CREEP-RUPTURE BEHAVIOR OF A WOVEN CERAMIC
MATRIX COMPOSITE AT ELEVATED TEMPERATURES IN
A HUMID ENVIRONMENT

THESIS

Jennifer L. Ryba, 2nd Lieutenant, USAF

AFIT/GMS/ENY/06-M02

DEPARTMENT OF THE AIR FORCE
AIR UNIVERSITY

AIR FORCE INSTITUTE OF TECHNOLOGY

Wright-Patterson Air Force Base, Ohio

The views expressed in this thesis are those of the author and do not reflect the official policy or position of the United States Air Force, Department of Defense, or the United States Government.

AFIT/GMS/ENY/06-M02

CREEP-RUPTURE BEHAVIOR OF A WOVEN CERAMIC
MATRIX COMPOSITE AT ELEVATED TEMPERATURES IN
A HUMID ENVIRONMENT

THESIS

Presented to the Faculty

Department of Aeronautics and Astronautics

Graduate School of Engineering and Management

Air Force Institute of Technology

Air University

Air Education and Training Command

In Partial Fulfillment of the Requirements for the

Degree of Master of Science (Materials Science)

Jennifer L. Ryba, BS

2nd Lieutenant, USAF

March 2006

AFIT/GMS/ENY/06-M02

CREEP-RUPTURE BEHAVIOR OF A WOVEN CERAMIC
MATRIX COMPOSITE AT ELEVATED TEMPERATURES IN
A HUMID ENVIRONMENT

Jennifer L. Ryba, BS
2nd Lieutenant, USAF

Approved:

//signed//

_____   _____
Dr. Shankar Mall (Chairman)   date

//signed//

_____   _____
Dr. Ted Nicholas (Member)   date

//signed//

_____   _____
Dr. Vinod Jain (Member)   date

AFIT/GMS/ENY/06-M02

Abstract

For high temperature applications, ceramic matrix composites (CMCs) are ideal because of their high strength and toughness, low density, and durability. A CMC manufactured with silicon carbide fiber and silicon carbide matrix, the focus of this research, maintains its strength and toughness at low and high temperatures, but experiences embrittlement at intermediate temperatures (450-900°C). This study focused on moisture and temperature effects on the embrittlement and stress-rupture life of the SiC/SiC CMC Syl-iBN/BN/SiC. The Syl-iBN/BN/SiC is composed of Sylramic™ fibers with an in-situ layer of boron nitride (Syl-iBN), boron nitride interphase (BN), and SiC matrix.

Stress rupture tests and monotonic tests were performed on the specimens. Tests were conducted under 100% humidity and laboratory air environments at three temperatures, 450°C, 750°C, and 950°C. These temperatures were chosen because they fall below the intermediate range, within the range, and above the range, respectively. This study found that while this CMC does experience embrittlement at intermediate temperatures, it also occurs at temperatures above the intermediate range. Scanning Electron Microscopy (SEM) analysis showed the embrittlement and pesting in the specimens increased with time, temperature, and moisture exposure, leading to premature failure. An analysis of the data confirmed that with increase in temperature and exposure to moisture, the stress-rupture life of the Syl-iBN/BN/SiC was considerably shortened.

Acknowledgments

First and foremost, I would like to thank my family for their unwavering support during my time at AFIT. Without their love and encouragement this endeavor would not have been possible. I would also like to thank my friends for giving me reasons to take time away from work, and a place to vent my frustration. Thanks also to Dr. Mall, for his guidance and support throughout the course of this thesis effort. To Ms. Robb, for giving me a place to relax at AFIT. Finally I would like to thank John Mehrman, John Balaconis, Pat Jackson, and Eric Dittman for keeping me sane when I was stuck in the lab.

Table of Contents

List of Figures

List of Tables

CREEP-RUPTURE BEHAVIOR OF A WOVEN CERAMIC
MATRIX COMPOSITE AT ELEVATED TEMPERATURES IN
A HUMID ENVIRONMENT

I. Introduction

"It is a truism that technological development depends on advances in the field of materials. One does not have to be an expert to realize that a most advanced turbine or aircraft design is of no use if adequate materials to bear the service loads and conditions are not available. Whatever the field may be, the final limitation on advancement depends on materials" [1].

In an industry continuously driven to develop lighter, stronger, and more durable materials in an effort to design more efficient and safer products, Ceramic Matrix Composites (CMCs) are emerging as vital elements in the advancement of engineering design. Some of the earliest tests on ceramic composites were conducted during the 1980s to try to understand the applications where the performance of the CMC exceeded the performance of the materials used at that time, especially under high temperature conditions. The primary objective in developing new material applications is to find a material that surpasses current materials' capabilities in the areas of environmental effects, thermal resistance, structural integrity, economical burden, and durability [2].

The ceramic matrix composite application considered in this study is for the applications in combustor liners. Aerospace designers place high importance on aircraft emissions and the adverse effect of some of these emissions on the atmosphere. In the case of combustor liners, the primary concern is NO_x emissions. These emissions usually result from the introduction of cooling air film during the combustion process. Advanced, low NO_x combustors will not be able to incorporate this type of cooling process.

1

Therefore, the new materials must be able to withstand the higher temperatures, while still remaining durable [3]. Of eleven materials studied for different applications in High Speed Civil Transport (HSCT), the High Speed Research (HSR) and Enabling Propulsion Materials (EPM) programs at NASA concluded that "the non-oxide SiC/SiC CMC had the most promise for high temperature, high oxidation applications [3] such as the combustor liner"[4]. The disadvantage to this winning material is its tendency towards embrittlement. This is one of the challenges that must be overcome before the CMC is a feasible alternative to its metal counterparts.

1.1 Embrittlement

For high temperature applications, ceramics are the best option, as they are the only class of material (between ceramics, metals, and polymers) that can be used at extreme temperatures. Figure 1 shows the service temperature limit of polymers, metals, and ceramics [5].
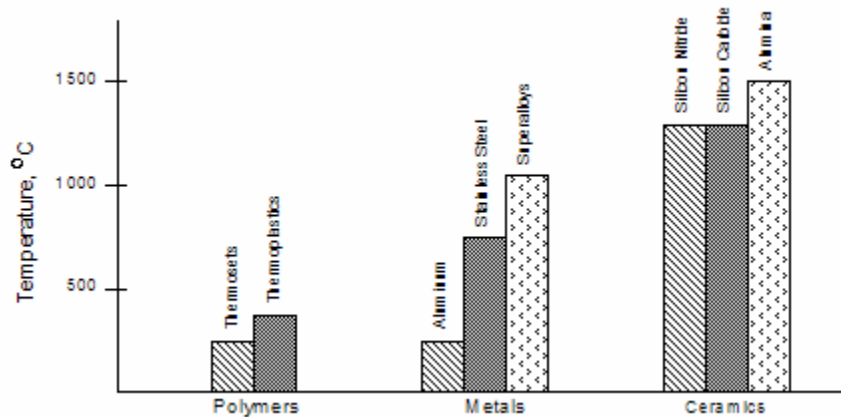
Figure 1: Service Temperature Limit of Polymers, Metals, and Ceramics [5]

Ceramics have higher hardness, strength and elastic modulus than metals and polymers. Their low density means important cost savings in designing aircraft components. However, ceramics have extremely low fracture toughness, meaning they are susceptible to crack-like defects [5]. This leads to catastrophic brittle failure. A solution to this problem is to reinforce the ceramic with a fiber matrix to increase the fracture toughness of the material and these are known as ceramic matrix composites (CMCs). Unfortunately, the addition of a fiber, and in this case an interphase, does not make the CMC perfect. The CMC is now prone to embrittlement.

The embrittlement of SiC/SiC CMCs, which is the test material of this study, is the oxidation embrittlement of the fiber/matrix interphase [6, 7, 8]. Embrittlement occurs when the composite is exposed to a harsh environment and its constituents are altered. This causes degradation in the composite's ultimate tensile strength, toughness, and damage tolerance. From previous works [6, 7, 8] it has been discovered that the testing environment attacks the interior of the specimen after entering through cracks caused by thermal stresses and applied loads. The amount of embrittlement depends on the temperature and moisture content of the air in the test or operating environment.

According to previous research, SiC/SiC CMCs work effectively outside the intermediate range (<450 °C and >900 °C), and within the intermediate range experience embrittlement [9, 10, 11]. More accurately, all temperature ranges might experience some embrittlement/ degradation, but it occurs most rapidly or significantly in the intermediate range [12]. So, while one might expect the degradation of the SiC/SiC to be proportional to the temperature, it instead performs worse than would be expected in the intermediate temperature range. The following figure explains this schematically (Figure 2).
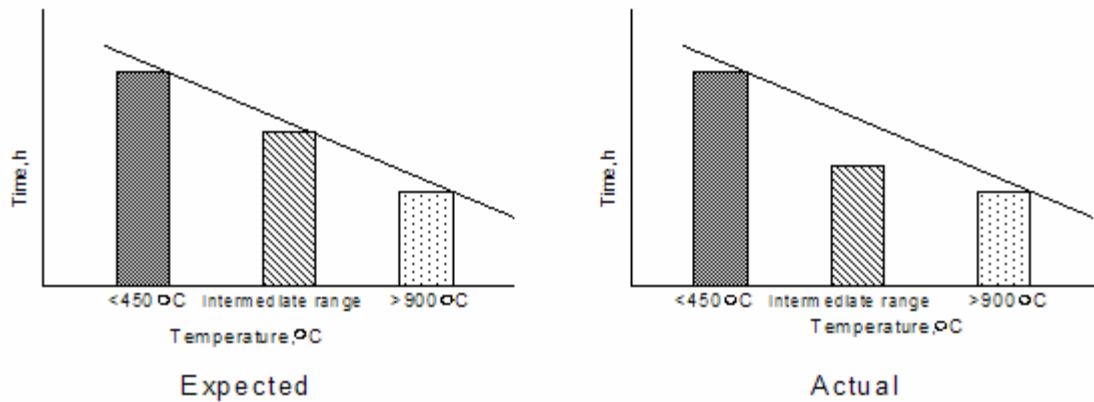
Figure 2: General Expected vs. Actual Specimen Performance

A term that will be used in this thesis with respect to embrittlement is "pesting" [4]. Pesting occurs when oxygen from the environment penetrates the specimen through matrix cracks in the composite. The oxygen reacts with the BN fiber coating and the fiber, causing the fibers and the interphase material to become bonded to each other and the matrix. For SiC/SiC CMC fibers, the product generated from the reaction of oxygen and BN fibers is a brittle silicate glass. So rather than the interphase functioning to protect the fiber, it is instead the instrument of its destruction, as it is replaced with a solid brittle glass. This glass has none of the toughness mechanisms inherent in a CMC, and fails easily and prematurely [4], not only because of the degradation of fiber strength, but also the stress concentration resulting from the formation of the glass [12].

In the case of a combustor liner, the ceramic matrix composite is exposed to a great deal of thermal stress – both through the thickness of the liner and due to the flow path of combustion products. Further loading is contributed by the thermal differential at attachment points and the high pressure environment of the combustor. The residual compressive stresses in the CMC can be overcome, and cracks can form in the matrix [4].

4

As the material is continuously loaded, at temperatures below 1000 °C, these cracks remain open, providing an opportunity for the environment to penetrate the CMC and attack the interphase material and fibers in the interior of the specimen. Above 1000°C the cracks are sealed by SiO_2 formation, repelling the environment.

The susceptibility of ceramic matrix composites to embrittlement and pesting has not been emphasized in literature prior to the mid 1990s. According to Heredia, et al. [12], there are three possible reasons for this:

(1) Instead of conducting load-bearing tests under high temperature conditions, specimens were heat treated, then tested. These two procedures produce different results, as the latter does not create the matrix cracks that lead to oxygen exposure in the interior of the specimen.

(2) Tests have been conducted above 1000 °C, which is above the pesting temperature, or intermediate range. At these temperatures, the formation of the silicate seals the cracks, preventing the pesting phenomenon.

(3) "Tests have been performed in flexure, rather than in tension. In such tests, load redistribution occurs" [12]. So due to the diminished strength degradation in flexure tests, even when embrittled regions have been created, they might not be apparent.

To correct this lack of understanding, tests have been conducted since the mid 1990s. As embrittlement is a major concern with CMCs, more effort was made to test specimens in a way that promote embrittlement [4]. After studying embrittlement behavior research can be done to produce materials that can better resist and overcome the effects of embrittlement.

1.2 Problem Statement

The focus of this study was to determine the effects of stress rupture loading, temperature, and moisture on the specimens of the Syl-iBN/BN/SiC CMC. The Syl-iBN/BN/SiC consists of a "Sylramic™ (Syl) fiber with an in-situ boron nitride (iBN) layer, boron nitride interphase, and silicon carbide (SiC) matrix" [4]. The SiC/SiC system studied is comparable to a material called 01/01 developed by NASA's Ultra-Efficient Engine Technology (UEET) Program [4]. This SiC/SiC system is the strongest and most creep resistant system developed thus far. This study seeks to investigate the stress rupture behavior of the material, or how it weakens over time, and how the environment effects this degradation.

During this study, tests were run in two separate environments – 100% humidity, and in air. A relationship was sought between the ceramic matrix composite degradation and the temperature, and/or the moisture content of the environment. Analysis of the failed specimens using a Scanning Electron Microscope showed how the introduction of high amounts of moisture into the testing environment affected the matrix, interphase, and fibers of the sample.

In the jet engine combustor applications, the liners are exposed to moisture levels much higher than those found in typical lab air. It is important to study how a material behaves with various temperatures, moisture, and applied stress conditions. Previous studies have investigated the behavior of CMCs at elevated temperature, under atmospheric pressure, and in ambient lab air [4]. A study conducted by LaRochelle [4] dealt with the Syl-iBN/BN/SiC CMC at various moisture content levels and stresses, at intermediate temperatures, 550°C and 750°C. While it is now not only understood and

accepted that moisture at elevated temperatures will degrade the CMC, the quantitative effects on the material have been shown at intermediate temperatures. However, this study will continue the research began in LaRochelle's study [4] by finding quantitative relationships between tests conducted below the intermediate temperature range, within the intermediate range, and above the intermediate range.

1.3 Approach

This research expanded the experiments conducted by LaRochelle [4]. It involved tests that generated stress rupture data to characterize the stress rupture behavior of the Syl-iBN/BN/SiC CMC system. The test environments consisted of three temperatures: 400 °C - below the intermediate range, 750 °C – within the intermediate range, and 950 °C – above the intermediate range. The tests run at 750 °C were intended to be compared with those run by LaRochelle. At these temperatures, tests were run at both 100% humidity conditions, and in laboratory air. A test duration, or run-out, time of 100 hours was used, to ensure exposure to the test environment, and to allow for the completion of as many experiments as possible.

Stress rupture tests are important to aircraft engineers because they show how long a material can withstand a certain load in a particular environment. The stress rupture loads in these tests were designed to imitate the tendency of CMC combustor liners to fail due to stress rupture at attachment points, because of the thermal and mechanical stresses the CMC experiences for long periods of time [4]. A ceramic susceptor that fit the test section of the specimen was used to maintain a humid environment during the duration of

the test. The environment was assumed to be 100% humid, due to a continuous input of steam.

The plan for this research was to test specimens at the three temperatures, with different stress levels, in lab air and humid environments. Stress rupture tests would be used for all specimens, and for those specimens that did not fail in the 100 hour test duration, monotonic tests were used to determine the effect of the environment on the elastic modulus and ultimate tensile strength of the specimens. The environmental stress rupture data provided the behavior of the material as temperature and moisture were varied. The research conducted by LaRochelle [4] was used for panel data, as the specimens used in this study were from the same panels as those used by LaRochelle. The experimental data of this study were normalized by dividing by the panel's room temperature ultimate strength. This accounted for the slight difference in mechanical properties of each panel, so their results could be compared.

Once a specimen failed, the hydraulic system of the test machine would remove the bottom half of the specimen from the test environment. This fracture surface was studied under the scanning electron microscope (SEM), as it had only been exposed to the test environment for the duration of the test, as opposed to the upper half of the specimen, which continued to be exposed to the testing environment until the equipment was turned off. Analysis using the SEM provided the details of failure mechanisms and the embrittlement phenomenon.

1.4 Chapter Summary

This research continues the study into the behavior of the Syl-iBN/BN/SiC composite in an environment that exposes it to conditions in a lab setting similar to conditions the composite would be under in a working situation, such as the jet engine combustor liner application. This section summarizes the layout of the thesis. Chapter II provides the background for the composite, its components, and its method of failure. Chapter III discusses the manufacture of the composite, and the specimen dimensions. Chapter IV describes the mechanical and environmental equipment used, the methodology of the tests run on the specimens, and the equipment used for analysis of the failed specimens. Chapter V presents the test results. Chapter VI discusses the results and their relevance to the current and future uses of the CMC. Chapter VII summarizes the research presented, and provides recommendations for future work with this composite.

II. Background

A ceramic matrix composite (CMC) is typically composed of, at the least, fibers and the matrix surrounding them. Some CMCs incorporate an interphase between the fibers and the matrix. These separate components are chemically and usually physically distinct materials [5]. The matrix is the continuous phase, and the fibers are the reinforcement phase. Together the different phases have better properties than they do separately. CMCs are used for their high strength and toughness, low density, ability to withstand extreme temperatures, and their durability. There are four broad categories of ceramic composite materials. Particulate composites consist of particles of various sizes and shapes randomly dispersed within the matrix. The discontinuous or short-fiber composites contain short fibers, or whiskers, as the reinforcing component. These fibers can be randomly oriented, or oriented all in the same direction. Continuous fiber composites are reinforced by long continuous fibers. The fibers can all be parallel to each other, at right angles, or oriented along several directions. These are the most efficient in terms of stiffness and strength. The final category is laminate composites. These consist of thin layers of lamina bonded together. The lamina can contain large numbers of continuous fibers oriented in the same or multiple directions. Composites can also consist of continuous fibers bundled in tows that are woven together to make two- or three-dimensional configurations, as is the case with the CMC in this experiment. Each fiber configuration provides different material properties to the CMC. The fiber configuration required for an application is dictated by the design requirements of that application.

This chapter will describe the principal constituents of ceramic matrix composites and the potential CMCs for combustor liner applications. It will provide an overview of the failure behavior experienced by CMCs and explain the embrittlement phenomenon experienced by the Syl-iBN/BN/SiC CMC at intermediate temperatures.

2.1 Principal Constituents of Ceramic Matrix Composites

2.1.1 Fibers

Ceramic fibers provide CMCs high strength and high elastic modulus in addition to their high temperature capability. Fibers are typically manufactured as multifiber tows consisting of 100-1000 smaller diameter fibers (5-15μm) or as single large fibers (50-100 μm). These monofilament fibers are mainly used in metal composites. Ceramic composites make use of the multifiber tows, as the smaller diameter and larger quantity of fibers reduces the microstructural defects associated with using larger fibers [13]. Ceramic composites can consist of oxide and non-oxide components. CMCs have been manufactured with oxide fibers within an oxide matrix, like the Nextel 720/alumina CMC system, non-oxide fibers within oxide matrices, like the carbon (C)/alumina silicate CMC system, and with non-oxide fibers within non-oxide matrices, like the SiC/SiC CMC system [4].

Oxide fibers have been commercially available since the 1970s [5]. Oxide fibers are mostly alumina (Al_2O_3) based and may contain small amounts of SiO_2. By definition, these fibers are impervious to oxidation. Unfortunately, they are extremely expensive, and have a temperature limitation of approximately 1000-1200°C [4]. For high temperature applications, a large grain size is desired because grain boundary sliding can

lead to large creep strains in fine-grained material. A 10 ATM Kaiser Rig test with 10% H_2O environment was run on the Nextel 720/alumina and showed that this CMC could survive 3000 and 1000 hour tests at 1137°C and 1200°C, respectively, with no loss of strength [4,14]. It is possible to use this ceramic at higher temperature applications, with the use of an all-alumina based, friable insulation that could keep the ceramic at 1200°C. However, this does not improve the CMCs performance at the desired operating temperature of 1300°C for the combustor liner, removing CMCs with oxide constituents from consideration as a liner material [15]. This leaves the non-oxide/non-oxide CMCs.

2.1.2 Matrix

Ceramic matrix materials can withstand very high temperatures, making them ideal for high temperature applications. Ceramics are composed of a metal combined with a nonmetal, generally with a fixed ratio of cations to anions, for example, alumina (Al_2O_3), silicon carbide (SiC), and silicon nitride (Si_3N_4) [13]. Ceramic matrices can also be classified as oxide and non-oxide. The most common oxide matrices are alumina and zirconia. While these are more resistant to oxidation, they are not capable of handling temperatures higher than 1200°C. Common non-oxide matrices include silicon carbide, silicon nitride, and titanium diboride [13]. These ceramics are viable at high temperatures, but require a layer of silica (SiO_2) to prevent oxidation. This silica layer is still susceptible to environmental degradation. This leaves silicon carbide and silicon nitride for consideration.

When matching fiber and matrix materials, it is important to consider the coefficient of thermal expansion. If the ratio of the coefficients of thermal expansion of the matrix

and the fiber is considerably less than one, premature matrix cracking occurs. If the ratio is considerably greater than one, thermal debonding of the fiber/matrix occurs. To avoid these situations, a ratio of close to unity is desired [16]. As the best fiber choice is a SiC fiber, the most logical matrix material would be the SiC CMC over the silicon nitride, as the silicon carbide would match coefficients of thermal expansion [4].

2.1.3 Interphase

It is desirable for a ceramic composite to have a weak fiber/matrix interphase. The debonding of the fiber and matrix allows the composite to still carry a load while the matrix was cracking. Oxide/oxide composites have sufficiently porous matrices that allow fiber/matrix debonding, and deflect matrix cracks. However, for more dense matrices, such as the SiC matrix, a coating is needed for the fiber to provide the weak interphase, and help the fiber withstand environmental degradation. The interphase decides the tensile axial properties of the composite material [16].

Originally carbon was considered a very good interphase material because of its mechanical properties and low cost [4]. Unfortunately, in environments with any humidity, carbon oxidizes and volatizes as CO and CO_2. The disappearance of the carbon leaves a space between the fiber and the matrix, increasing the surface area of the fiber subjected to the environment. Filippuzzi et al [17] tested SiC/C/SiC composites in oxidizing and inert atmospheres, and by using thermogravimetric analysis, found that these composites experience an initial weight loss in the oxidizing environments due to the oxidation of C [4].

The susceptibility of carbon to oxidation has led researchers to investigate other materials. One such material is boron nitride (BN). While it still experiences oxidation, it does not oxidize as readily as carbon. Boron nitride is as effective as carbon, and can withstand temperatures below 450°C and above 900°C. This is because at low temperatures, the rate of oxidation is low enough to be of little concern. Above 900°C, the formation of a layer of silica seals the cracks, reducing the exposure of the BN interphase to the environment [4].

Research was performed by Sheldon et al [18] concerning the oxidation of BN and SiC at 1000°C. They analyzed their data using thermodynamic calculations and found that "at 1000°C the BN would not oxidize to form B_2O_3 until all Si has formed SiO_2 and all C has formed CO [18]". As previously stated, at this high temperature the silica formation seals the cracks, and extends the life of the material. Ogbuji [19] conducted a test above 450°C and below 900°C, at 800°C, in the intermediate range. In place of the BN interphase he found silica formation. From the results of previous tests, the amount of silica formation was more than was expected at 800°C. He postulated that the liquid B_2O_3 dissolved the SiC matrix cladding to form a liquid borosilicate. This liquid was eutectic at any temperature above 372°C, which led to alterations in the constituents of the CMC, in this case the interphase, causing the CMC to fail at a stress level lower than expected. This is the phenomenon known as embrittlement which will be discussed in section 2.4.

2.2 Potential Ceramic Matrix Composite for Combustor Liner Application

The previous section narrowed down the list of acceptable materials for a high temperature, high humidity environment. The final choice for the fiber and matrix

material was a SiC/SiC CMC as it is the only material that can perform at temperatures above 1300°C. Two interphase materials were considered, carbon and boron nitride. They are both typically used with SiC fibers, and provide the best material properties for the combustor liner application. Both materials oxidize in high moisture environments which leads to failure, especially in the intermediate range, >450°C and <900°C. A review of previous studies will show which material, of carbon and BN, is better suited to the combustor liner application. These studies were in SiC/SiC composites with C or BN interphases, where mechanical stress on the specimens cause matrix cracks, exposing the interior of the material to the test environment [4].

A study performed by Heredia et al [12] on a two-dimensional NiC/C/SiC system found that stress rupture tests performed in air at 800°C resulted in a drastic reduction of rupture strength as a function of time. For example, one specimen was 33% of the ultimate strength at room temperature after a 12 hr period [4]. Heredia et al [12] also conducted a cyclic study on the NiC/C-B/magnesium aluminosilicate system at 500°C, where the system failed at a peak stress of 50% of the ultimate strength at room temperature at 104 cycles. The NiC/C/SiC system was also studied by Lin and Becher [20] and Lin et al [21] at temperatures of 600°C, 900°C, and 950°C. Their tests had similar results to those performed by Heredia et al [12]. The specimens were analyzed using electron microscopy and the researchers concluded that "the life of the CMC was controlled by the oxidation of the C interphase and the formation of glass from the oxidation of the fiber and matrix [4]". They also concluded the behavior of the interphase strongly depends on the inherent porosity of the SiC/SiC CMCs.

The NiC/C/SiC system behavior was studied at 425°C and 950°C by Lara-Curzio et al [22] and Lara-Curzio [23], respectively. They collectively found that the oxidation of the carbon interphase exposed an increased gage length of the fiber to the stress-rupture environment, leading to degradation in strength and shortened life. The study conducted by Lipetzky et al [24] on this CMC at 1000°C showed no influence from moisture in the test results due to the formation of the silica layer, which sealed the cracks and prevented the environment from attacking the interphase and exposing the fibers.

Another system tested using the carbon or boron nitride interphase was the Hi-Nicalon (HN)/SiC system. Martinez-Fernandez and Morscher [25] found that HN/C/SiC minicomposites outperformed the NiC/C/SiC minicomposites, but did not perform as well as the HN/BN/SiC minicomposites in the 700-1200°C temperature range. A minicomposite is one tow of fibers that have gone through the manufacturing process. By testing the stress rupture and low-cycle fatigue behavior of the HN/BN/SiC CVI minicomposites and composites in air between 600-1300°C, Morscher [9, 26] found the degradation in strength was a result of the fiber exposure to the test environment and reaction to the liquid by-product of the oxidation of the interphase material, in this case the oxidation of BN to form a borosilicate glass. Another cause of the premature failure was the pesting of the fibers resulting from the solidification of the liquid [4].

Morscher and Cawley [27] studied the stress rupture behavior of the HN/BN/SiC MI matrix and the Syl/BN/SiC Mi matrix at 815°C in air and found that the Sylramic fibers outperformed the Hi-Nicalon fibers. After conducting a test to study the stress rupture behavior and low cycle fatigue behavior of the HN/BN/SiC MI matrix system, Morscher et al [28] concluded that the embrittled fibers failed before the pulled-out fibers,

16

although the pulled-out fibers failed shortly after, and that the bridging fibers were exposed to the environment for long periods of time. In this study, they used a SEM to identify embrittled and untouched areas on the fracture surface, and electron dispersive spectroscopy (EDS) to compare the different O:C ratios for the failed fibers. From these tests, Morscher et al [28] determined a failure mechanism for this CMC: first the applied loads cause cracking in the matrix material, allowing the environment to infiltrate the interior of the specimen and attack the interphase and fiber materials, causing embrittlement. This leads to the degradation of fiber strength, and when an embrittled fiber fails, it begins a domino effect resulting in the failure of all the neighboring fibers pested together. Finally, the increased load on those fibers untouched by the environment causes them to experience pull-out and failure.

Some of the data from the previously discussed studies with HN/SiC systems are summarized in Figure 3 and Figure 4. The stress in these plots was calculated by dividing the composite stress by the volume fraction of fibers in the loading direction so that the results could be compared with data for the as-produced fibers [4]. The Figure depicting the results for a carbon interphase test show a slightly lesser slope in the HN/C/SiC experimental data compared with the as-produced HN fiber data. This shows the material initially experiences minor embrittlement, and as the temperature increases above 700°C, more embrittlement occurs with longer times and higher temperatures [4]. Figure 4 shows that the HN/BN/SiC system failed at similar fiber stresses as the as-produced HN fibers. A comparison of Figure 4 to Figure 3 shows the superior performance of the BN interphase to the carbon interphase. These figures indicate that the BN is more durable in oxidizing environments than the C.
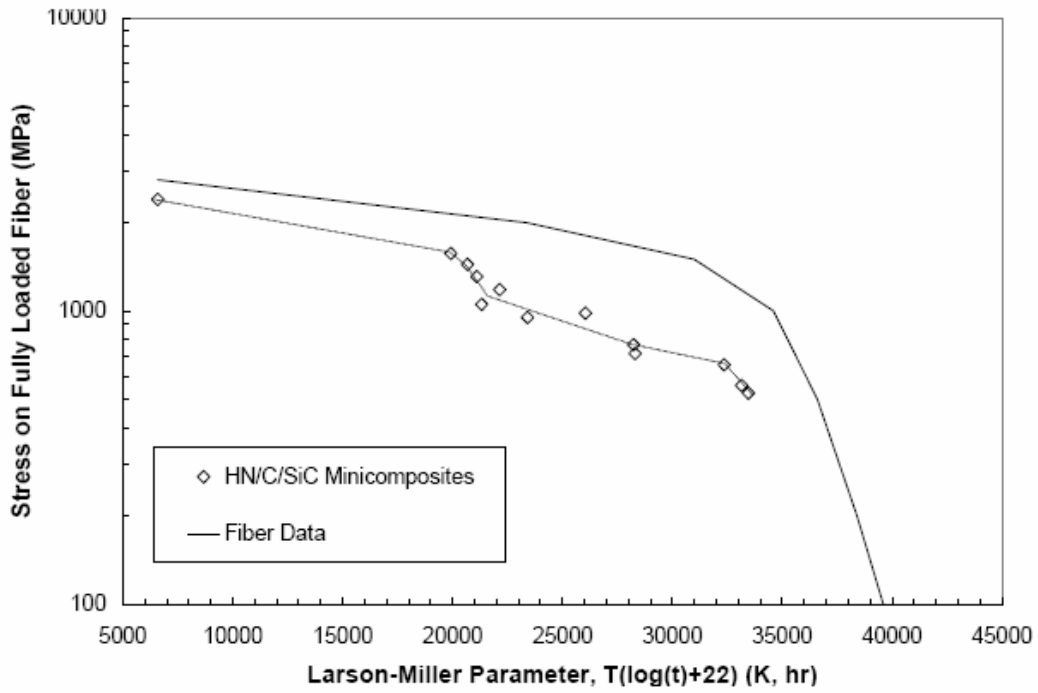
17

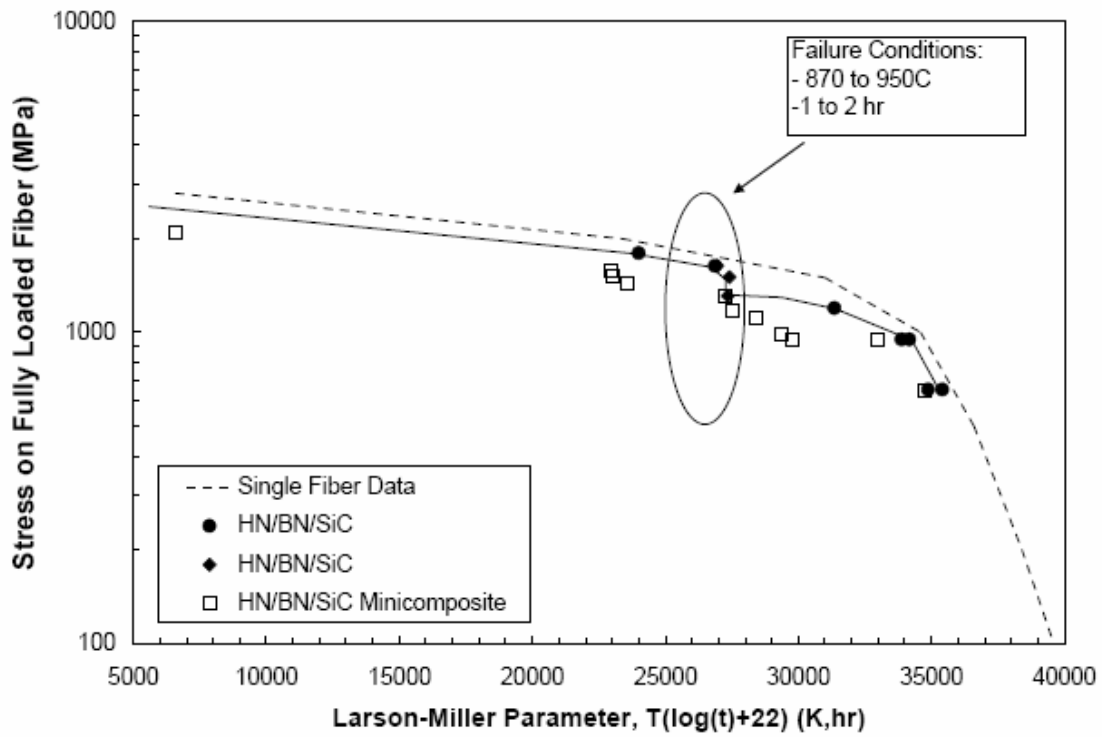**Figure 3: Larson-Miller Plot of HN/C/SiC [4, 9]**

Figure 4: Larson-Miller Plot of HN/BN/SiC [4, 9]

18

The material used in this study was a Syl-iBN/BN/SiC CMC, consisting of Syl-iBN SiC fibers, a BN interphase, and a SIC matrix. The SiC/SiC fiber/matrix combination was chosen for its high performance at high temperatures, and for the comparable coefficients of thermal expansion, and the BN interphase was chosen over the C for its higher durability in oxidizing environments.

2.3 CMC Failure Behavior

2.3.1 Overview

The fiber reinforcement in ceramic matrix composites makes them more resistant to damage than a pure ceramic material. In an undamaged CMC, all of its constituents share the applied load depending on the volume fractions and elastic properties of the constituents. The first sign of damage in a CMC under mechanical and/or thermal stress is the appearance of micro-cracks in the matrix. The first cracks typically begin at places in the specimen that are not uniform, i.e. within the cross tows, where there is a higher concentration of pores and surface flaws, and at places with higher stress concentrations, such as corners and attachment points of the specimen [4]. As the specimen continues to load, these micro-cracks grow and combine to form even larger cracks. Eventually these cracks work through the thickness of the specimen, and it fails. Due to the additional support of the fibers, the matrix cracking stress is greater than the catastrophic fracture stress of the pure ceramic material [29, 30].

As micro-cracks grow and propagate in the matrix they continue until they meet a fiber aligned perpendicular to the crack plane, and parallel to the loading direction. When the crack encounters the fiber, the interphase fails, allowing the fiber to slide through the

19

matrix (pull-out), and relieving the stress concentration at the crack tip. These fibers become bridging fibers, and effectively stop the crack propagation. When the bridging fiber fails, the stress concentration at the crack tip increases, and if enough fibers fail, the stress increases enough that the crack continues to propagate [4]. This process repeats as the cracks continue to propagate through the matrix and encounter other fiber tows. A typical stress strain curve for a CMC material is shown in Figure 5.
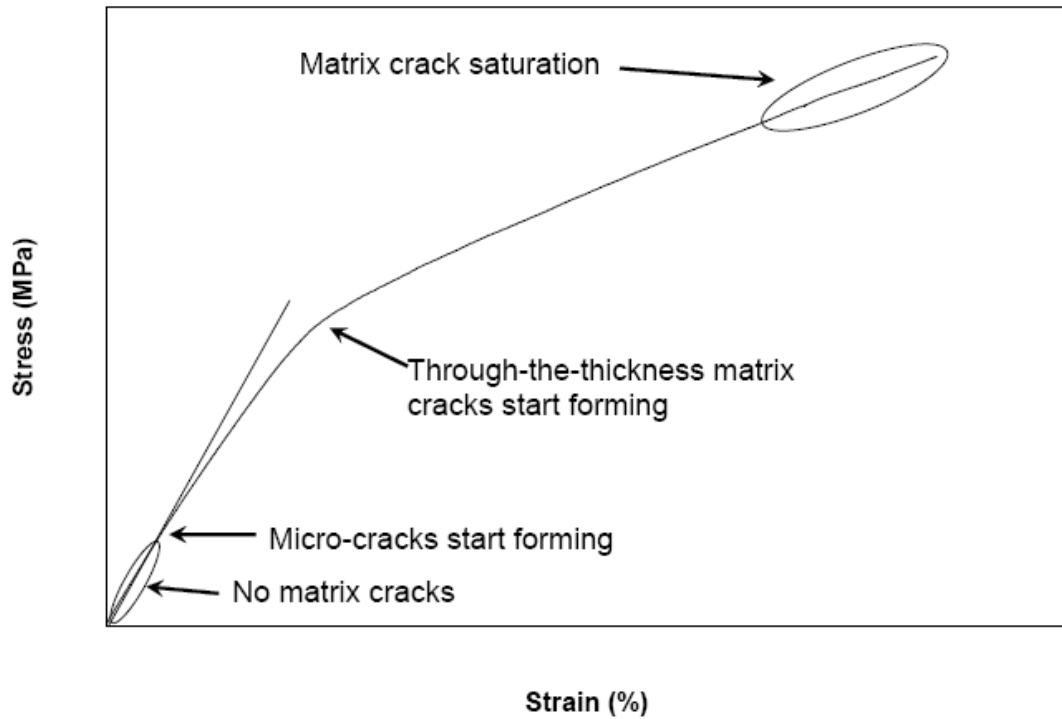
Figure 5: Typical Stress Strain Curve for a CMC Material [4]

The "knee" in Figure 5 represents when either one crack propagates through all the fibers, or when many cracks combine to form a large crack that continues through the thickness. In a through-the-thickness crack, the fibers support the entire load on the specimen. As the fibers fail, the load is redistributed among the remaining fibers [4]. In a study performed by Yun et al [31], they found that under a stress rupture condition at

intermediate temperatures failure occurs by local overloading due to the stress concentration resulting from the strong bond of the fibers to the matrix. It does not even mean that the fibers are weakened. It means that the strongly bonded fibers are as strong as their weakest link. When the weakest strongly bonded fiber fails, it causes all the other strongly bonded fibers to fail due to their "inability to globally share the increased stress applied to the nearest neighbor fibers and unbridged crack growth [31]". Normally in a CMC with an interphase, the interphase fails, allowing the fibers to slip. But in the case of the Syl-iBN/BN/SiC CMC at high temperature and moisture levels, the fibers and matrix become strongly bonded through the solidification of the interphase material, leading to the failure of groups of fibers.

As shown in Figure 5, the two extremes of matrix cracking are no matrix crack and matrix crack saturation. There are no cracks when the applied stress is below the matrix cracking stress. When the applied load is high enough that the distance between cracks is shorter than the slip transfer length, the matrix material has reached matrix crack saturation [32]. In between these two extremes, the matrix will experience either partial cracks or through-the-thickness cracks. In a through the thickness crack, the bridging fiber carries the entire load. In a partial crack, the stress on the fiber is reduced because there is still matrix material at the crack tip to carry some of the load [4].

In stress rupture loading, the specimen will eventually reach a steady state crack density composed of partial and through-the-thickness cracks. Any cracks open to the surface of the specimen can allow the environment into the interior, leading to attack on the interphase and fibers, causing embrittlement [4]. Only the interphase and fibers exposed to the environment will experience stress-oxidation strength degradation and

21

embrittlement due to that environment. The parts of the sample protected from the environment will only experience failure due to thermal and mechanical stresses.

2.3.2 Creep (Stress)-Rupture Behavior

In designing aerospace components, the creep resistance of a material is a critical factor in testing its performance. Creep is deformation that occurs over a period of time when a material is subjected to constant stress at constant temperature. By studying the creep behavior of a material, a limit for the maximum operation temperature for that material can be established.

In testing ceramic composites, creep is often used to analyze the oxidation of the composite components. During a creep test, cracks form in the matrix and expand, exposing the fibers and interphase to the test environment, leading to degradation of the fiber strength. In oxide composites, the damage done to the matrix resulting from creep stress is a primary factor in determining creep-rupture life. In non-oxide composites, all the damage is a result of the cracks formed in the matrix, but the final failure is attributed the oxidation of the fibers and interphase.

A common problem in composites is the disparity between the creep strength of the fiber and the strength of the matrix. However, in a strongly bonded fiber/matrix system, the axial stresses in the fiber and matrix equilibrate, as shown in Figure 6.
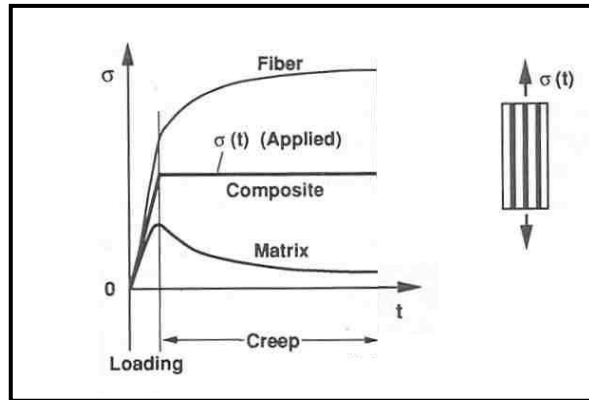
Figure 6: Stress Redistribution during Creep [13]

2.4 Embrittlement of SiC/BN/SiC CMCs at Intermediate Temperatures

As previously discussed, the presence of O_2 and H_2O in a testing environment
severely degrades the performance of the Syl-iBN/BN/SiC CMC, if cracks form in such a
way that the load-bearing fibers and interphase material are exposed to that environment.
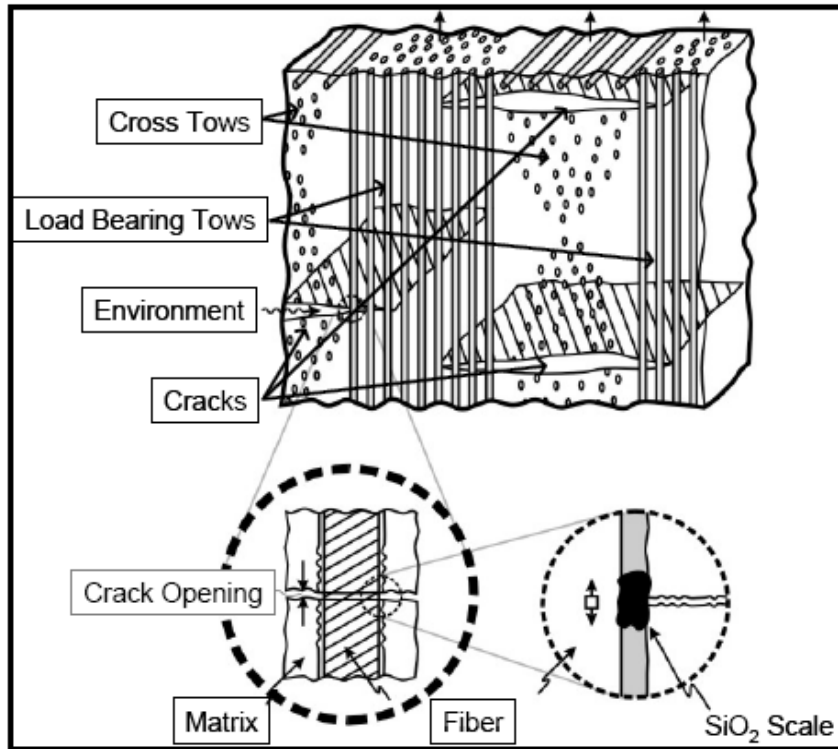Figure 7 [4] is a schematic of the embrittlement of CMCs.

Figure 7: Model of Environmentally Assisted Embrittlement of CMCs [4]

At an intermediate temperature the major reactions of the Syl-iBN/BN/SiC CMC
are the oxidation of the BN to form the borosilicate glass, B_2O_3, as [11]

$$2BN + \frac{3}{2}O_2(g) \rightarrow B_2O_3(l) + N_2(g) \qquad\qquad 2$$
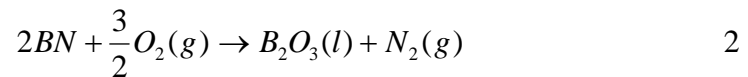
Coffer and Economy [33] verified that the BN oxidizes to form B_2O_3 by using
thermogravimetric analysis. There are several ways the liquid B_2O_3 product can become a
borosilicate glass. One way is for it to react with any SiO_2 from the oxidation of the SiC
fiber and/or matrix. This is supported by Ogbuji [19], who reported that the phase
diagrams for the SiO_2-B_2O_3 system show that B_2O_3 can dissolve its own weight in SiO_2 at
800°C, resulting in the borosilicate liquid. The following reaction describes how the

liquid B_2O_3 formed by reaction (2) dissolves the SiC fiber and matrix to form the viscous

borosilicate liquid [19]:

$$B_2O_3(l) + SiC(s) + \frac{3}{2}O_2(g) \rightarrow B_2O_3 \cdot SiO_2(l) + CO(g) \qquad 3$$
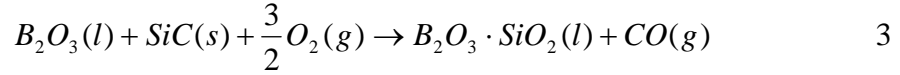
The SiO_2 can also be formed through oxidation of the fibers and matrix as

$$SiC + \frac{3}{2}O_2(g) \rightarrow SiO_2(s) + CO(g) \qquad 4$$
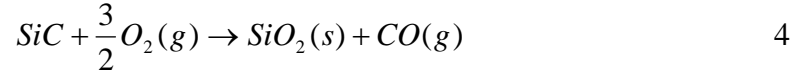
The borosilicate liquid is volatized by moisture according to the following reactions

[4]

$$B_2O_3(l) + 3H_2O(g) \rightarrow 2H_3BO_3(g) \qquad 5$$

$$3B_2O_3(l) + 3H_2O(g) \rightarrow 2H_3B_3O_6(g) \qquad 6$$

$$B_2O_3(l) + H_2O(g) \rightarrow 2HBO_2(g) \qquad 7$$

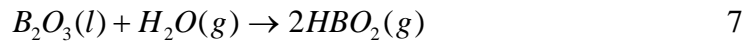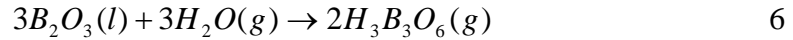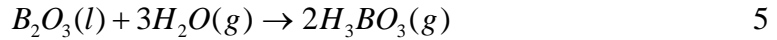Equation (7) describes the primary reaction in volatilization at intermediate

temperatures. This equation was found to be stable in the gaseous form at 700°C by

Coffer and Economy [33]. Through the use of SEM images, EDS for elemental

identification, Rutherford backscattering spectroscopy for composition measurement of

B_2O_3, and wavelength dispersive spectroscopy for boron detection, Morscher et al [11]

found that the BN was converted to liquid then to borosilicate. The resulting glass was

predominately SiO_2. This is supported by Jacobson et al [10, 11]. In the mid-1960s, it

was found that B_2O_3 and borosilicates are strongly hydrophilic [34]. Jacobson and co-

workers found that in the liquid form, B_2O_3 and borosilicates are rapidly hydrolyzed,

even in air. This hydrolysis reaction liberates gaseous boron hydroxides, and with this

loss of boron from the borosilicate liquid, its viscosity increases until it is transformed

into a solid SiO_2 glass [19]. This glass formation results in the pesting of the fibers, leading to the failure of neighboring fibers in groups. There are two reasons fibers fail due to pesting. The first is that when one fiber fails, the neighboring pested fibers experience an abrupt increase in load. The second reason is that the pesting of the fibers provides an easy path for failure cracks to propagate across [4].

The above studies led to further research by Morscher [9] and Morscher and Cawley [27] into the embrittlement behavior of SiC/SiC CMCs at 815°C in ambient laboratory conditions [4], and a study by LaRochelle into the embrittlement effects on a Syl-iBN/BN/SiC CMC at 550°C and 750°C with controlled moisture content levels. The present research investigates embrittlement effects at 400°C, 750°C, and 950°C with ambient air, and high moisture levels.

III. Material and Specimen Description

This chapter will discuss the material, the specimen preparation, and the dimensions of the specimen. This will allow for a better understanding for the behavior of the specimen.

3.1 Material

The material tested in this experiment was a non-oxide fiber/non-oxide matrix ceramic composite. The Syl-iBN fiber performs were provided to Honeywell Advanced Composites, Inc. for manufacturing by NASA Glenn Research Center. Six panels were produced, with 15 specimens cut from each panel. The technique used to apply the BN interphase layer to the in-situ BN performs, and a thin layer of SiC to the BN layer was Chemical Vapor Infiltration (CVI) [4]. In the CVI process a solid material is deposited from gaseous reactants onto a heated substrate. A CVI technique provides good mechanical properties at high temperatures, but takes a long time to complete the process, and can be expensive. The addition of the BN layer to the fiber preform resulted in a $10.64 \pm 0.34\%$ weight gain. The layer of SiC added a $53.40 \pm -5.99\%$ weight gain [4]. The bulk of the matrix was SiC, which was infiltrated by slurry into the preform. This caused a $30.10 \pm 1.50\%$ weight gain. A $13.92 \pm 0.80\%$ weight gain resulted from the melt infiltration of molten Si. The final material was a mostly nonporous composite comprised of 8 piles of woven Syl-iBN tows, with each tow having 800 fibers [4]. The fibers are woven in a five-harness satin weave. Figure 8 depicts a five-harness satin weave.
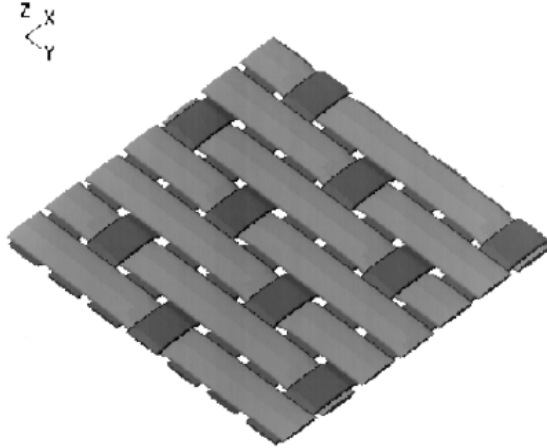
Figure 8: Five-harness Satin Weave [3]

For a five-harness satin, the warp ends (warp fibers in longitudinal direction, fill fibers in transverse direction) go over four fill fibers then under one fill fiber. The satin weave is more durable and pliable than the plain weave (over, under a fill yarn). It is also less porous than the plain weave. Properties of the constituents of the Syl-iBN/BN/SiC CMC are listed in Table 1.

Table 1: Composite Constituent Properties [4]

Constituent	Material	Volume Fraction (%)	Weight Gain (%)	Elastic Modulus (GPa)	Remarks
Fiber	Syl-iBN	37.10	N/A	380	5 Harness Satin 20 ends/inch
Interphase	BN	6.62	10.64	Unknown	~ 0.45 μm
Matrix	CVI SiC	19.33	53.40	425	~ 4 μm
	MI SiC		30.10		
	Si	36.95	13.92	345	Process Temp ~1400°C
	Porosity		0.00		

3.2 Specimen Geometry

The specimens were cut in a dog-bone configuration to encourage failure within the gage section of the specimen. Figure 9 depicts the specimen dimensions.
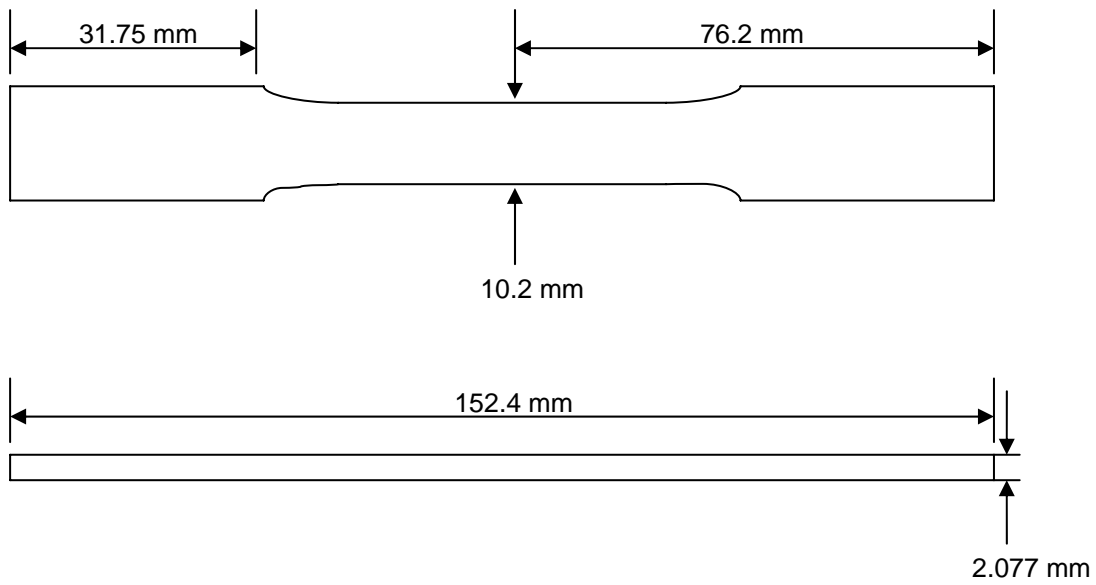
Figure 9: Specimen Dimensions

IV. Experimental Set-Up and Procedures

This section describes the details of the experimental set-up and procedure. It will discuss the different testing methods as well as post-failure analysis of the specimens.

4.1 Test Equipment

This section discusses the equipment used to create the environment and conditions under which the specimens were tested. It shows the arrangement of the testing equipment through figures.

4.1.1 Mechanical Test Apparatus

There were four main components of the mechanical testing apparatus for testing the SiC/SiC CMC; the servo-hydraulic machine, the water chiller, the extensometer, and the high temperature equipment.

All monotonic and creep testing was performed using a vertically configured Material Test Systems (MTS) Corporation servo-hydraulic machine (model 810) with a 25 kN (5500 lb) capacity. The load measurement was used to compute the axial stress, σ, experienced by the specimen using the following equation:

$$\sigma = \frac{P}{A}$$

where P is the applied load, and A is the cross-sectional area of the test section. A load cell, MTS model 661.20E-01, also with a 25 kN capacity, measured the load applied to the specimen by the hydraulic piston.

The test specimens were secured using a pair of MTS 647.02B-03 Hydraulic Wedge Grips. The grips consisted of a pair of interchangeable wedges coated with a layer of a surf alloy to provide a better surface for gripping the specimens. To maintain a suitable grip temperature, each grip wedge had an inlet and outlet to allow cooling to water to pass through. It was important to maintain a moderate grip temperature so an extreme temperature condition at the gripped section of the specimen did not adversely affect the specimen outside the test section. The grips were cooled using a NESLAB HX-75 Refrigerated Recirculator. Distilled water was kept at a temperature of 14°C and continuously circulated through the grips during the test. The grip pressure was controlled by an MTS 685.53 Hydraulic Grip Control attached to the test stand, capable of exerting pressures up to 20.7 MPa (3000 psi). The grip pressure used during the test was 8 MPa. The grip pressure could not be too high, or it would damage the specimen, possibly causing it to break in the grips, instead of the test section. If the pressure were too low, the specimen would slip in, or out of, the grips, affecting the test data. Figure 10 shows the test stand with the servo-hydraulic machine, the furnace, and the extensometer assembly.
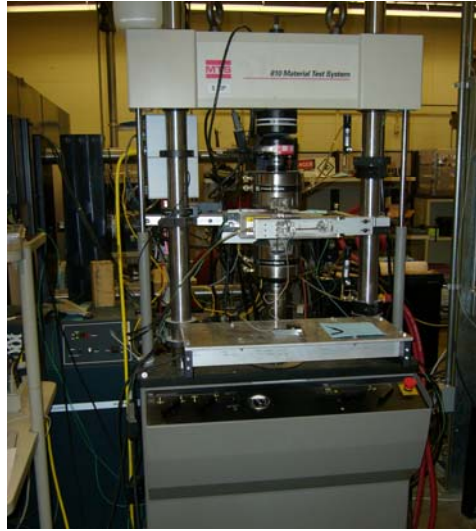
Figure 10: Experimental Test Set-Up

The strain on the specimen was measured using an MTS High Temperature Axial Extensometer, model number 632.53E-14. The extensometer had two 3.5 mm diameter alumina rods, with a 12.7 mm gage length that extended from the sensor to rest on the specimen. Each rod had a cone-shaped tip, for mounting on flat specimens. The extensometer maintained contact with the specimen using constant spring pressure. To protect the extensometer and its electronics from the heat radiating from the oven, it had a heat shield and constant air flow over the body of the extensometer. The airflow was regulated by a valve, and held at about 20 psi. Maximum extension of the rods was 16.8 mm, although the test specimen never stretched enough to test this parameter. The extensometer could measure strains between +20 and -10% for a maximum specimen temperature of 1200°C, and could provide up to 300g of contact force through spring tension. The accuracy of the extensometer results was tested by periodically testing the Young's Modulus of aluminum samples. Figure 11 shows the extensometer set-up.
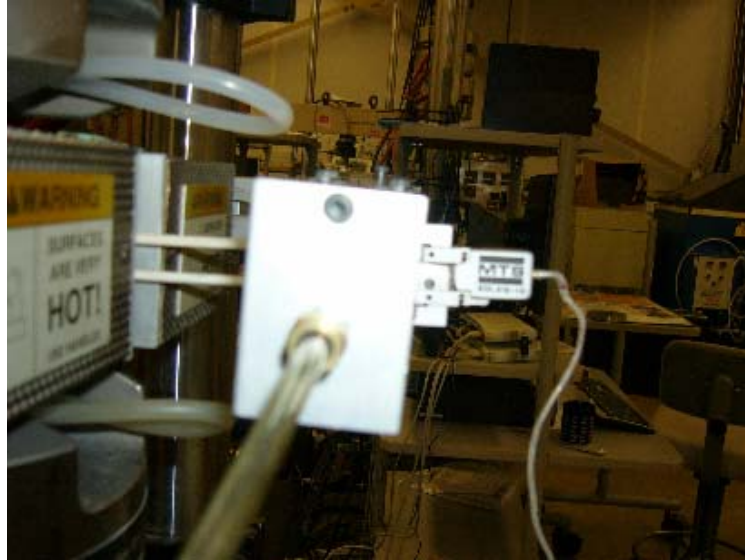
Figure 11: Extensometer

The test software used to control the hydraulics and the furnace, and to gather data from the extensometer, was the MTS TestStar IV. Each type of test was programmed, and data was acquired, using the software's Multi Purpose Testware (MPT) feature. After writing the program, setting up the specimen, and starting the test, all of the testing and data acquisition was automated. After the test concluded, the results were analyzed and plotted using the Microsoft Office Excel spreadsheet program. Figure 12 shows an example of an MPT test program used during a creep test.

Type	Name	Start	Interrupt
	temp data	\<Procedure\>.Start	oven heat up.Done
	oven heat up	\<Procedure\>.Start	
	circular data file	\<Procedure\>.Start	
	data ramp up	oven heat up.Done	ramp up.Done
	ramp up	oven heat up.Done	
	data creep	ramp up.Done	
	creep	ramp up.Done	
	ramp down	creep.Done	
	oven off	creep.Done	

Procedure is done when | ramp down.Done

Figure 12: MPT Test Program

4.1.2 Environmental Equipment

The environmental equipment included a furnace, an external temperature controller, a steam generator, and a ceramic susceptor. The furnace used to heat the specimen was a two-zone AMTECO Hot-Rail Furnace System. It was made up of two halves, each containing one silicon carbide heating element, mounted to either side of the specimen. Temperature feedback control was achieved using two R-type thermocouples, one for each half of the furnace. They extended slightly below the interior wall of the furnace, and were exposed to the heated air within the chamber. The furnace was controlled by two MTS model 409.83B temperature controllers, one for the left element, and one for the right element. To reduce heat loss from the furnace, the furnace insulation was carved to fit around the extensometer rods, and the inlet tube for the steam. Figure 13 shows a close-up of the furnace.
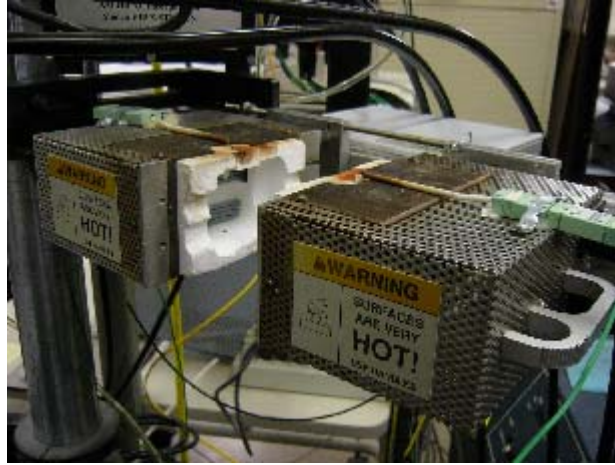
34

Figure 13: Furnace

The furnace was regularly calibrated using a specimen fitted with two S-type thermocouples, one on either side of the test section. The thermocouples had been fitted with sections of ceramic insulators to separate the wires, instead of one long piece - to increase their flexibility (to fit through the openings in the furnace). The thermocouples were glued to the specimen using Zircar High Temperature Alumina Cement, and set over a 24 hour period.

Tests in the steam environment required an alumina susceptor to maintain high humidity around the test section of the specimen. The furnace chamber was designed to fit around the susceptor, and the inlet tube for the steam. The susceptor consists of 6 parts; two halves of a tube, an end with holes for the extensometer, and end with a hole for the steam inlet tube, and two rings that fit over the chamber to keep it together. The susceptor is assembled around the specimen once the specimen is in the grips. The susceptor is approximately 56 mm long, with a 36 mm diameter. For purposes of this experiment, it was assumed that the use of the susceptor helped enable the 100% steam environment around the test section of the specimen. A schematic of the humid environment assembly is shown in Figure 14.
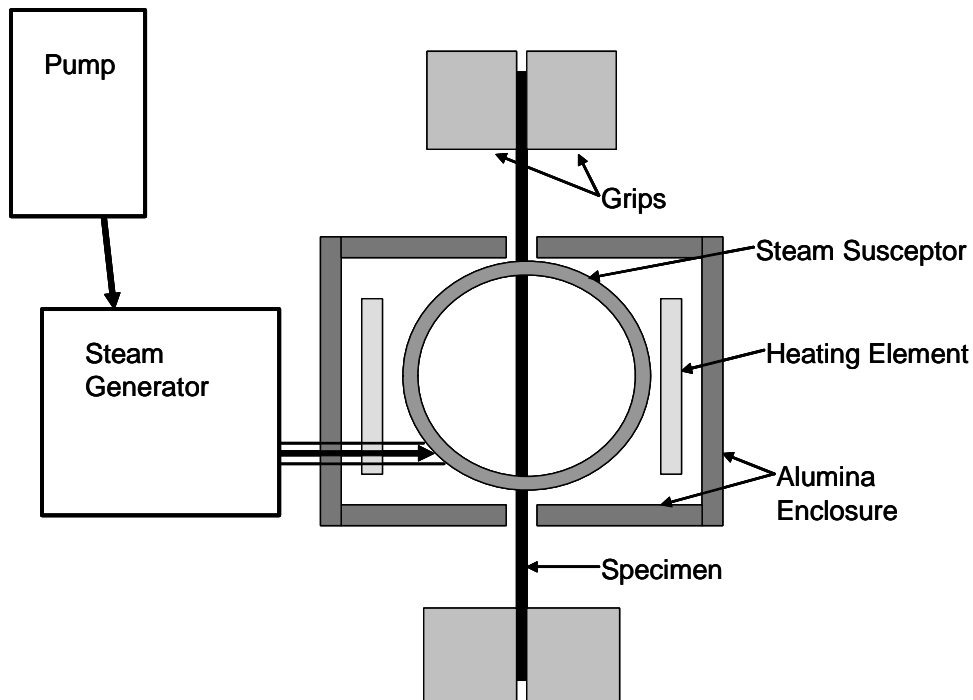
Figure 14: Schematic of the Heating Chamber with Susceptor

Two components were required to provide steam for the test, a water pump, and a steam heating unit. These components made up the AMTECO HRFS-STMGEN Steam Generation System. The unit pumped approximately 30 mL/h into the susceptor. The system used distilled water contained in a jug set above the testing unit. The water traveled first through the pump, then the steam heating unit, and from that unit through a ceramic feed tube into the susceptor. A slight positive pressure removed the dry air from the susceptor, and allowed for a 100% steam environment. Figure 15 shows the water pump and steam heating unit.

Figure 15: Water Pump and Steam Heating Unit

4.2 Test Procedures

This section discusses the temperature calibration for the specimens, and the preparation for the specimens and the equipment for the tests. It also describes the types of testing done.

4.2.1 Test Temperature

When testing a specific temperature, the ambient air temperature was not as important as the specimen temperature. It was important to calibrate the set-point for the furnace at each temperature tested to ensure the specimen was at the correct temperature. This was achieved by using the specimen outfitted with the thermocouples in the gage section, and a portable, two channel temperature sensor, the Omega Engineering, Inc. OMNI-CAL-8A-110. The temperature specimen was mounted in the grips under no

37

stress, and the thermocouples were attached to the temperature sensor, so each side of the specimen could be monitored. The MPT software was used to increase the temperature of the specimen to within 150 degrees of the desired temperature, then controlled manually until the correct specimen temperature was reached. The temperatures were set to within ± 10 degrees of the desired temperature. It was difficult to have the exact same temperature on both sides of the specimen, due to the differing conditions of the heating elements in each side of the furnace. Due to replacement of heating elements during the course of the tests, different calibration settings were used. Table 2 depicts one of the calibration settings.

Table 2: Temperature Controller Settings

Specimen Temp Left Side (°C)	Controller Setting Left Element (°C)	Specimen Temp Right Side (°C)	Controller Setting Right Element (°C)
400	403	400	408
750	335	750	653
950	834	950	824

4.2.2 Specimen and Equipment Preparation

When preparing to begin the testing for the thesis, all potential specimens were examined for any visible damage that may have occurred during processing and fabrication. The test section of each specimen was measured across the width and thickness, to determine the affected surface area. A Mitutoyo Corporation Digital Micrometer, model CD-S6"CT was used to measure the specimens. After each specimen was determined to be usable, and measured, fiberglass tabs were attached to each end of the specimen, on both sides. The tabs served to reduce the stress concentration on the

specimen ends induced by the grips. The tabs also protected the specimen from surface damage caused by the grips. The tabs consisted of a glass fabric/epoxy material. The tabs were glued to the specimen using M-Bond Catalyst. 3 drops were applied to each surface, and then pressure was applied for about a minute, to ensure good contact between the tab and the specimen. Figure 16 shows a tabbed specimen.

Figure 16: Tabbed Specimen

Before starting each test, the hydraulics in the machine were warmed up by using a function generator (a feature of the MTS system software) to cycle the actuator (lower grip) in a sinusoidal wave form. This typically ran for a half hour. After the hydraulics were warmed up, the actuator was returned to the zero position, and the specimen was mounted in the grips, making sure that the test section was perfectly perpendicular so that the extensometer would rest properly on the specimen. Then, for the humid condition tests, the susceptor was assembled around the specimen and the furnace closed around the susceptor. Because the susceptor fit over the entire specimen; if it were not supported, it would slide to the bottom of the specimen, the susceptor had to rest in the furnace. This later caused problems with extensometer readings, as the holes for the extensometer in the susceptor were not positioned perfectly. After the furnace was closed, the extensometer was attached, ensuring proper contact with both rods. One also had to be careful that the extensometer was not touching the susceptor or the extensometer mount, as this would prevent it from taking accurate readings.

For the non-room temperature tests, the temperature would be raised over a 25 minute period, and then allowed to equilibrate over 25 minutes. During the steam tests, the steam pump and generator would be turned on at the beginning of the test, and remained on for the duration of the test.

4.2.3 Monotonic Tensile tests

The monotonic tensile tests determined the ultimate tensile strength of the specimens at different temperatures. Due to a limited supply of specimens, and the fact that comparative data had been taken previously from specimens from the same panels as were used in this experiment, a monotonic tensile test was run at 400°C and 950°C, to compare results for the Young's Modulus. The ultimate tensile strength for the panels at room temperature was used as a normalization factor throughout the testing.

For both the monotonic and creep tests, data was collected for time, temperature of element 1, temperature of element 2, displacement, force control, force, and strain.

4.2.4 Creep-Rupture Tests

The creep test was the focus of this experiment. The tests were run under load control mode. Load was determined by using a percentage of the ultimate tensile strength of the specimen (at room temperature), and multiplying by the surface area of the gage section. Load was applied over a five minute period, during which data points were collected every half second so a more accurate Young's Modulus could be calculated. After this period, data was collected every minute.

The set run-out time for the tests was 100 hours. A long testing period was desired, to maximize the exposure of the specimens to the adverse environments. In those cases that the specimen did not fail during the specified testing time, a residual strength test

was performed, to determine the effect of the environment on the final strength of the material.

4.3   Test Summary

The following table (Table 3) presents a summary of all of the tests run during this experiment. A total of 17 specimens were tested.

Table 3: Test Summary

Panel	Specimen	Test Condition	Applied Stress (MPa)
3	13	400C Monotonic	333.96
2	8	100% humid 400C Creep	290.02
2	7	100% humid 400C Creep	254.65
2	13	100% humid 400C Creep	212.00
1		750C Monotonic	326.88
1	2	0.6 atm pH2O 750C Creep	259.04
1	3	0.6 atm pH2O 750C Creep	254.49
1	5	0.6 atm pH2O 750C Creep	218.42
2	9	100% humid 750C Creep	176.04
1	4	0.6 atm pH2O 750C Creep	206.42
6	7	950C Monotonic	309.43
2	10	100% humid 950C Creep	187.45
5	14	100% humid 950C Creep	167.30
5	9	100% humid 950C Creep	155.81
2	12	100% humid 950C Creep	120.00
3	13	400C Monotonic	333.96
5	11	Air 400C Creep	280.12
1		750C Monotonic	326.88
3	14	Air 750C Creep	251.69
5	13	Air 750C Creep	202.70
6	7	950C Monotonic	309.43
5	15	Air 950C Creep	206.20
3	7	Air 950C Creep	162.91

4.4   Post Failure Analysis

This section discusses the Scanning Electron Microscope (SEM) analysis performed on the failed specimens. Further analysis of SEM results is found in chapter V.

The Scanning Electron Microscope creates magnified images by using electrons instead of light waves. It can achieve higher magnifications and more detailed three-dimensional images than are possible with a light microscope (like the optical microscope. The images created without light waves are black and white. The sample is placed in an air-tight chamber, and the air is pumped out to create a vacuum. To create an image, an electron gun at the top of the column emits a beam of high energy electrons. The beam travels downward through a series of magnetic lenses designed to focus the beam to a very fine spot. A set of scanning coils cause the beam to move back and forth across the specimen, the speed of which is determined by the desired resolution. The higher the resolution, the slower the beam moves. As the electron beam hits each spot on the sample, secondary electrons are knocked loose from its surface. These electrons are counted by a detector, which then sends the signals to an amplifier. The final image is built up from the number of electrons emitted from each spot on the sample.

Analysis of the specimens under this microscopy showed physical changes in the fibers, matrix, and interface of each sample. It provided a way to compare the effects each environment had on the samples.

The SEM used to analyze the specimens for this experiment was a FEI FP 2011/11 Quanta 200 HV Scanning Electron Microscope shown in Figure 17. The SiC/SiC specimens were relatively good conductors, and while the pictures did show some charging in the specimen, the results were not distorted enough to require coating the specimens.

Figure 17: Scanning Electron Microscope

During the tests, as soon as a specimen would break, the lower part would be removed from the heat/humid environment due to the hydraulics shutting off. The upper part of the specimen was exposed to the heat and humidity until the steam generator was turned off, and the furnace cooled down. Analysis of the upper portion of the specimen would not be accurate, as it would be influenced by the excess exposure to the adverse environment, even though the sample was not under stress. For this reason, the specimens examined under the SEM were from the lower half of the sample. The fracture surface specimens were cut using a SHERLINE model 5410 with a full diamond saw blade approximately 6 mm away from the fracture surface and then mounted on silver SEM posts using conductive carbon paint. In the SEM, the samples were imaged at a 15-degree tilt to emphasize the fiber lengths and surface topography.

V. Results and Discussion

5.1 Experimental Results

This chapter will discuss the experimental results of this research. The scanning electron microscopic analysis done on the failed specimens is also presented.

5.1.1 Experiments

The stress rupture tests conducted in this research were a continuation of the work done by LaRochelle [4]. In his tests, he varied the moisture content level from 0.0, to 0.2, to 0.6 atm partial pressure of water vapor, pH_2O, at 550°C and 750°C. Both of these temperatures are within the intermediate temperature range. LaRochelle [4] conducted monotonic tension tests at room temperature to establish a baseline for comparison of data collected in the different moisture and temperature environments, and monotonic tests at 550°C and 750°C with the three moisture content levels. This research tested specimens at two moisture levels, ambient lab air, or 0.0 atm H_2O, and at 100% humidity, at three different temperatures, 400°C, 750°C, and 950°C. The results for the 750°C tests were comparable to the results obtained for LaRochelle [4] in his tests, and so the data of his 750°C tests were combined with the data for the current tests. Monotonic tension tests were performed for this research in laboratory air at 400°C and 950°C, while the monotonic test at 750°C in laboratory air was done in a previous study [4].

The monotonic uniaxial tension tests were performed by steadily increasing the load applied to a specimen over a short period of time. The load was applied parallel to the longitudinal direction of the specimen. Stress strain data was collected throughout the

44

entire test to measure the material properties of the specimens. The room temperature

tests provided baseline data to compare material properties across different panels, and

the ultimate stress and strain data for each panel. The room temperature ultimate tensile

strength was used to normalize the applied stress so that data obtained for specimens

from different panels could be compared, and to remove any scatter associated with

individual panel properties.

The procedure for the monotonic test consisted of loading the specimen at a rate of

3333 N per minute. Each panel displayed slightly different material properties due to the

inherent scatter introduced by the current manufacturing process of SiC/SiC CMCs, for

example fiber spacing and voids. To ensure that the variations in material properties were

acceptable when compared to the properties of previously produced specimens, one

specimen from each of the six panels was tested in a room temperature monotonic tension

test. Three of the specimens were tested by the NASA Glenn Research center, and three

were tested by LaRochelle [4]. As the specimens used in LaRochelle's [4] research and

the experiments presented here are from the same panels, they were assumed to have the

same material properties. Figure 18 is a plot of the stress strain curves for each of the six

panels.
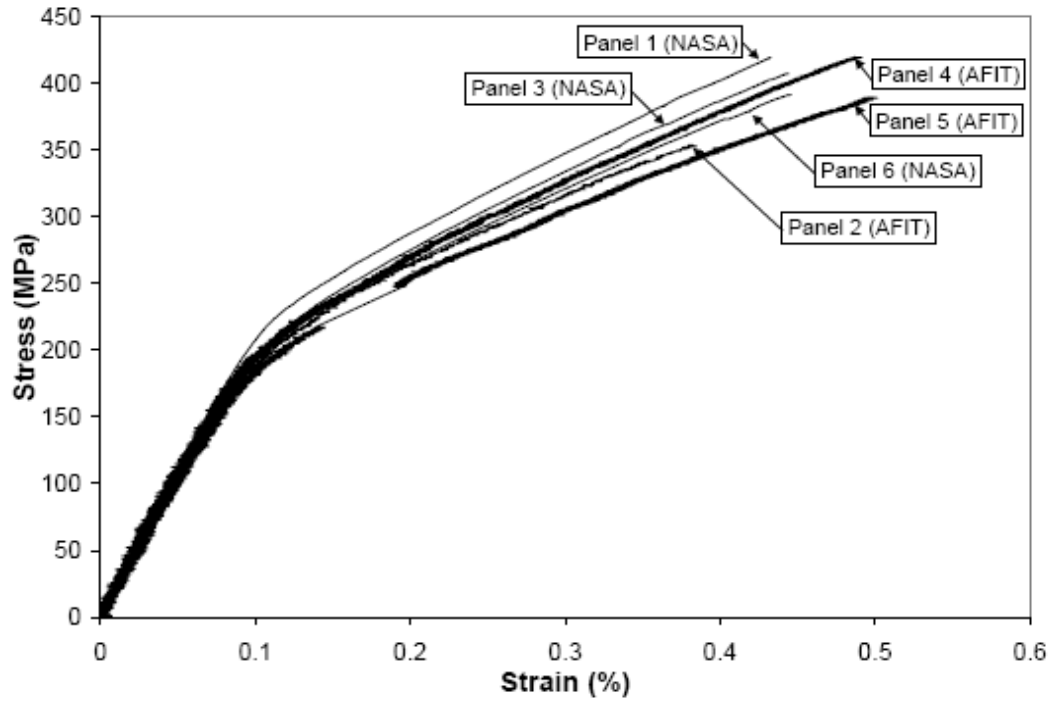
Figure 18: Stress Strain Curves for Six Panels [4]

LaRochelle [4] calculated the modulus of elasticity for the composite, the matrix, and the fibers using the rule of mixtures and measurements from Figure 18. This data is presented in Table 4, as well as the volume fraction (f), the ultimate strength (σ_{ult}), and ultimate strain (ε_{ult}) of each panel.

Table 4: Room Temperature Data - Monotonic Tests [4]

Panel Number	f (%)	σ_{ult} (MPa)	ε_{ult} (%)	E_c (GPa)	E_f (GPa)	E_m (GPa)
1	36.7	419.44	0.432	233	383	199
2	36.4	353.68	0.381	212	381	174
3	38.1	407.27	0.443	216	374	179
4	37.6	419.51	0.486	218	368	183
5	36.9	389.05	0.506	213	372	177
6	36.2	391.48	0.446	220	366	188
Average	37.0	396.74	0.449	219	374	183

LaRochelle [4] performed six monotonic tests at 0.0, 0.2, and 0.6 atm H_2O at 550°C and 750°C and found that the mechanical properties of the material are not affected by

the moisture in the environment in the elastic range. In this research, two monotonic tests were performed at 400°C and 950°C. A difference is not noted until the specimen is close to failure, and even then, the effect is mild. Figure 19 is a representative stress strain curve of the temperature effects on the properties of a specimen.
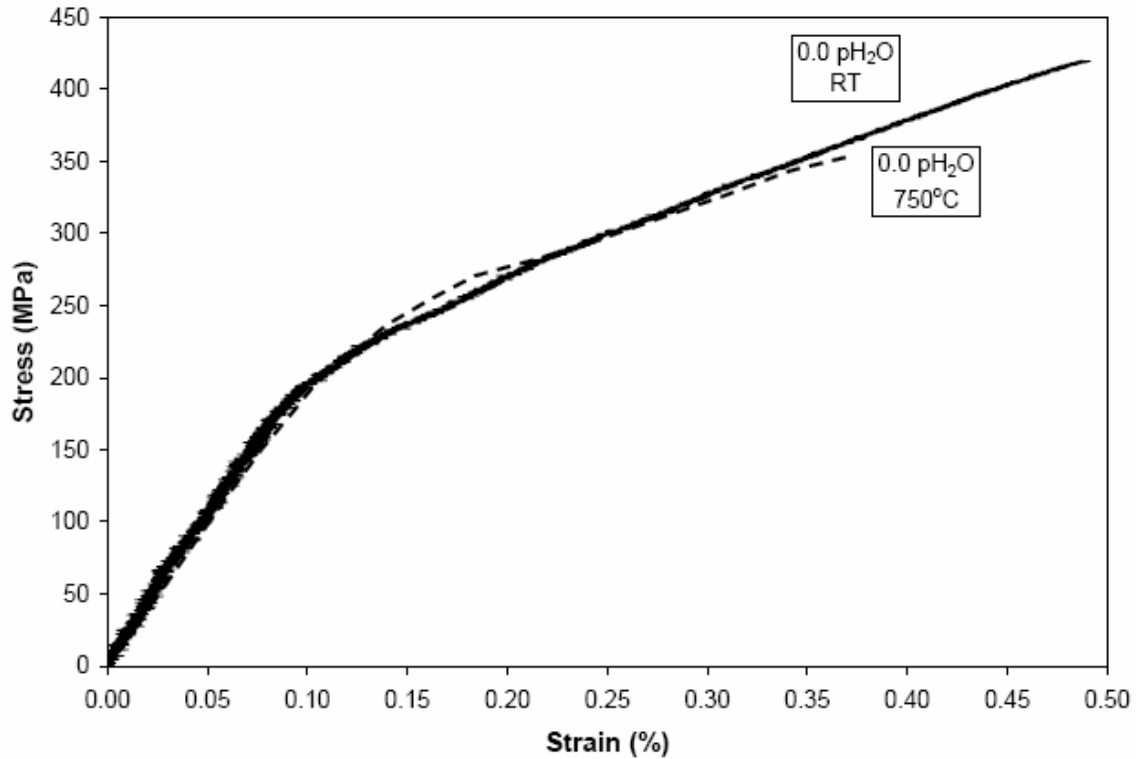
Figure 19: Temperature Effect on Stress Strain Curve [4]

Figure 20 depicts the effects of moisture on the mechanical properties of a specimen. In comparing Figure 19 to Figure 20, it is shown that the ultimate strength and failure strain reductions show no correlation with the moisture content level.
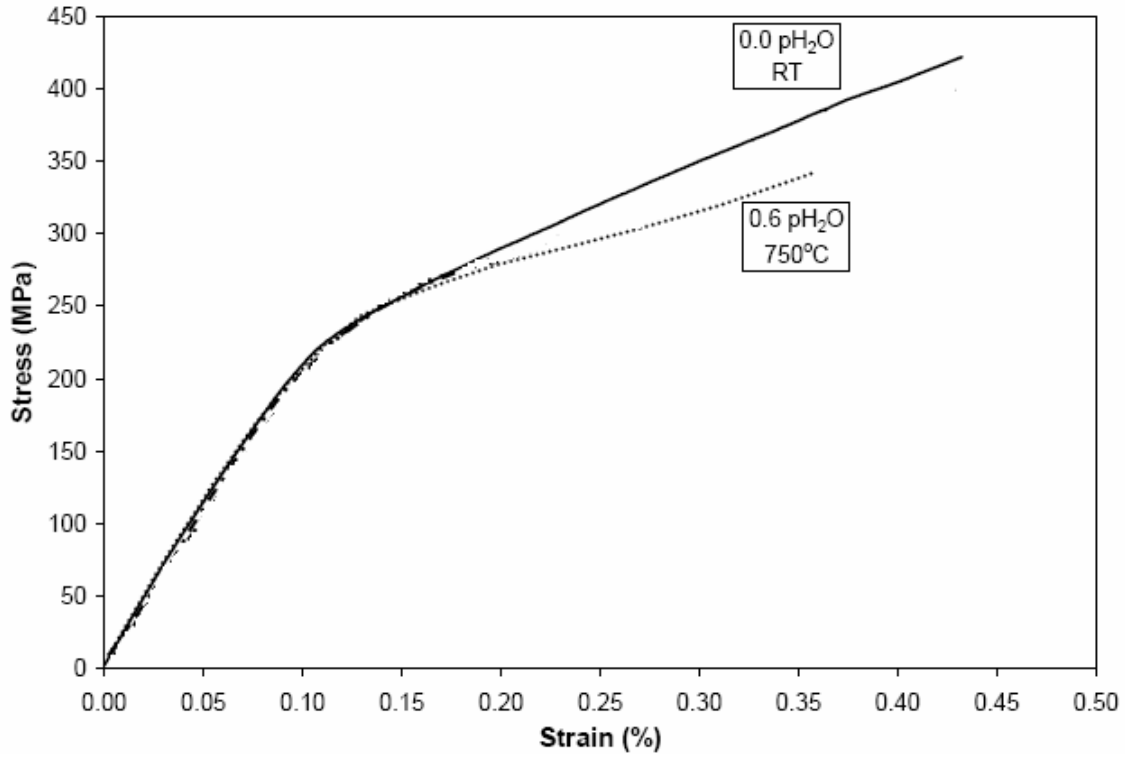
Figure 20: Moisture Effects on Stress Strain Curve [4]

Table 5 summarizes the normalized ultimate stress and ultimate strain values at 400,

750, and 950°C. Figure 21 and Figure 22 show the graphical representation of these

results. Figure 22 shows the data normalized with respect to each panel's room

temperature monotonic ultimate strength.

Table 5: Stress Strain Data – Environmental Monotonic Tests

Test Conditions	Young's Modulus (GPa)	Ultimate Strength (MPa)	Normalized w.r.t. RT σ_{ult} (MPa)	Room Temperature ε_{ult} (mm/mm)	ε_{ult} (mm/mm)
400°C	231	333.96	0.820	0.443	0.355
750°C	232	326.88	0.778	0.486	0.380
950°C	230	309.43	0.790	0.446	0.404
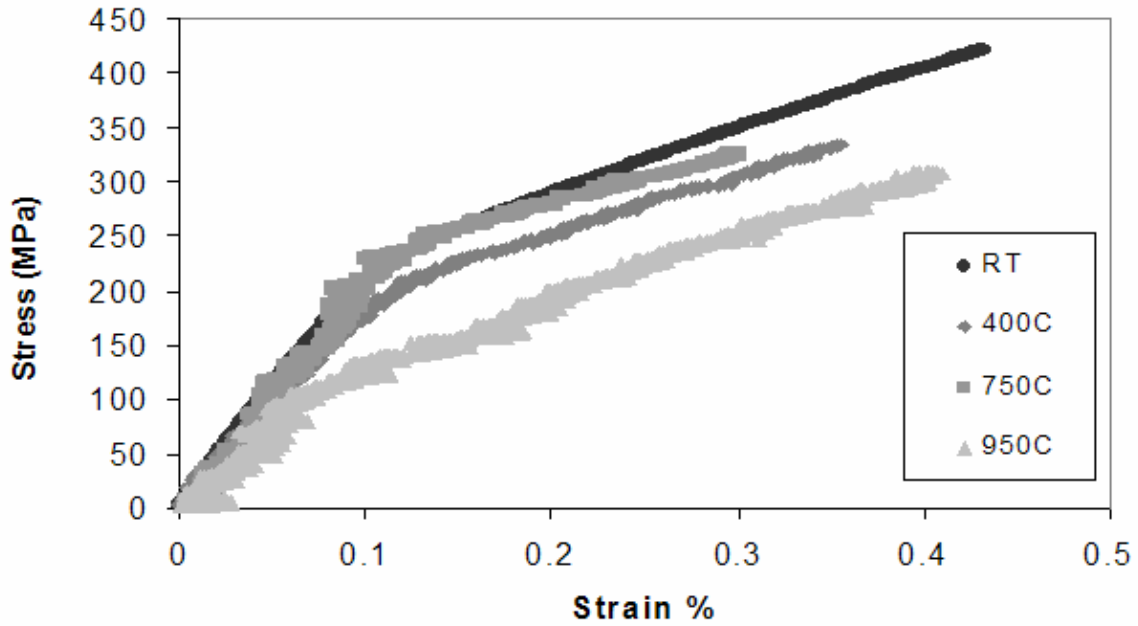
Figure 21: Environmental Monotonic Stress Strain Curves
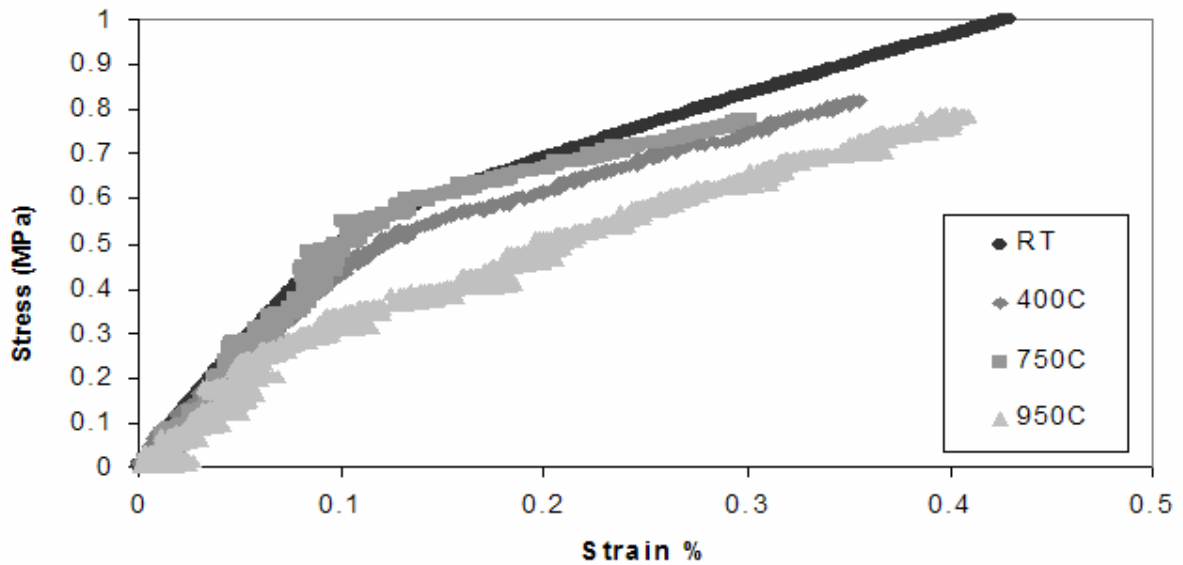
Figure 22: Environmental Monotonic Stress Strain Curves Normalized with respect to Room Temperature Ultimate Strength

A stress rupture tests consists of loading a specimen to a known load that produces

a desired stress in the test section based on the specimen's dimensions. Similar to a

monotonic tension test, the load is applied in the uniaxial direction parallel to the

longitudinal direction of the specimen and perpendicular to the transverse tows. This load

is held constant until the specimen fails, or until it reaches a predetermined end time. For these tests, the end time (run-out) was set to 100 hours, to allow the specimens sufficient time to be exposed to the environment, but also allow for enough tests to be run in order to collect usable data. Each stress rupture test provided stress-strain data, a fracture surface specimen, and provided applied stress versus failure time data. This data is important, as it shows how the environment affects the life of the composite.

The stress rupture tests consisted of allowing the specimen to reach the testing temperature, then applying the load to the desired amount over a period of five minutes, where it was maintained for the remainder of the test. This research collected data from fifteen stress rupture tests. Figure 23 summarizes the results of the stress rupture tests, including data from the monotonic tests, and from LaRochelle [4]. Open and closed symbols denote humid and dry conditions, respectively. The diamond, square, and triangle symbols represent 400°C, 750°C, and 950°C, respectively. The data points at 0 hours are the monotonic test results. The data points at 100 hours are the experiments where the specimen did not fail. Figure 24 and Figure 25 break down the results for the stress rupture tests into humid conditions and ambient air conditions.
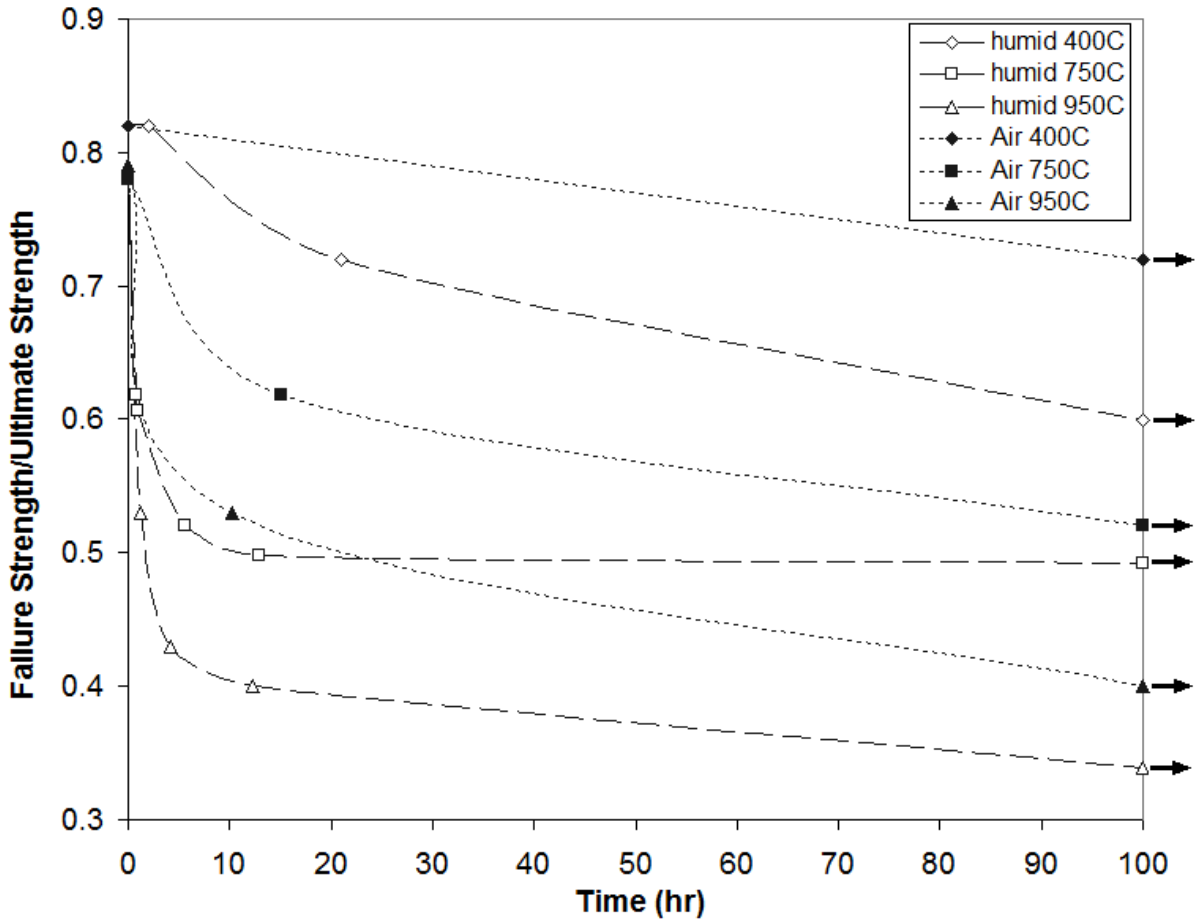
Figure 23: Stress Rupture Curves Normalized with respect to Room Temperature Strength

The degradation in strength due to increased temperature and moisture is apparent in the above figures. Due to variations in mechanical properties between panels, every attempt was made to use specimens from the same panels for the stress rupture tests. By normalizing the stress rupture curve by the individual panel's room temperature ultimate strengths, scatter caused by differences in panels was reduced. The normalized stress is the applied stress divided by the room temperature monotonic tensile ultimate strength for that panel. Table 6 presents the stress rupture data.

Table 6: Stress Rupture Data

Panel	Specimen	Test Condition	Applied Stress (MPa)	Normalized Stress (MPa)	Failure Time (hr)
3	13	400 C	333.96	0.820	0.00
2	8	100% humid 400 C	290.02	0.820	1.96
2	7	100% humid 400 C	254.65	0.720	21.02
2	13	100% humid 400 C	212.00	0.599	100.00
1		750 C	326.88	0.779	0.00
1	2	0.6 atm pH2O 750 C	259.04	0.618	0.78
1	3	0.6 atm pH2O 750 C	254.49	0.607	0.89
1	5	0.6 atm pH2O 750 C	218.42	0.521	5.64
2	9	100% humid 750 C	176.04	0.498	12.98
1	4	0.6 atm pH2O 750 C	206.42	0.492	100.00
6	7	950 C	309.43	0.790	0.00
2	10	100% humid 950 C	187.45	0.530	1.18
5	14	100% humid 950 C	167.30	0.430	4.20
5	9	100% humid 950 C	155.81	0.400	12.31
2	12	100% humid 950 C	120.00	0.339	100.00
3	13	400 C	333.96	0.820	0.00
5	11	Air 400 C	280.12	0.720	100.00
1		750 C	326.88	0.779	0.00
3	14	Air 750 C	251.69	0.618	15.10
5	13	Air 750 C	202.70	0.521	100.00
6	7	950 C	309.43	0.790	0.00
5	15	Air 950 C	206.20	0.530	10.20
3	7	Air 950 C	162.91	0.400	100.00

Normalizing the data by the room temperature ultimate tensile strength shows how the test environment affects the CMC life. The lines in the plots merely show the trend of the data, they are not curve fits. Due to the limited amount of specimens, there are not a lot of data points, so there is not much scatter in the plots. The majority of the data for the humid 750°C tests was from LaRochelle [4]. A test was run under humid conditions at 750°C to verify the assumption that the data from this test is comparable with the data from LaRochelle [4]. The data point obtained from this test fit the trend for the humid 750°C data. At times less than two hours, little distinction can be made in the data, as time progresses, the curves become distinct. It is apparent in Figure 23 that the data for humid and dry conditions show the same trends, although there is more strength degradation under humid conditions.
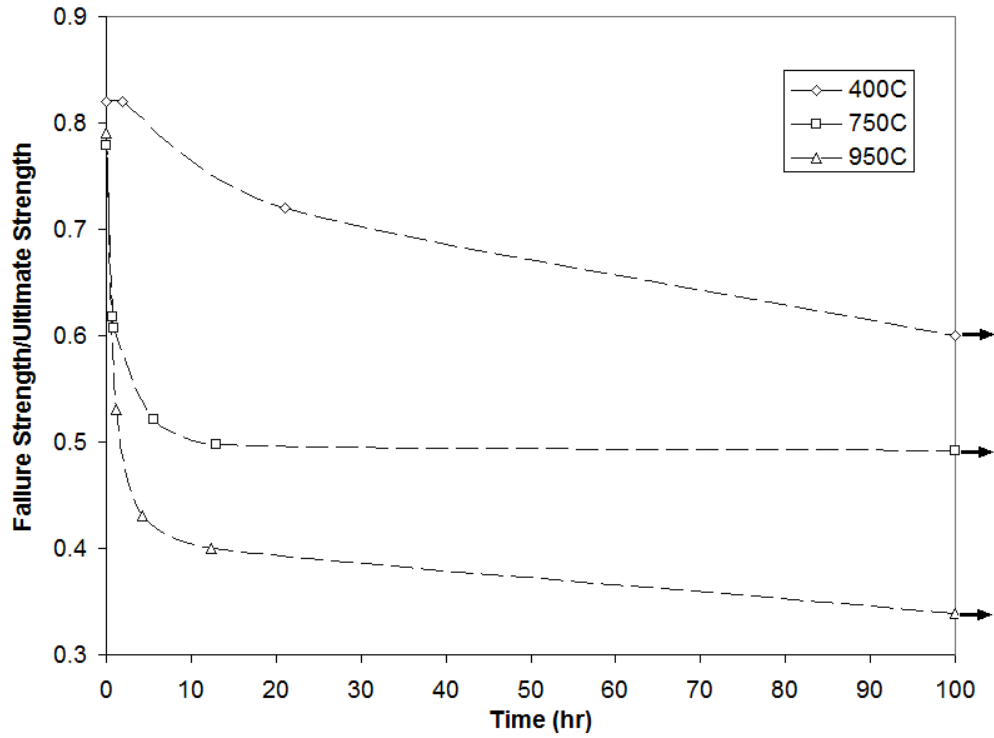
Figure 24: Stress Rupture Data for Humid Conditions Normalized with respect to Room Temperature Strength
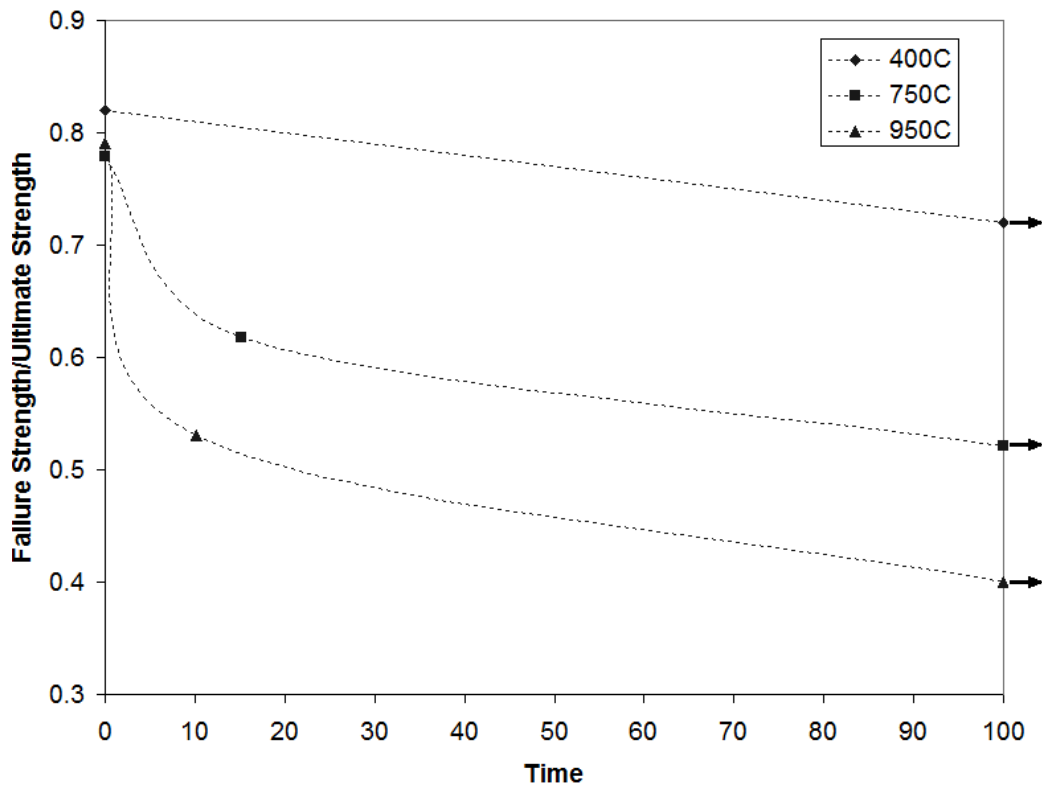
Figure 25: Stress Rupture Data for Ambient Air Conditions Normalized with respect to Room Temperature Strength
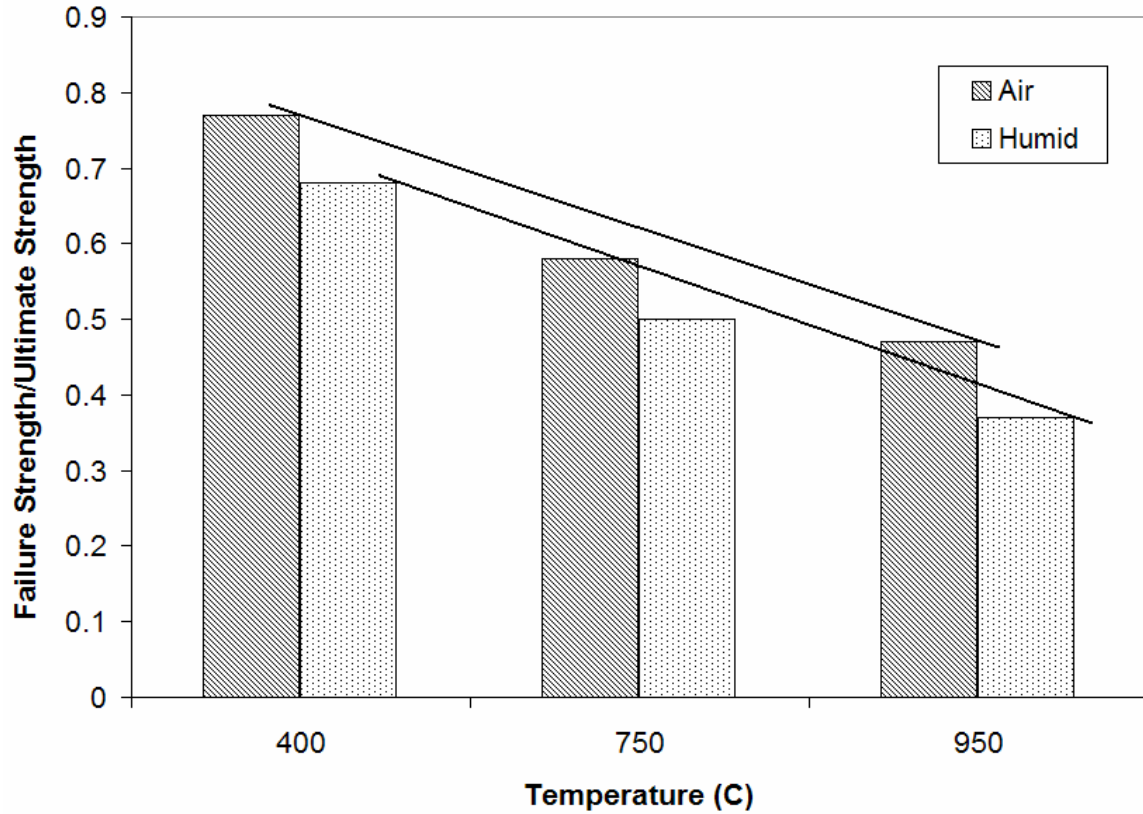
Figure 26: Normalized Failure Stress at 50 hours Estimated from Normalized Stress vs. Time Curves

Figure 26 compares the estimated normalized failure strengths at the different environmental conditions. Table 7 shows these values. Like Figure 2, Figure 26 shows poorer performance in the intermediate range.

Table 7: Estimated Normalized Failure Strength at 50 hours

Temperature (°C)	Normalized Stress with respect to Room Temperature UTS		Ratio Humid/Air
	Humid	Air	
400	0.68	0.77	0.88
750	0.50	0.58	0.86
950	0.37	0.47	0.73

Residual strength tests were run on the samples that did not fail in the stress rupture tests. The results are listed in Table 8. Figure 27 and Figure 28 show the trends for the residual strength tests.

54

Table 8: Residual Strength Data

Specimen	Test Conditions	Normalized Applied Stress (MPa)	RT Ultimate Tensile Strength (MPa)	Residual Strength (MPa)	% of Initial Strength
002-13	Humid – 400°C	0.599	353.68	328.25	0.928
001-04	60% pH$_2$O – 750°C	0.492	419.44	158.02	0.377
002-12	Humid – 950°C	0.339	353.68	303.96	0.859
005-11	Air – 400°C	0.720	389.05	402.08	1.03
005-13	Air – 750°C	0.521	389.05	224.39	0.577
003-07	Air – 950°C	0.400	407.27	310.78	0.763

One can see that the residual strength performance is much worse for the intermediate ranges, both in air and humid conditions. The high percentage of residual strength for the humid tests can be attributed to the low value for the room temperature strength. As one can see in Table 4, it is much lower than the ultimate strengths of the other panels. The increase in the ultimate tensile strength in the 400°C test can be attributed to scatter.
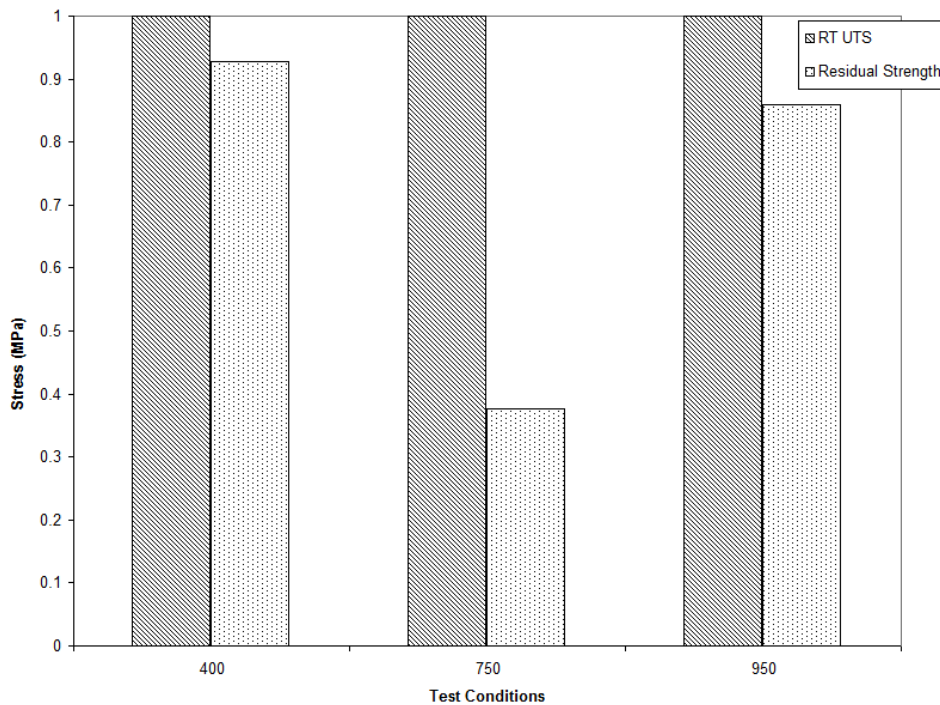
Figure 27: Humid Test Residual Strength with respect to Room Temperature Ultimate Strength
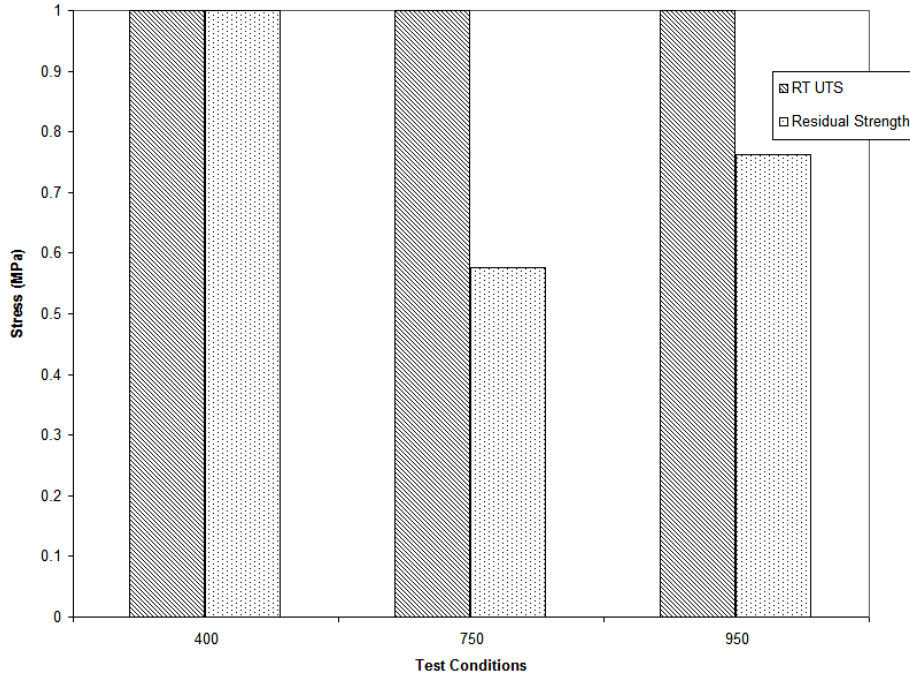
Figure 28: Residual Strength in Air with respect to Room Temperature Ultimate Strength

5.1.2 Scanning Electron Microscope

Scanning electron microscopy shows the physical characteristics of a fracture

surface using very high magnifications. A systematic approach was used to compare the

failure mechanisms of the damaged specimens. A specimen that failed in a pristine

environment, at room temperature and ambient air conditions, was used as a basis for

comparison with specimens that had failed in the various environmental conditions.

Images for this specimen were obtained from LaRochelle [4]. Analysis of these images

provides a better understanding of the instruments of failure under high humidity and

high temperature conditions.

Each specimen had approximately 25 SEM pictures taken using the following

magnifications: 3 at 50x, 5 at 100x, 6 at 1000x, 6 at 3000x, and 6 at 8000x. These levels

of magnification were chosen so a better comparison could be made between the images

from this study and those from LaRochelle [4]. LaRochelle used images at a

magnification of 30x which will be compared to the 50x images. The 50x images give good overall views of the topography of the specimen, and the general appearance of the fracture surface. The 100x images show the fracture surfaces of the tows, and tow failure characteristics. The 1000x images show interactions of large groups of fibers in a tow. The 3000x images show interactions of a small group of fibers, and 8000x images show fiber-to-fiber interactions [4]. The micron bars in the lower right corner of the images show values of 2mm, 1mm, 100 µm, 20 µm, and 10 µm for the 50x, 100x, 1000x, 3000x, and 8000x, respectively, for this study. For the pictures from LaRochelle [4], the micron bars read: 800, 200, 20, 8, and 2 µm for 30x, 100x, 1000x, 3000x, and 8000x, respectively.

In discussing the SEM analysis the terms used to describe the constituents of the CMC are SiC fibers, the CVI SiC layer, the MI SiC matrix, and the BN interphase. Figure 29 shows these constituents. Each fracture surface has a different appearance: the MI SiC has a random orientation around the fibers, while the CVI SiC seems to radiate out from each fiber with a fairly consistent thickness, the fibers fracture mostly flat and smooth.
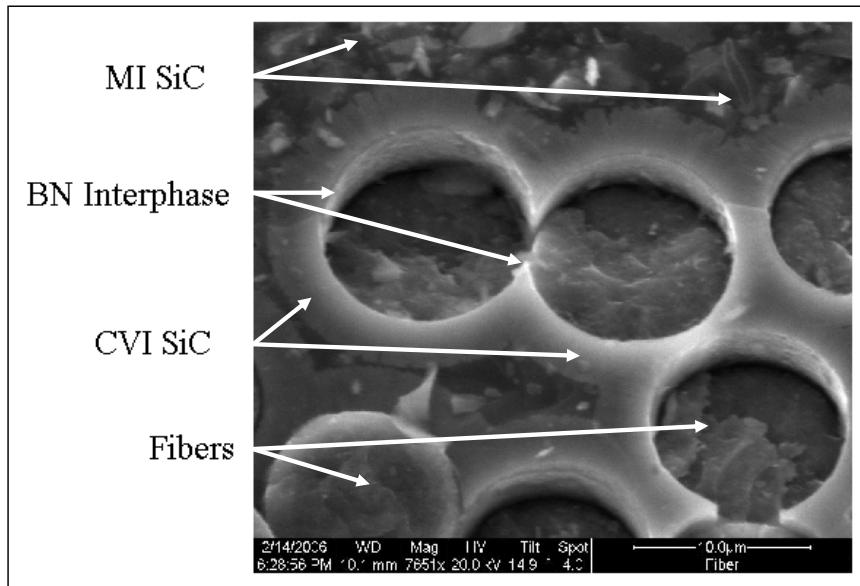
Figure 29: CMC Constituents

Figure 30 demonstrates fiber pullout. The fiber that "pulls out" of the matrix is one that has separated from the interphase, and so diverted a crack until the fiber finally failed. Figure 31 demonstrates fiber debonding, with interior debonding happening when the interphase remains with the matrix, and exterior debonding, when the interphase remains on the fiber.
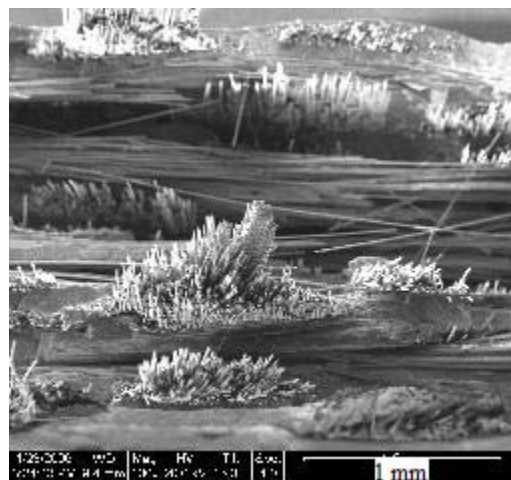
Figure 30: Fiber Pullout
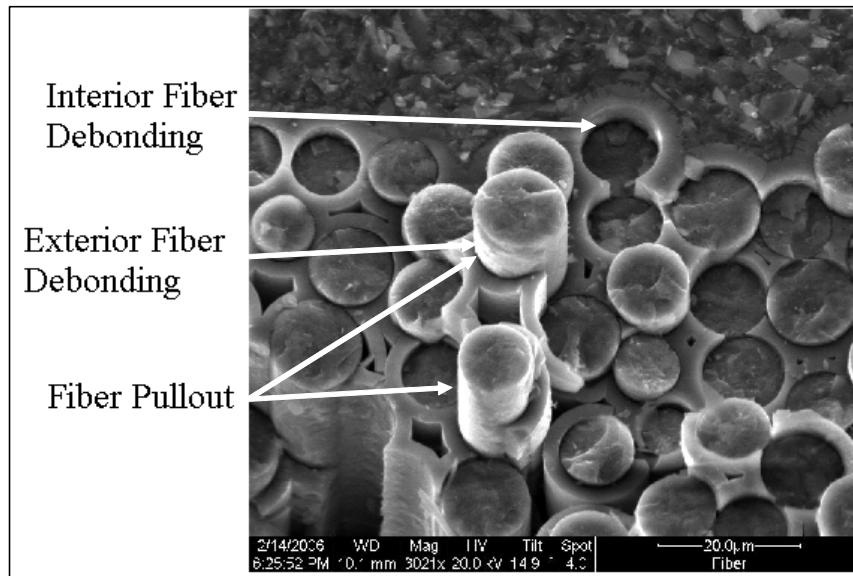
Figure 31: Fiber Debonding

The final terms that will be used in discussing the SEM analysis are puddling and

pesting. Puddling and pesting are results of embrittlement. Puddling is when massive BN

oxidation occurs, resulting in boria [4]. Pesting of the fibers is the effect of the

embrittlement, when the liquid borosilicate solidifies into a silicate glass, bonding the

fibers to each other and to the matrix. This prevents the fiber from slipping from the

matrix to distribute stress and prevent crack propagation, resulting in the crack continuing

across the solidified bundle of fibers. Figure 32 [4] shows puddling and pesting,

respectively
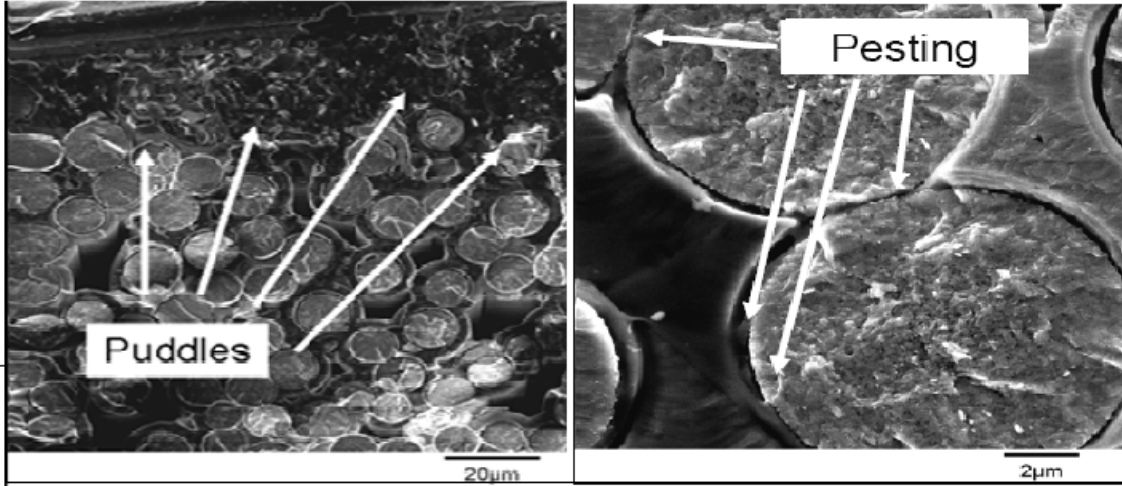
Figure 32: Embrittlement Features: Puddles and Pesting

The following figures compare the room temperature specimens from the previous study [4] with the 400°C monotonic test specimen from the current study. The similarity in the images shows that at low temperatures, the damage mechanisms are comparable to those at room temperature.
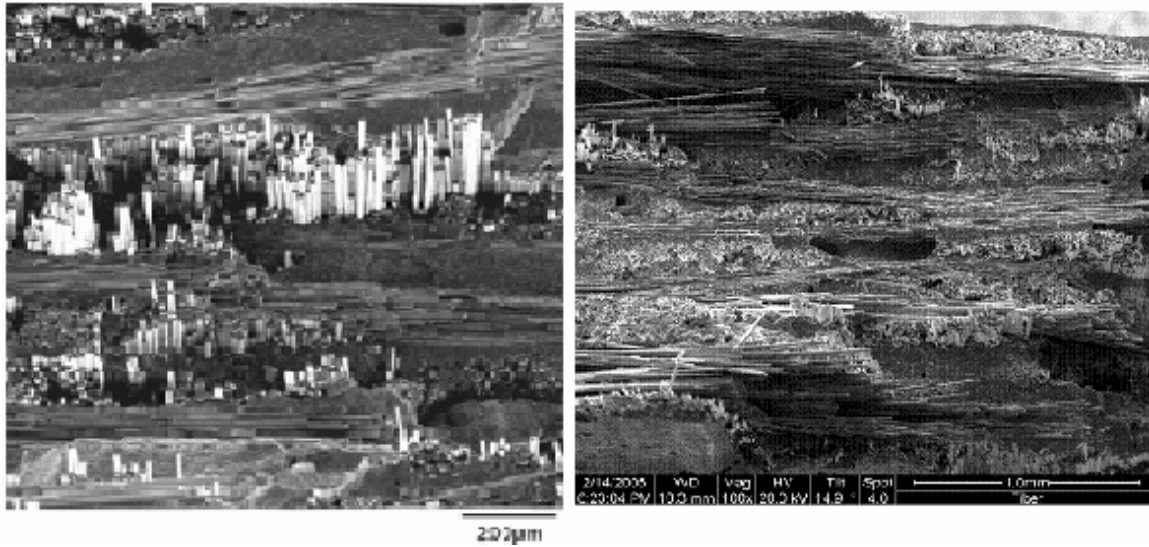
Figure 33: Fracture Surface Comparison - Room Temperature vs. 400°C - 100x
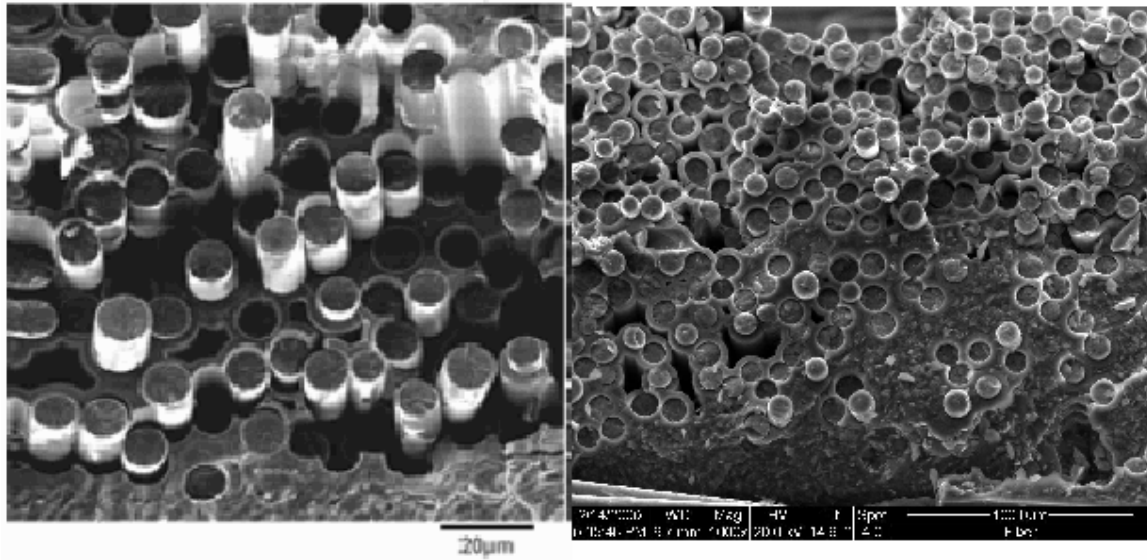
Figure 34: Fracture Surface Comparison - Room Temperature vs. 400°C - 1000x
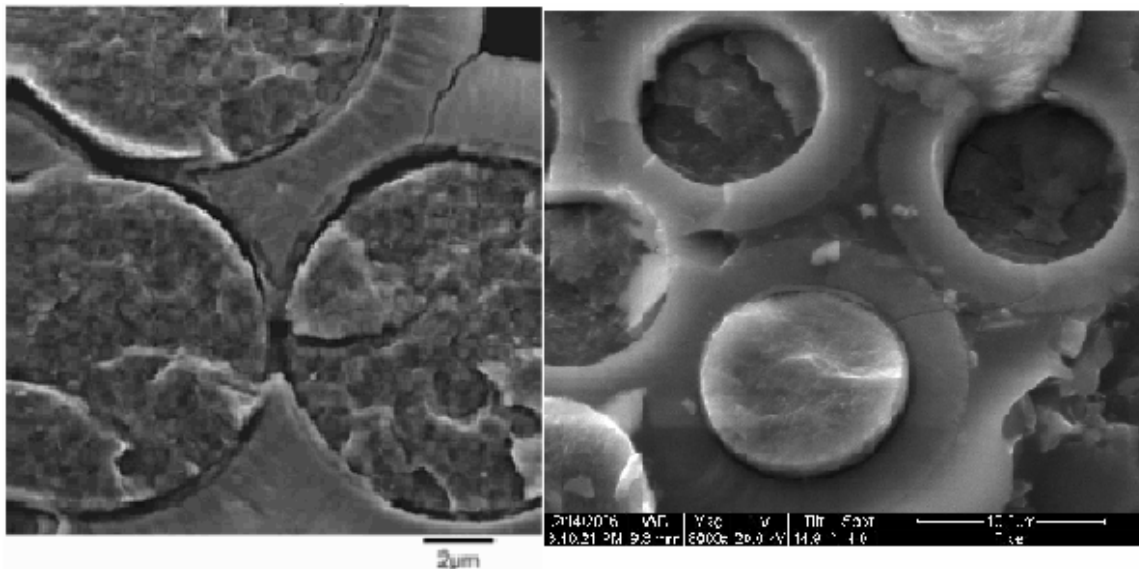
Figure 35: Fracture Surface Comparison - Room Temperature vs. 400°C - 8000x

The stress rupture tests in this study were conducted under humid and dry conditions at 400°C, 750°C, and 950°C. The effect of temperature and moisture on these specimens is shown in the SEM images of the fracture surfaces. The images from humid, or 100% humidity, tests are from the current study.

Tests at 400°C

The first analysis is of the tests run at 400°C (Figure 36 through Figure 45). The initials MT in the figures indicate a monotonic test. The initials RS in Figure 36 mean that the fracture surface is the result of a test run out in the environmental condition followed by a residual strength test. Comparison of the fiber pullout lengths of the different samples does not show much variation. At 50x, the samples seem to have very similar pullout, both in humid and air tests.
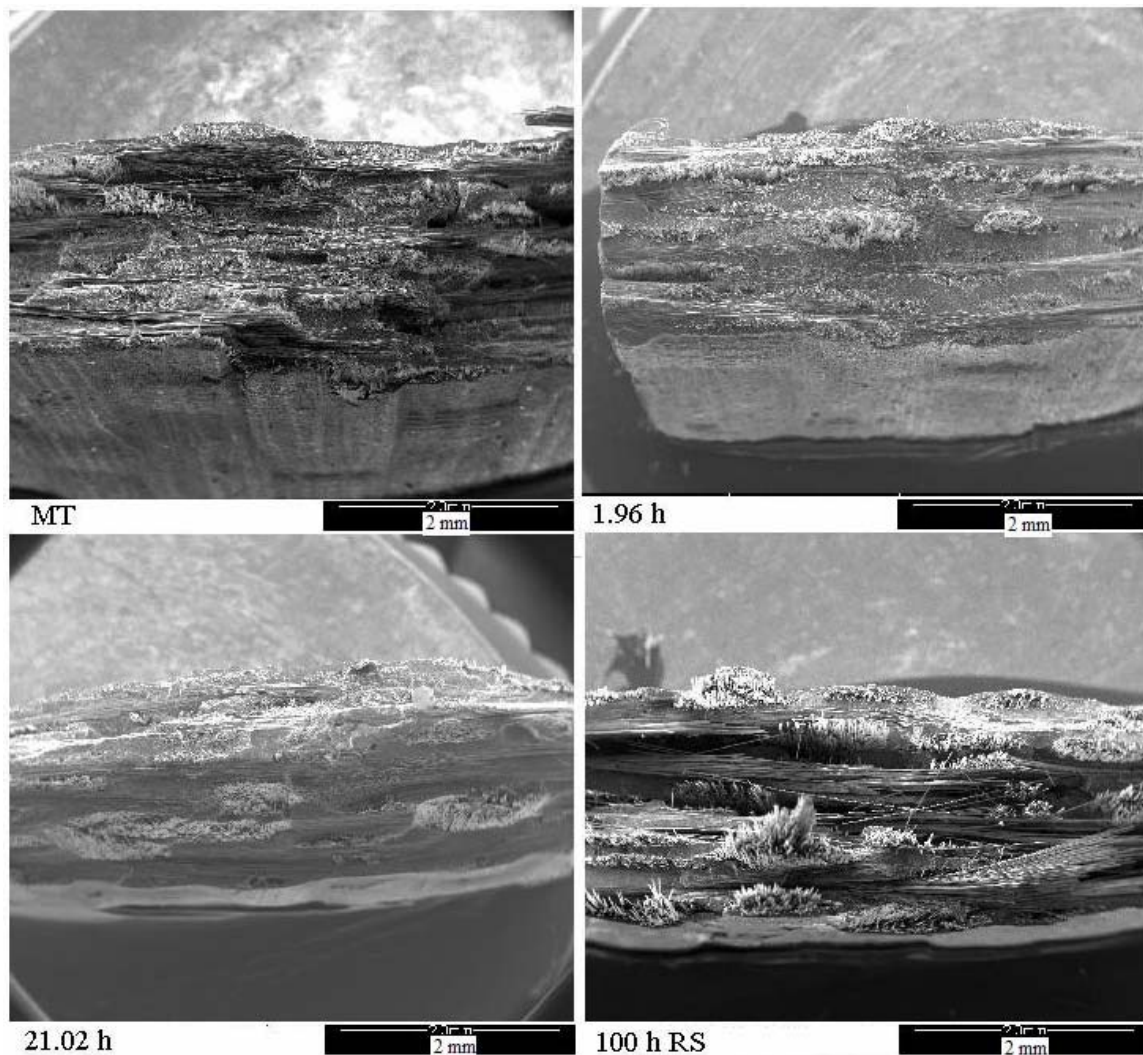
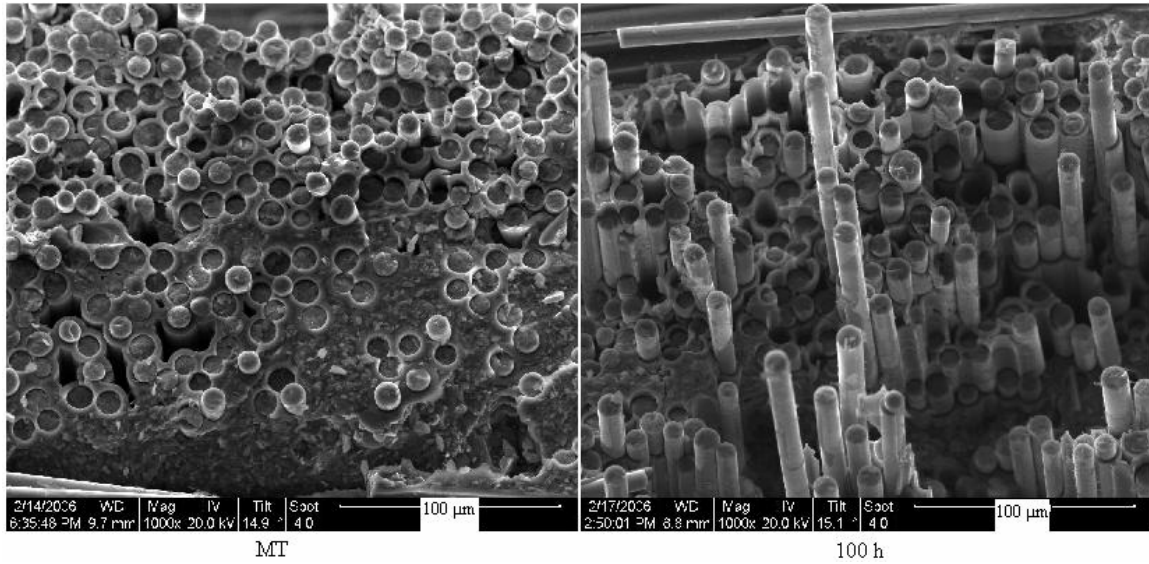**Figure 36: Stress Rupture Tests - Humid Conditions 400°C - 50x**
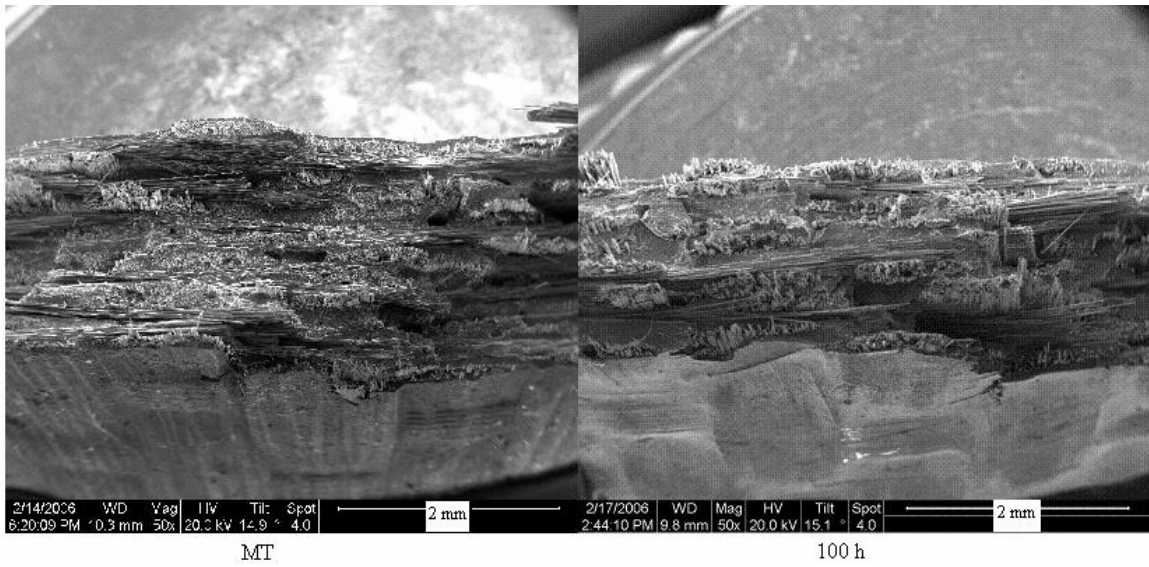
Figure 37: Stress Rupture Test - Ambient Air - 400°C - 50x
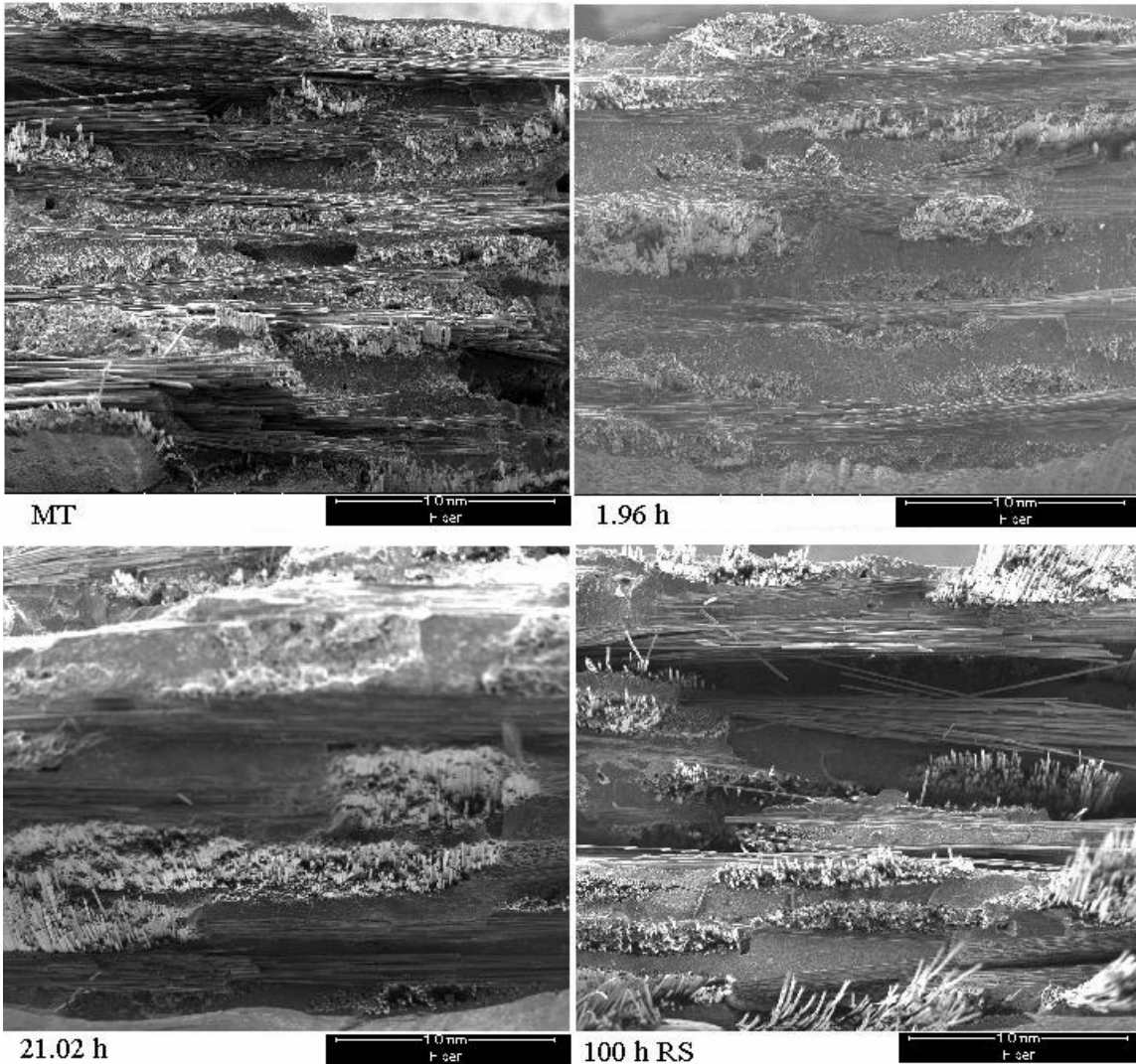
Figure 38: Stress Rupture Test - Humid Conditions - 400°C - 100x

The 100x images still maintain a consistent fiber pullout length between the specimens. Within each specimen there is a wide range of pullout lengths, but similar pullout lengths in tows. The residual strength specimen has a rather brushy appearance compared to the other three samples. The images (Figure 38 and Figure 39) from the ambient air and moisture tests are similar in appearance.
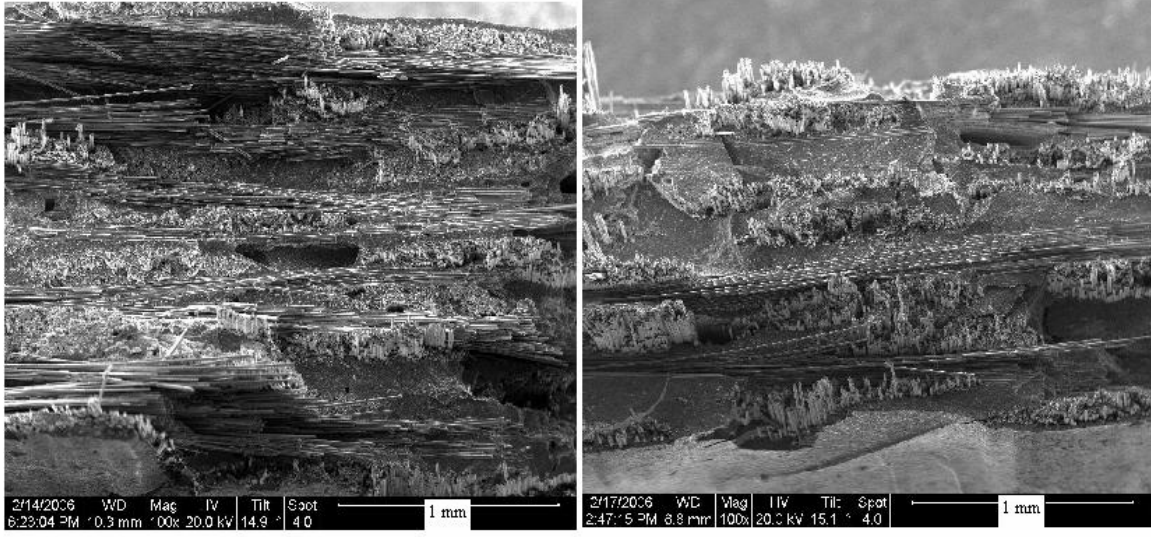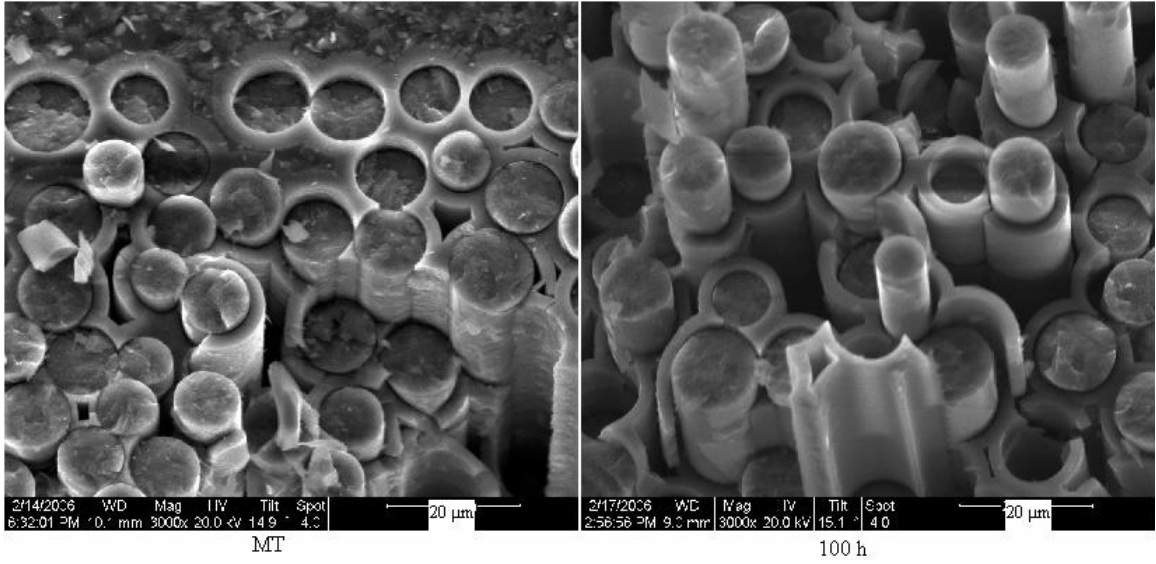
Figure 39: Stress Rupture Test - Ambient Air - 400°C - 100x
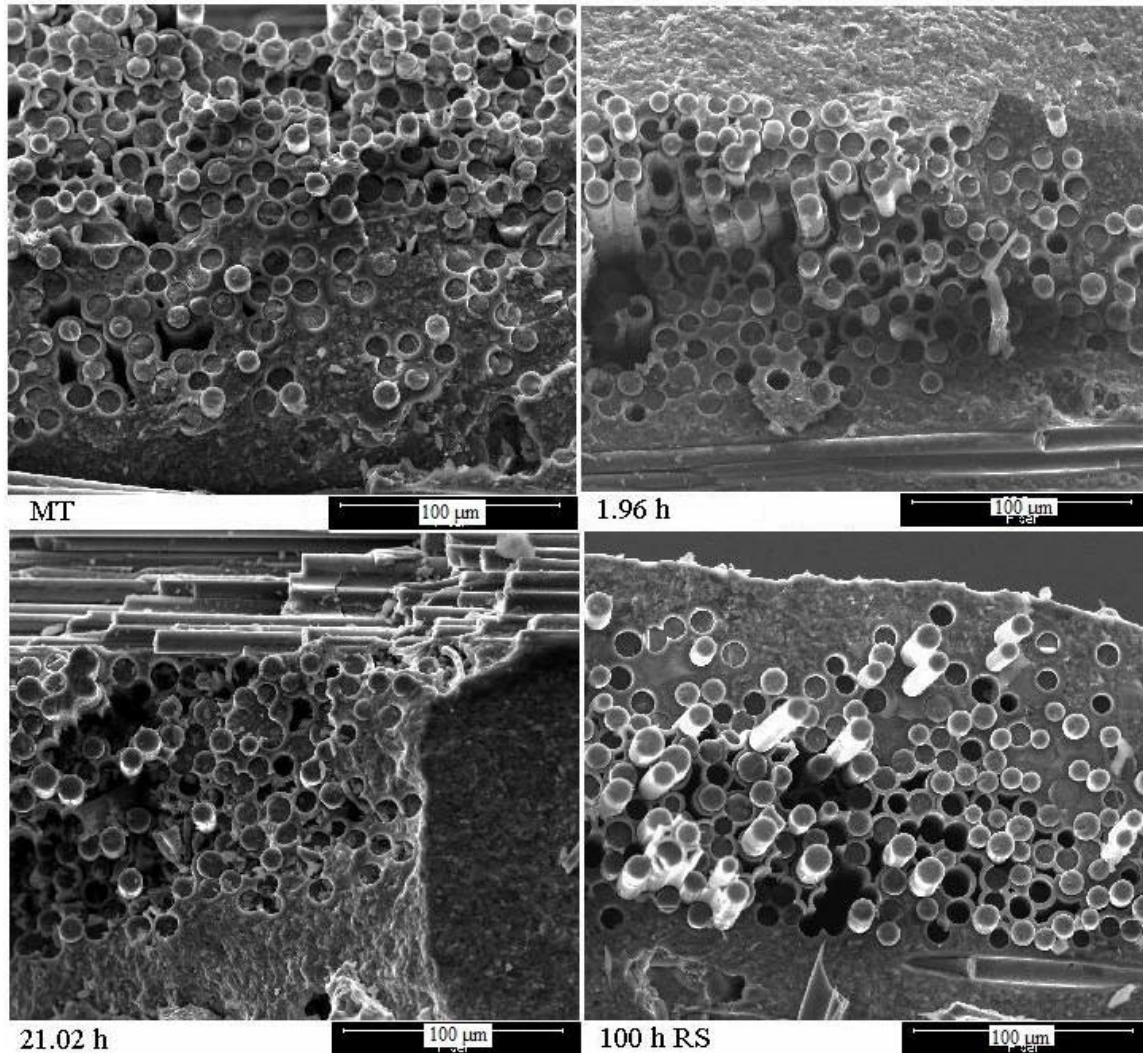
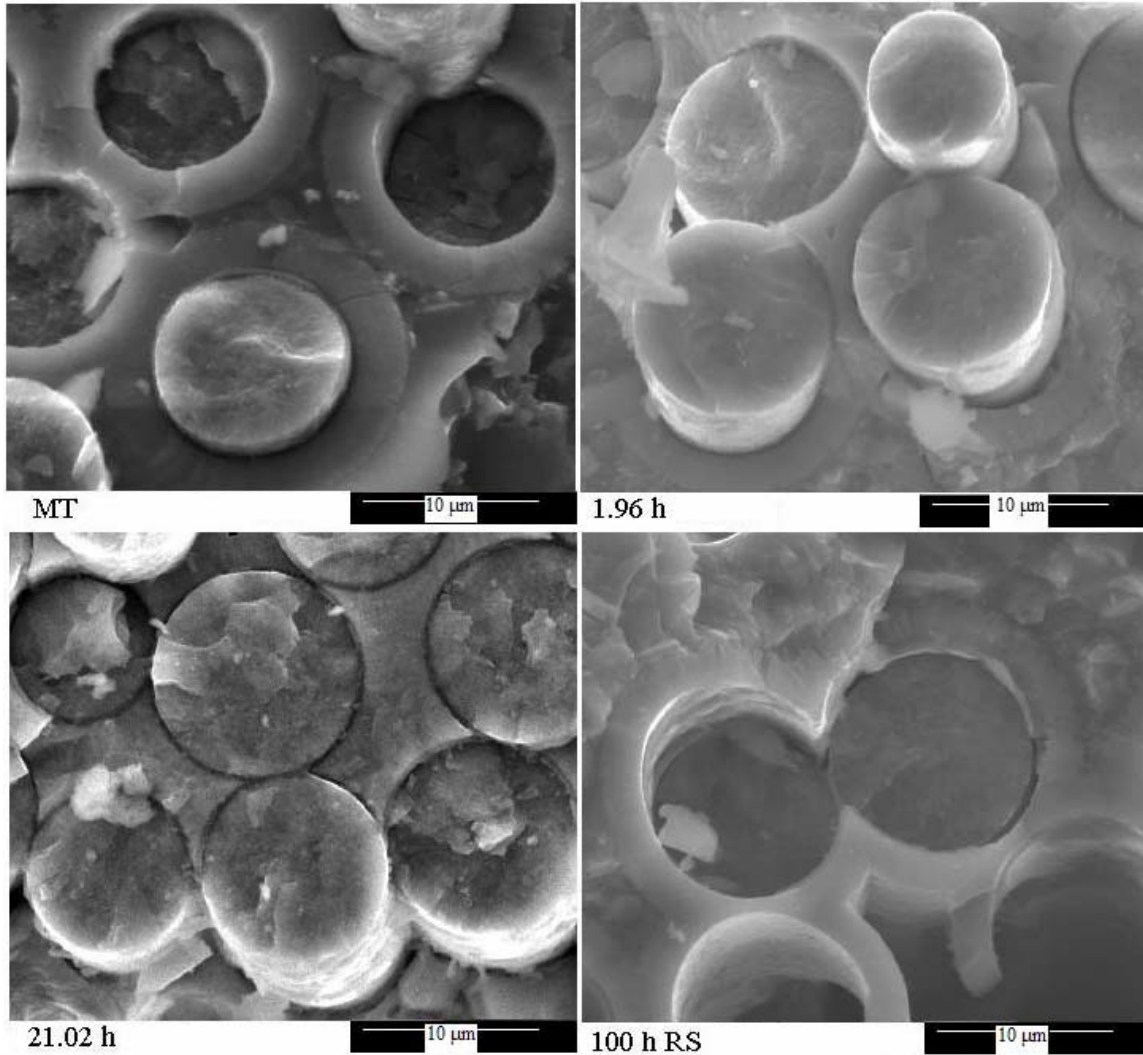**Figure 40: Stress Rupture Test - Humid Conditions - 400°C - 1000x**

Comparison of the 1000x images in Figure 40 and Figure 41 show that the fibers are experiencing interior and exterior debonding. The fibers are failing at different lengths, and there is no evidence of puddling.

Figure 41: Stress Rupture Test - Ambient Air - 400°C - 1000x
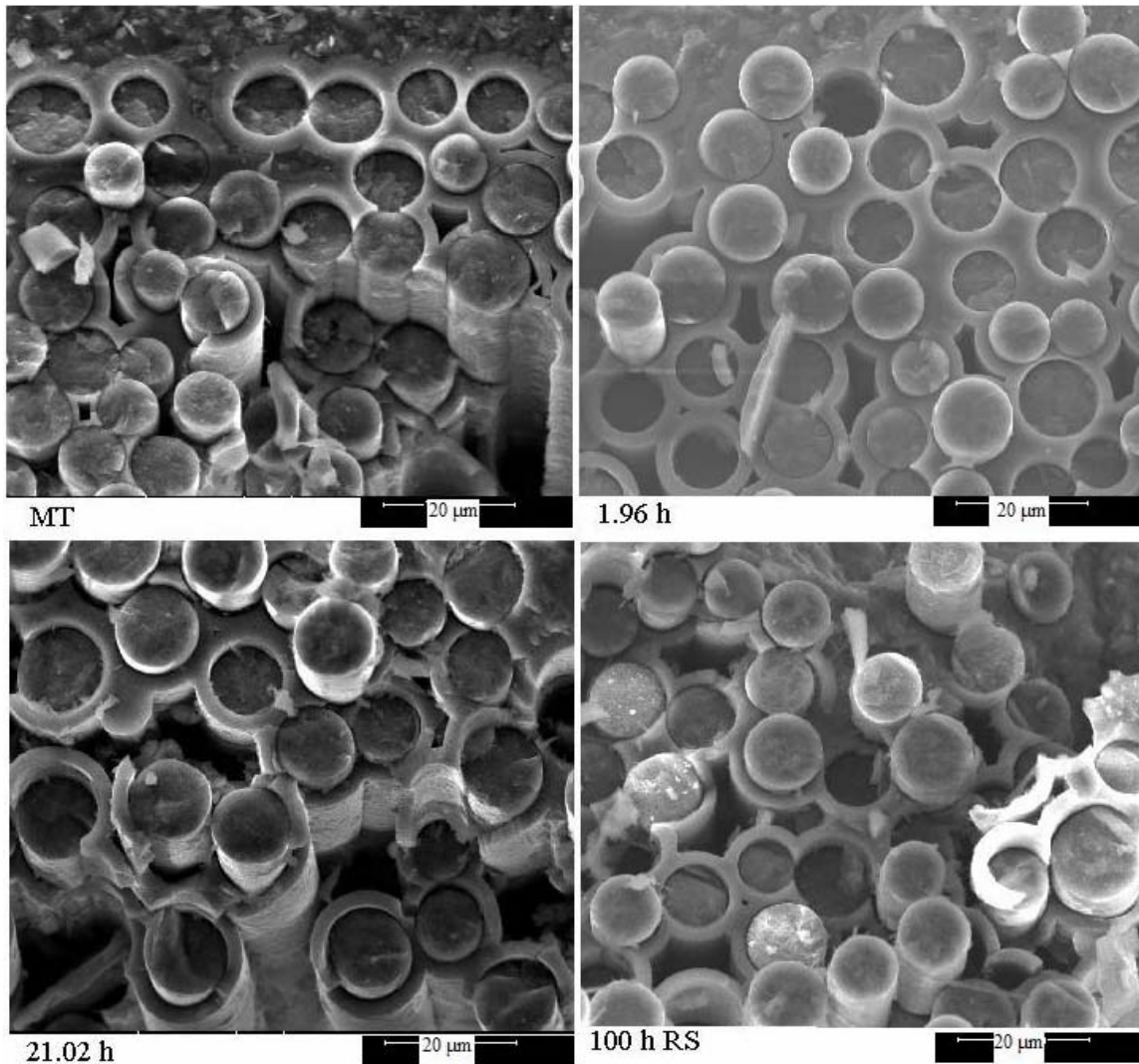
Figure 42: Stress Rupture Tests - Humid Conditions - 400°C - 3000x

Comparisons of the 3000x images in Figure 42 and Figure 43 show that at all times the BN layer is distinguishable from the fiber and the CVI SiC, that the fibers experience both interior and exterior debonding. It also shows that nearest neighbor fibers fail at different fiber locations.

Figure 43: Stress Rupture Test - Ambient Air - 400°C - 3000x

Figure 44: Stress Rupture Tests - Humid Conditions - 400°C - 8000x

Comparisons of the 8000x images in Figure 44 and Figure 45 show no distinguishable characteristics between the room temperature monotonic test and the tests run at 400°C, both humid and air. However, the brittle fracture of the matrix, fiber, and interphase is obvious.
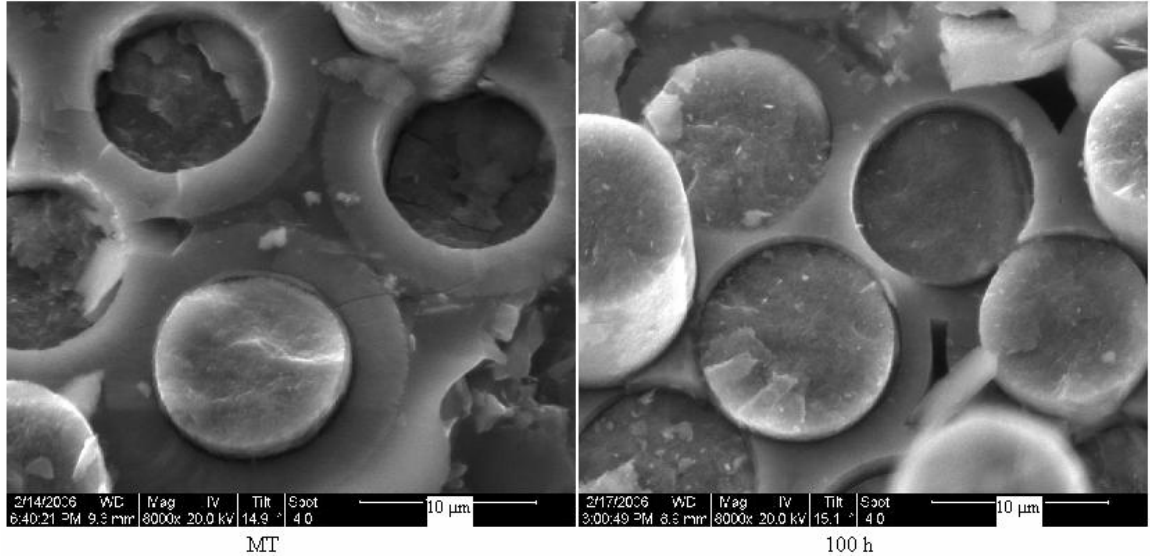
Figure 45: Stress Rupture Test - Ambient Air - 400°C - 8000x

The results from the 400°C test were as expected. There was little effect from moisture below the intermediate temperature range. Embrittlement did not seem to occur at this temperature.

Tests at 750°C

The second analysis is of the tests run at 750°C, in the intermediate range. Images for the 750°C monotonic test sample were obtained from LaRochelle [4], and used in combination with 100% humid tests conducted in this study, and with tests run in air (Figure 46 through Figure 55). They all show that the variability of the fiber pullout lengths decreases as the failure time increases, as the specimens spend more time exposed to the environment.
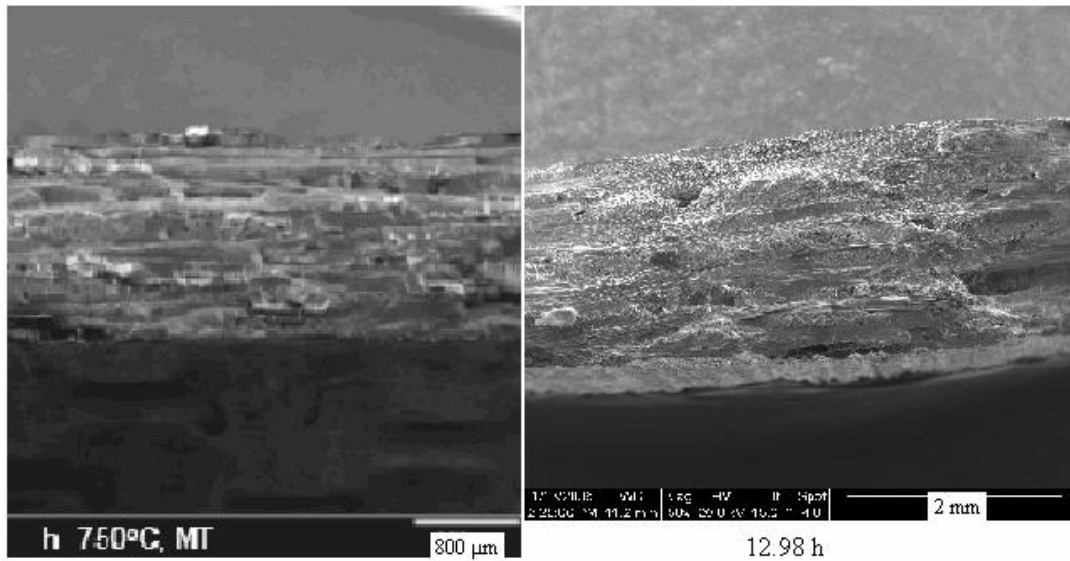
Figure 46: Stress Rupture Test - Humid Environment - 750°C – 30x and 50x

At 50x, in humid conditions and in air, the fracture surfaces appear relatively smooth, with little fiber pullout. However, the specimens tested in air have more pullout than the humid test specimens.
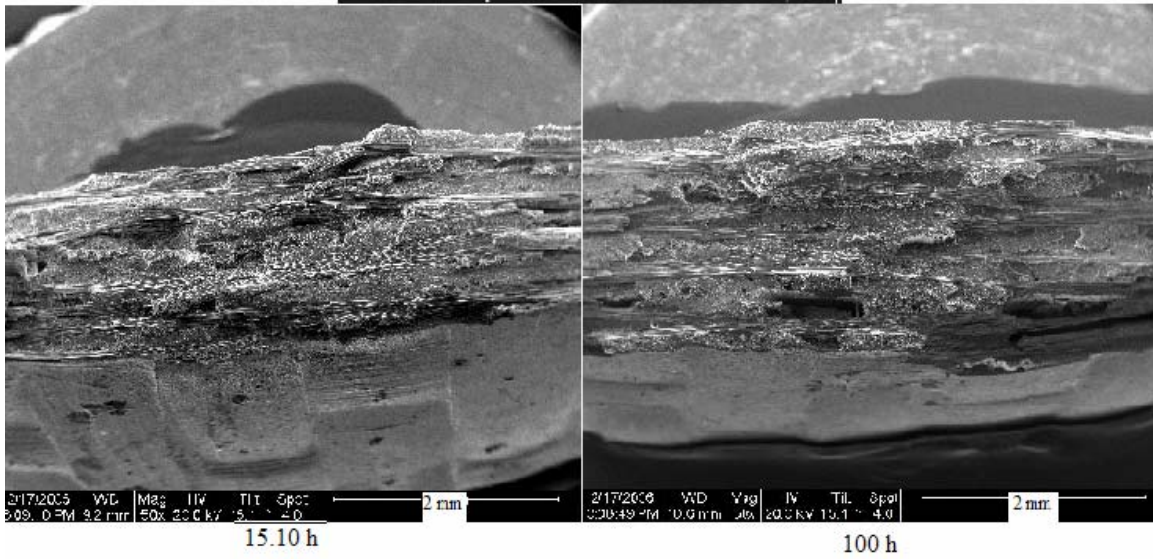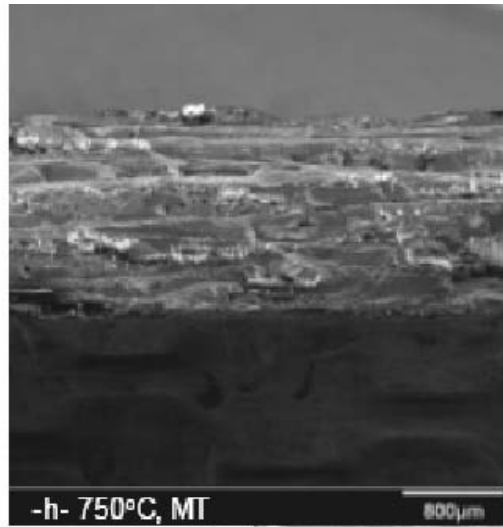
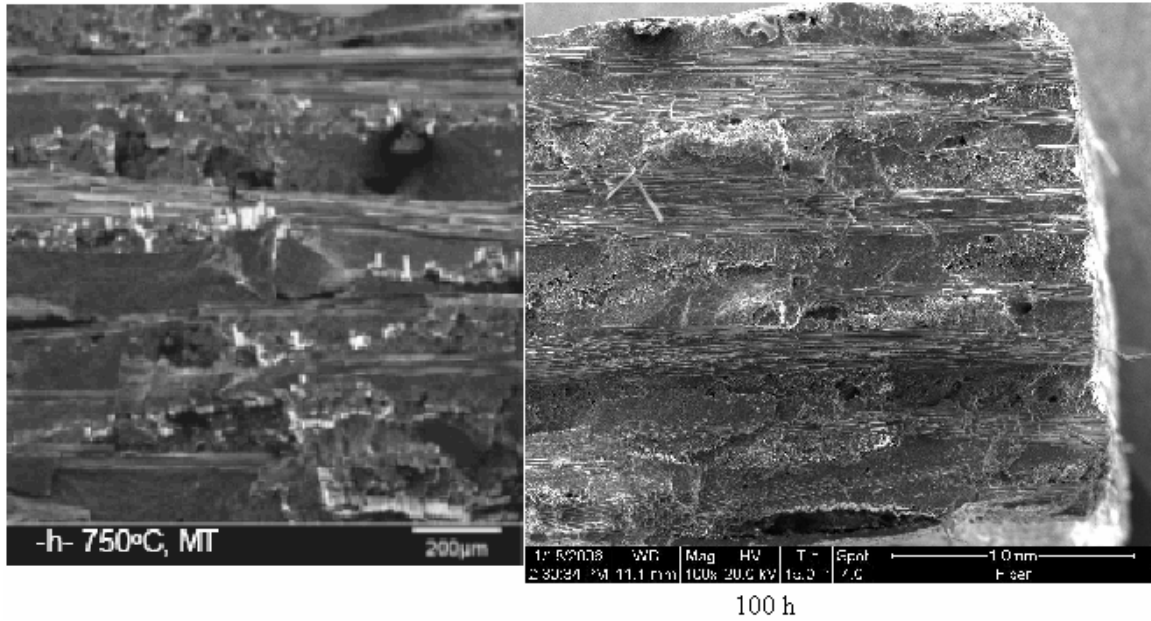**Figure 47: Stress Rupture Test - Ambient Air - 750°C - 50**

100 h

Figure 48: Stress Rupture Tests - Humid Environment - 750°C - 100x

The 100x images also show the variability in pullout lengths. Again, one can see that as the failure time, or exposure time, increases, the fiber pullout length decreases. One can see that the fracture surface is relatively smooth, with mostly planar fracture. The images in Figure 49 have similar pullout, even at different exposure times.
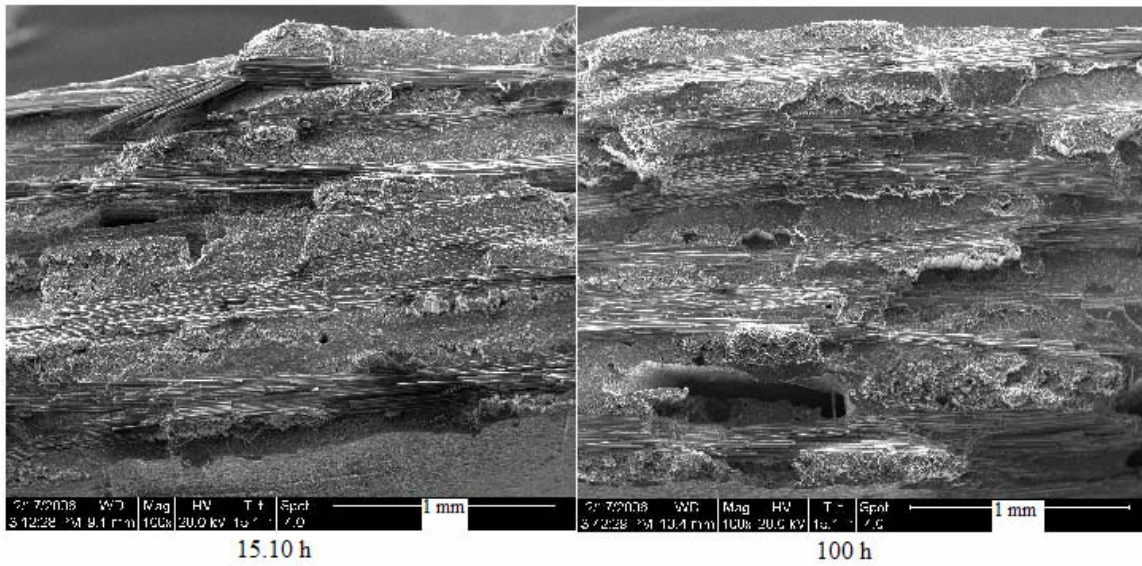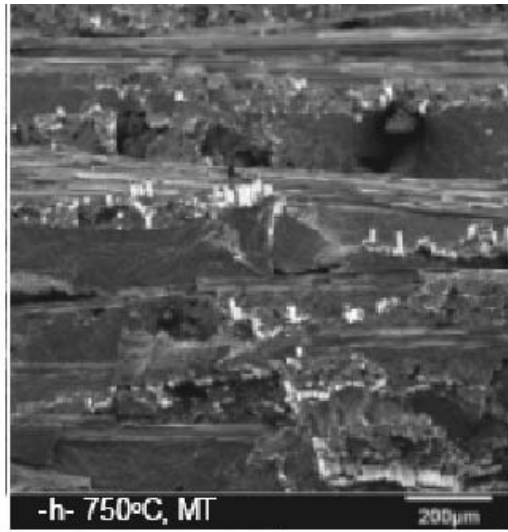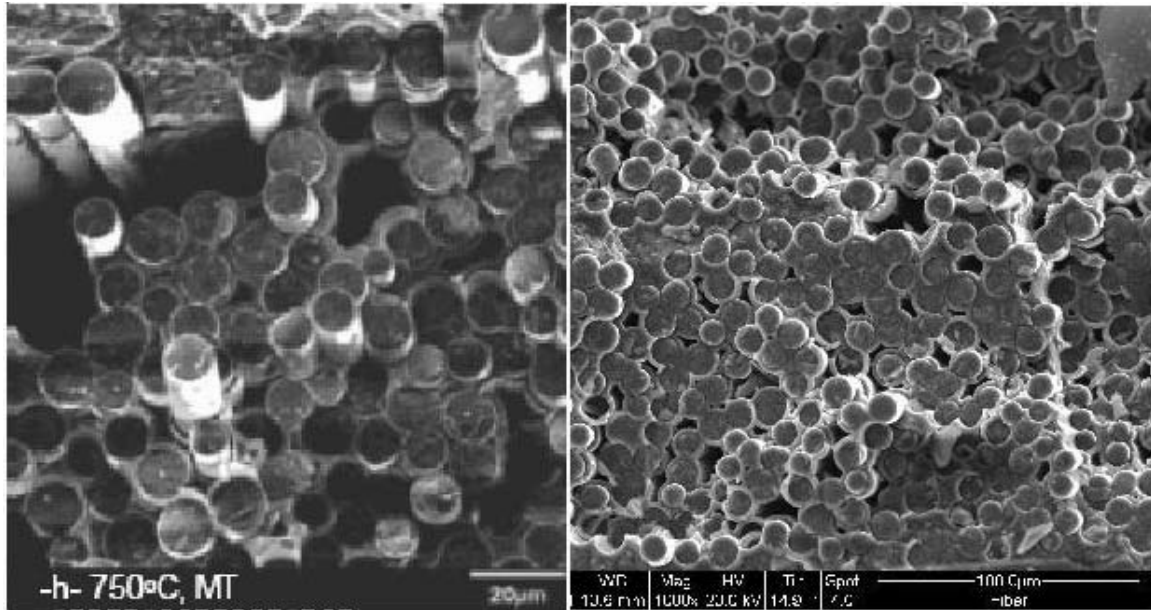
Figure 49: Stress Rupture Test - Ambient Air - 750°C - 100x

Figure 50: Stress Rupture Tests - Humid Environment - 750°C - 1000x

The 1000x images show that puddle formation has caused planar fraction in groups of fibers. The humid test shows much less fiber debonding than the air tests, although the air tests have little debonding themselves. Again, one can see very planar fracture.
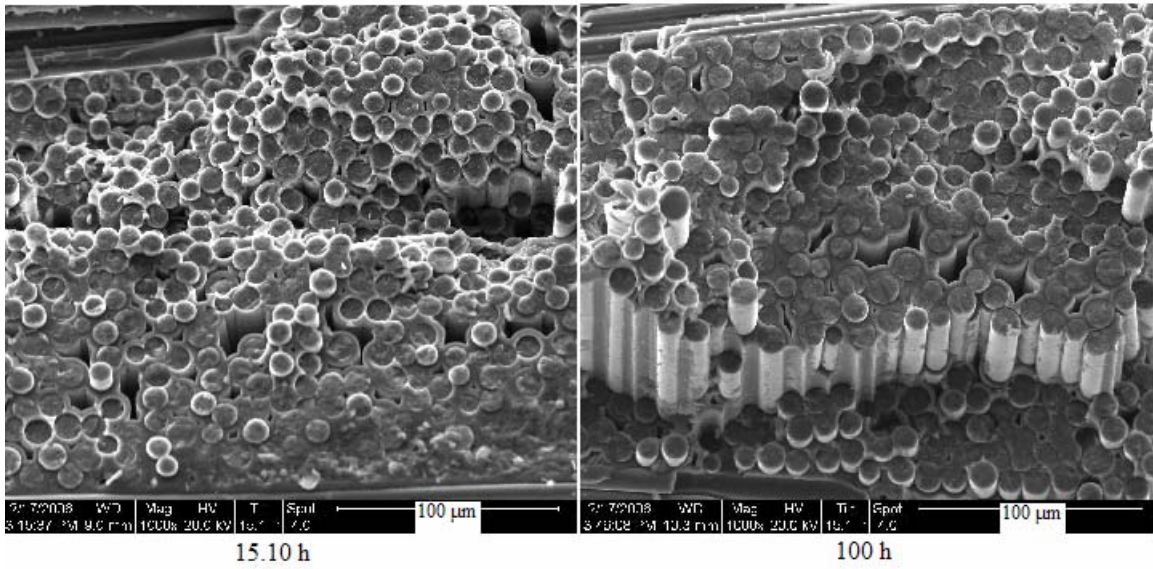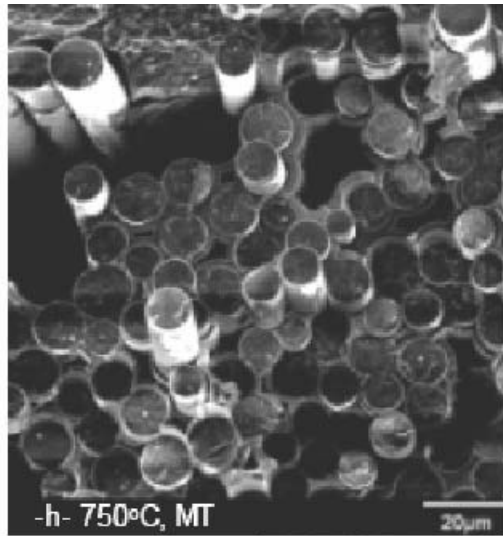
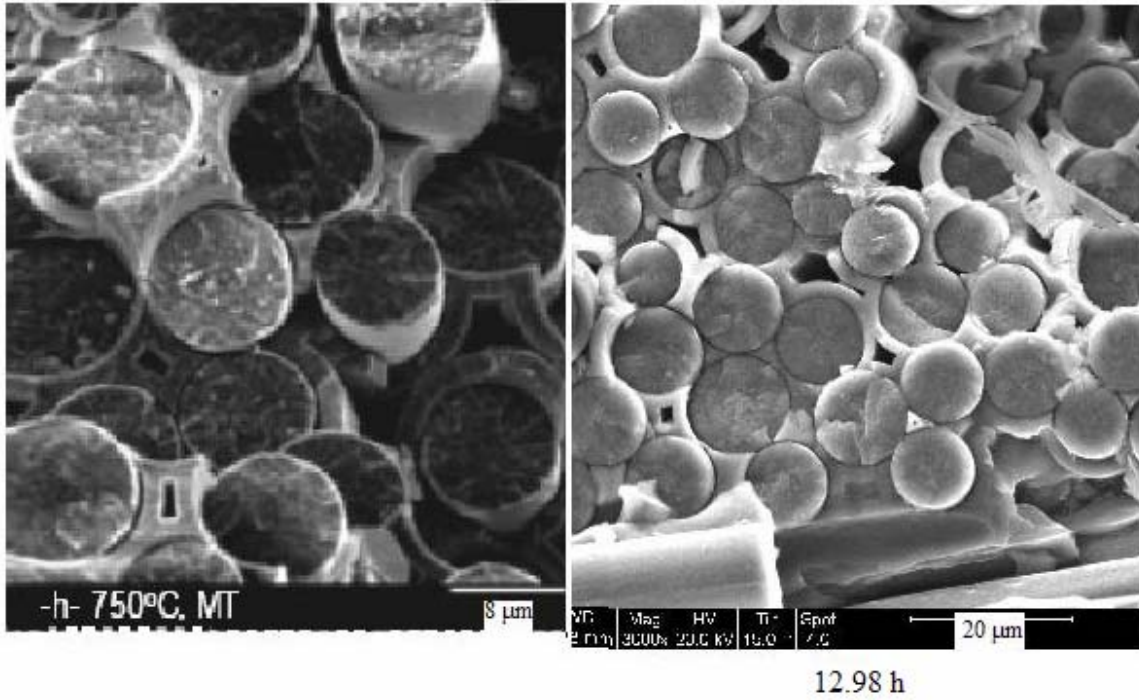**Figure 51: Stress Rupture Test - Ambient Air - 750°C - 1000x**

Figure 52: Stress Rupture Tests - Humid Environment - 750°C - 3000x

The 3000x images show that pesting has occurred in many of the fibers. It is more apparent that the neighboring fibers have failed along the same fracture surfaces. At longer exposure times, the featureless glass formation of the CVI SiC can be seen.
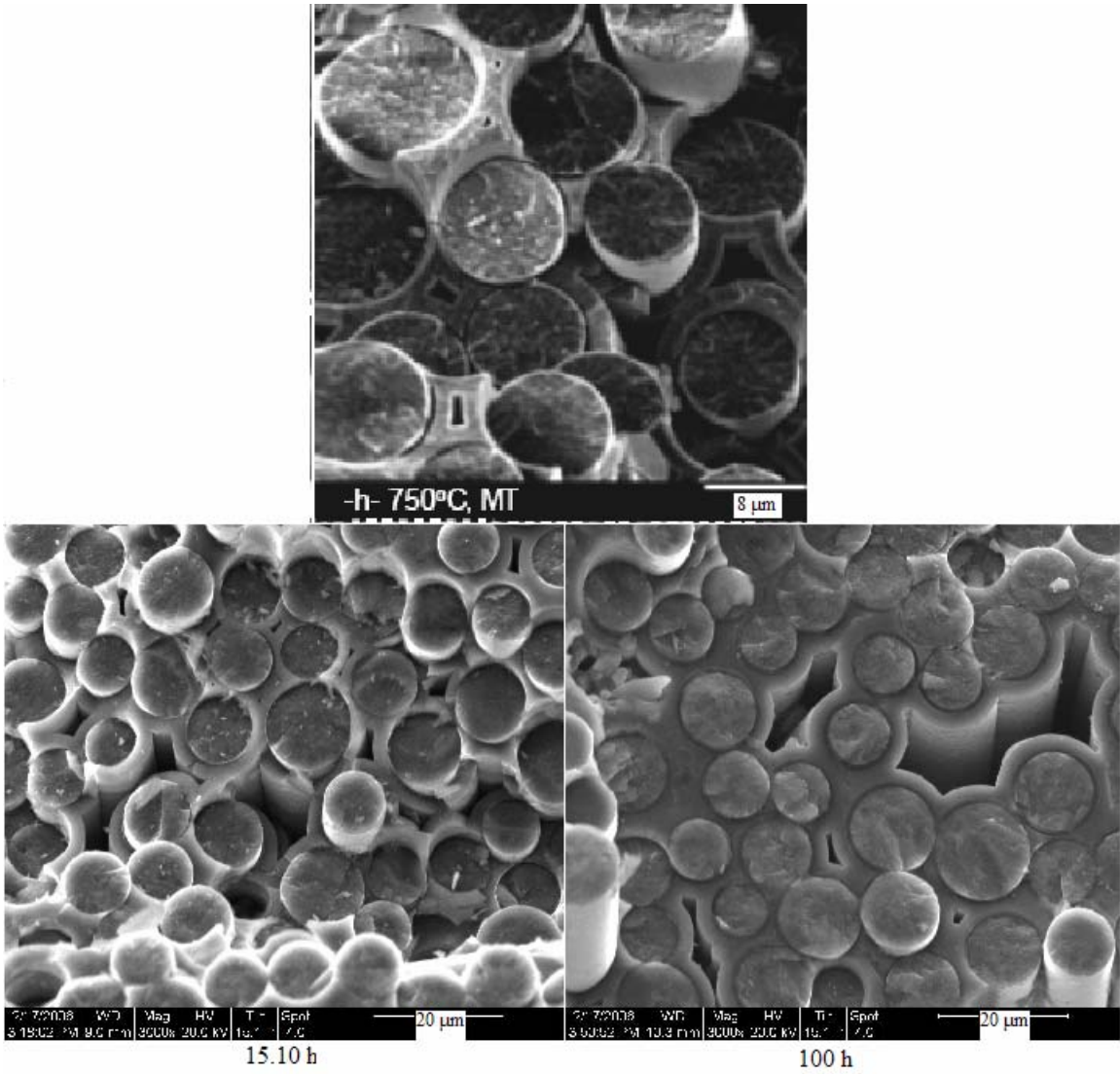
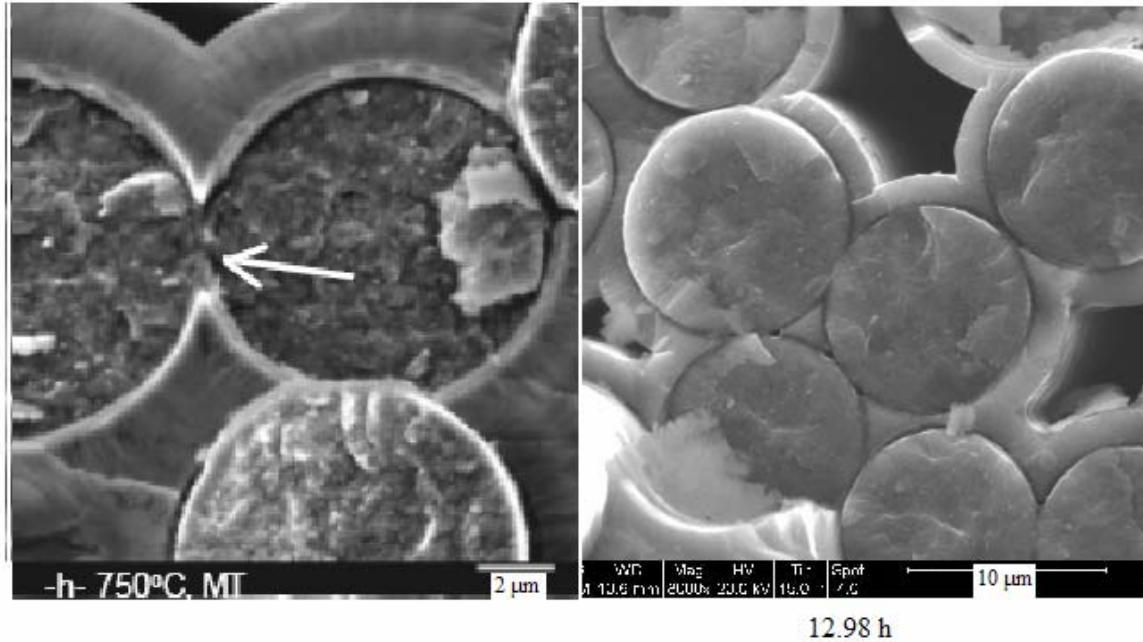**Figure 53: Stress Rupture Test - Ambient Air - 750°C - 3000x**

Figure 54: Stress Rupture Tests - Humid Conditions - 750°C - 8000x

The 8000x images show that the fracture patterns of fibers can be traced across neighboring fibers. This is occurring because the glass formation has pested these fibers together, preventing them from pulling out, and allowing the matrix cracks to propagate through the fibers. The pesting is also connecting the fibers to the matrix where the fiber and matrix are close. The recession of the BN interphase is also more apparent. It is apparent that the longer the samples were exposed to moisture, the more puddle formation and pesting occurred. In the ambient air tests, the exposure to the environment led to embrittlement as can be seen in the 100h test in Figure 55.
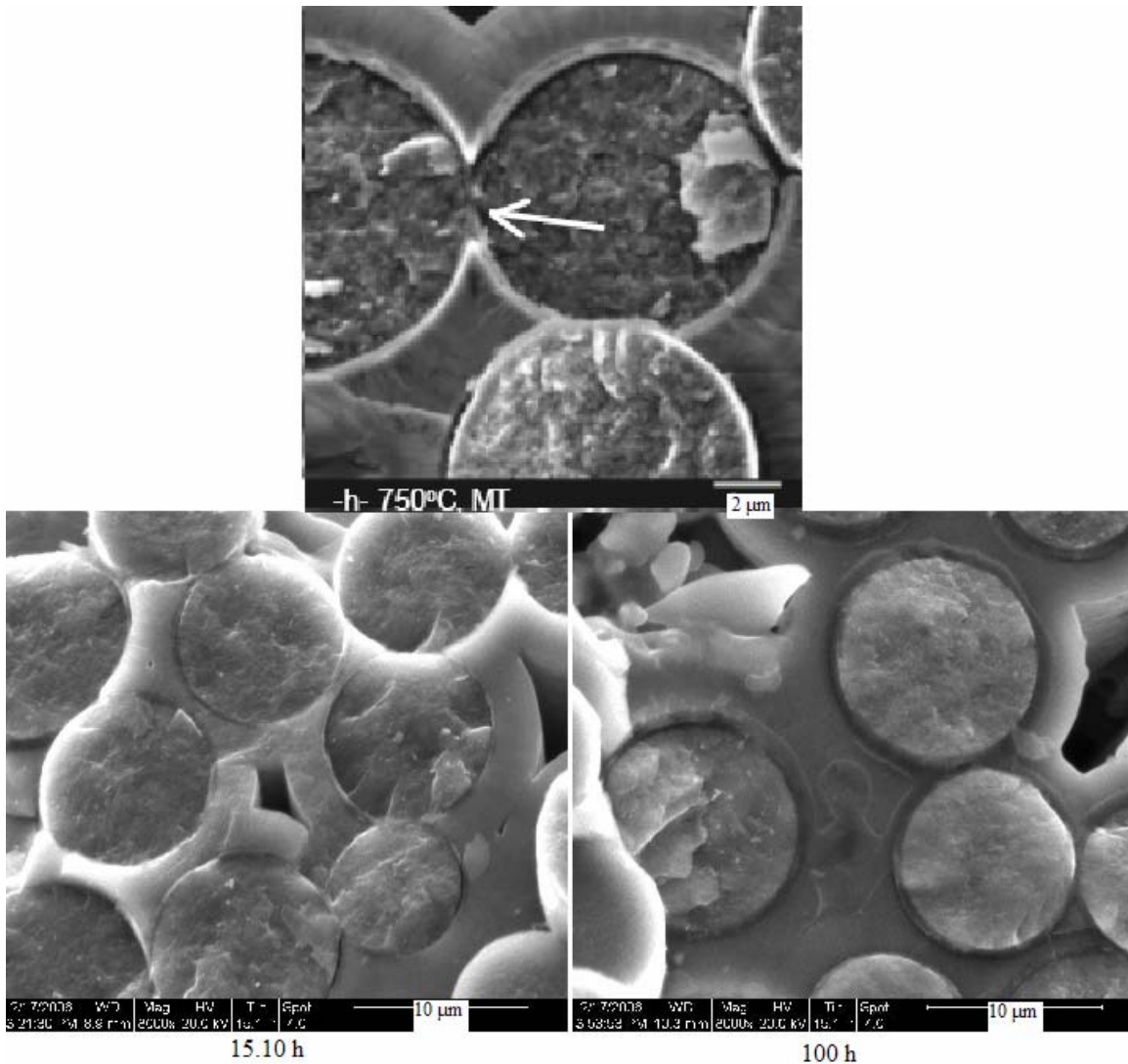
Figure 55: Stress Rupture Test - Ambient Air - 750°C - 8000x

A comparison of a LaRochelle [4] FESEM image and a SEM image from this study (respectively) from specimens tested under high humidity at 750°C are shown in Figure 56, Figure 57, andFigure 58. The term high humidity refers to the 60% pH_2O environment in the previous study and the 100% humid environment in the current study. The specimen tested in high humidity at 750°C appeared to experience less embrittlement and pesting than the specimens from the tests run by LaRochelle [4]. This could be due to

his test set-up having a direct flow of steam on the test section of the specimen, where in these tests the steam filled the susceptor, but was not directly on the specimen.
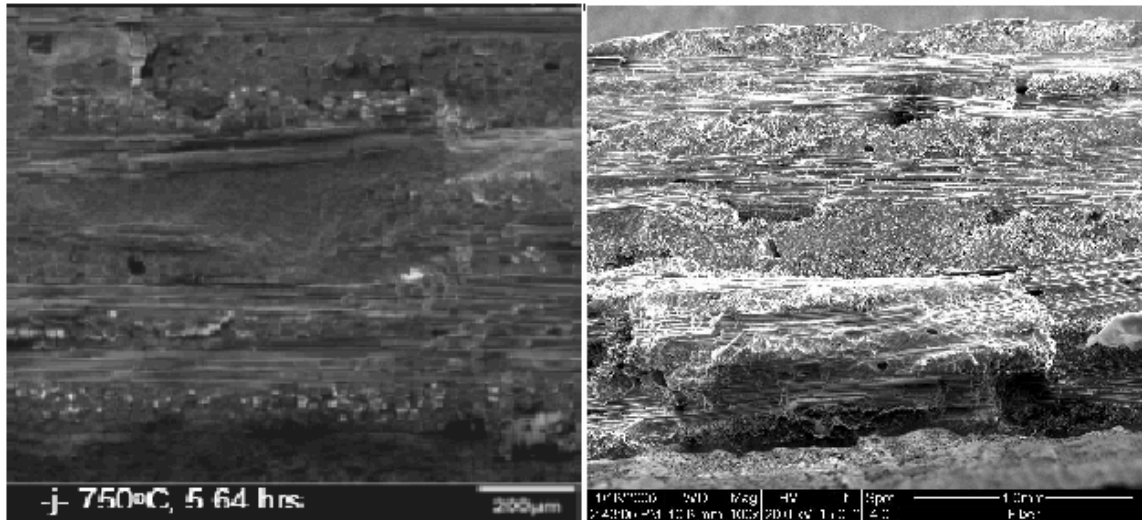

Figure 56: Comparison of Fracture Surfaces - 750°C High Moisture - 100x
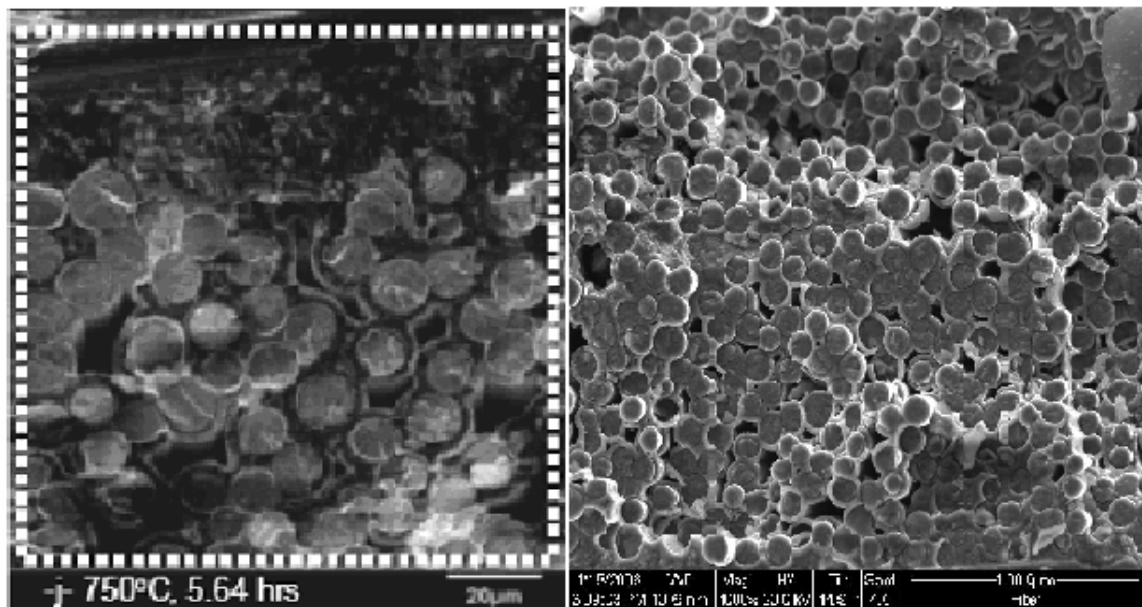
Figure 57: Comparison of Fracture Surfaces -750°C High Moisture - 1000x
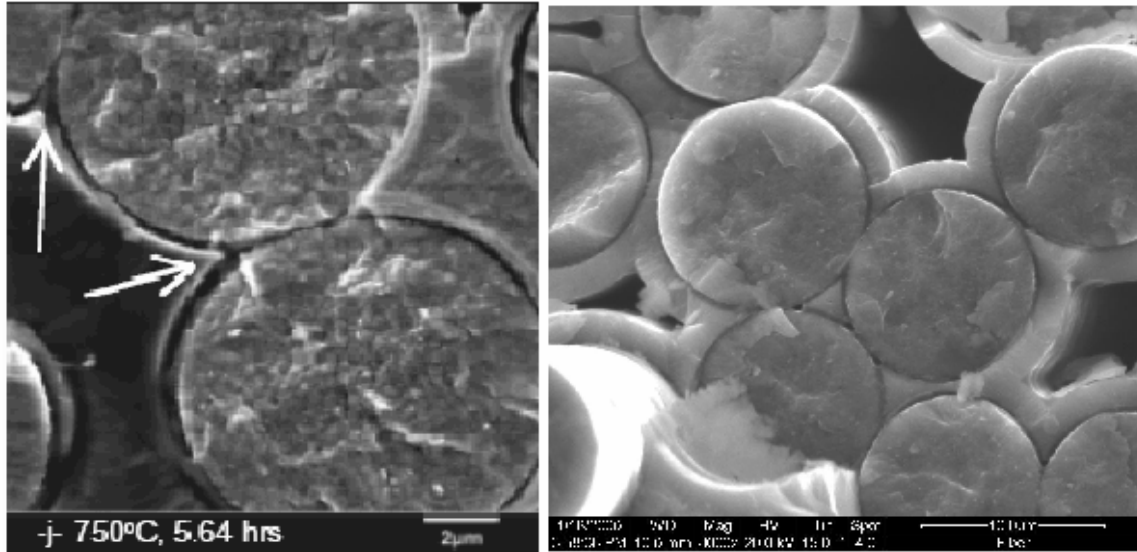
Figure 58: Comparison of Fracture Surfaces - 750°C High Moisture - 8000x

There are still puddles on the fracture plane, and it is apparent that fibers are failing in groups along the same fracture planes. The image from this study does not have as much featureless glass formation as the LaRochelle [4] image. However, the damage mechanisms are similar, and the failure time of the specimen from this test fits with the LaRochelle data extremely well, as seen in Figure 24.

Tests at 950°C

The third and final analysis was of the tests run at 950°C, above the intermediate range. The images for the 950°C tests are presented from Figure 59 through Figure 68.
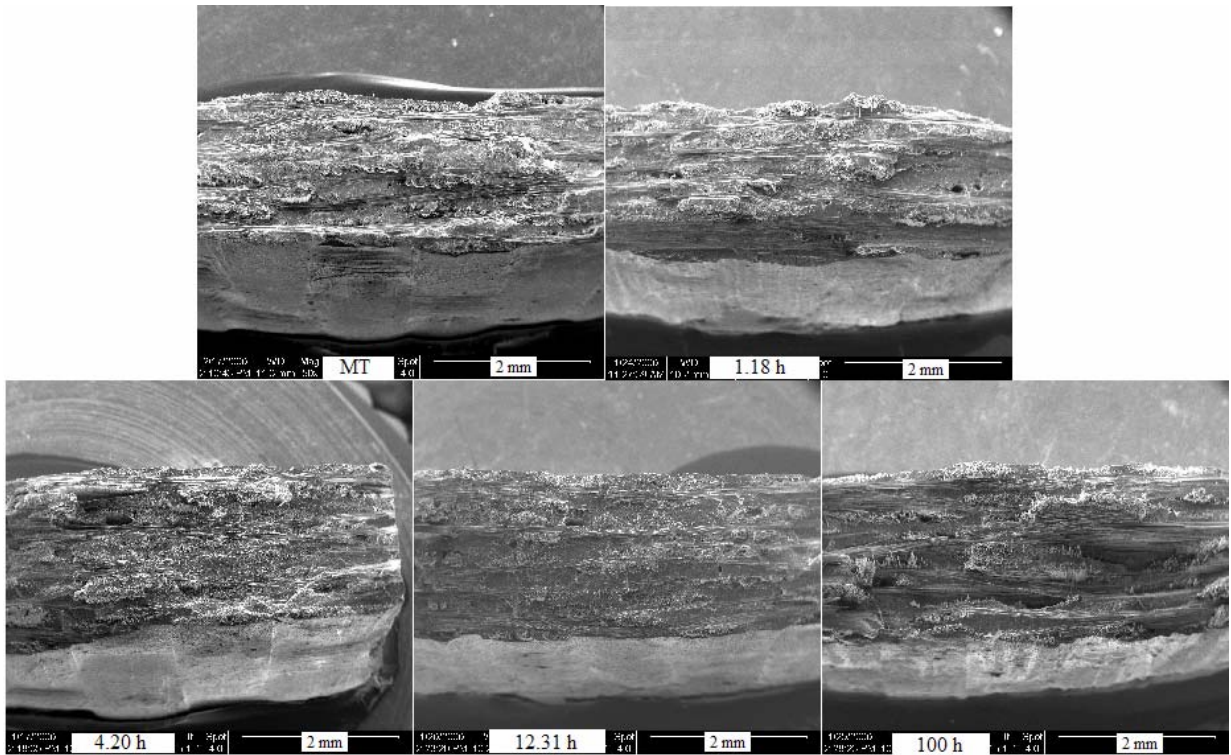
Figure 59: Stress Rupture Test - Humid Condition - 950°C - 50x

The 50x images show relatively smooth fracture surfaces, with fiber pullout occurring for the most part in tows. At this magnification, there is little difference in the humid and air tests.
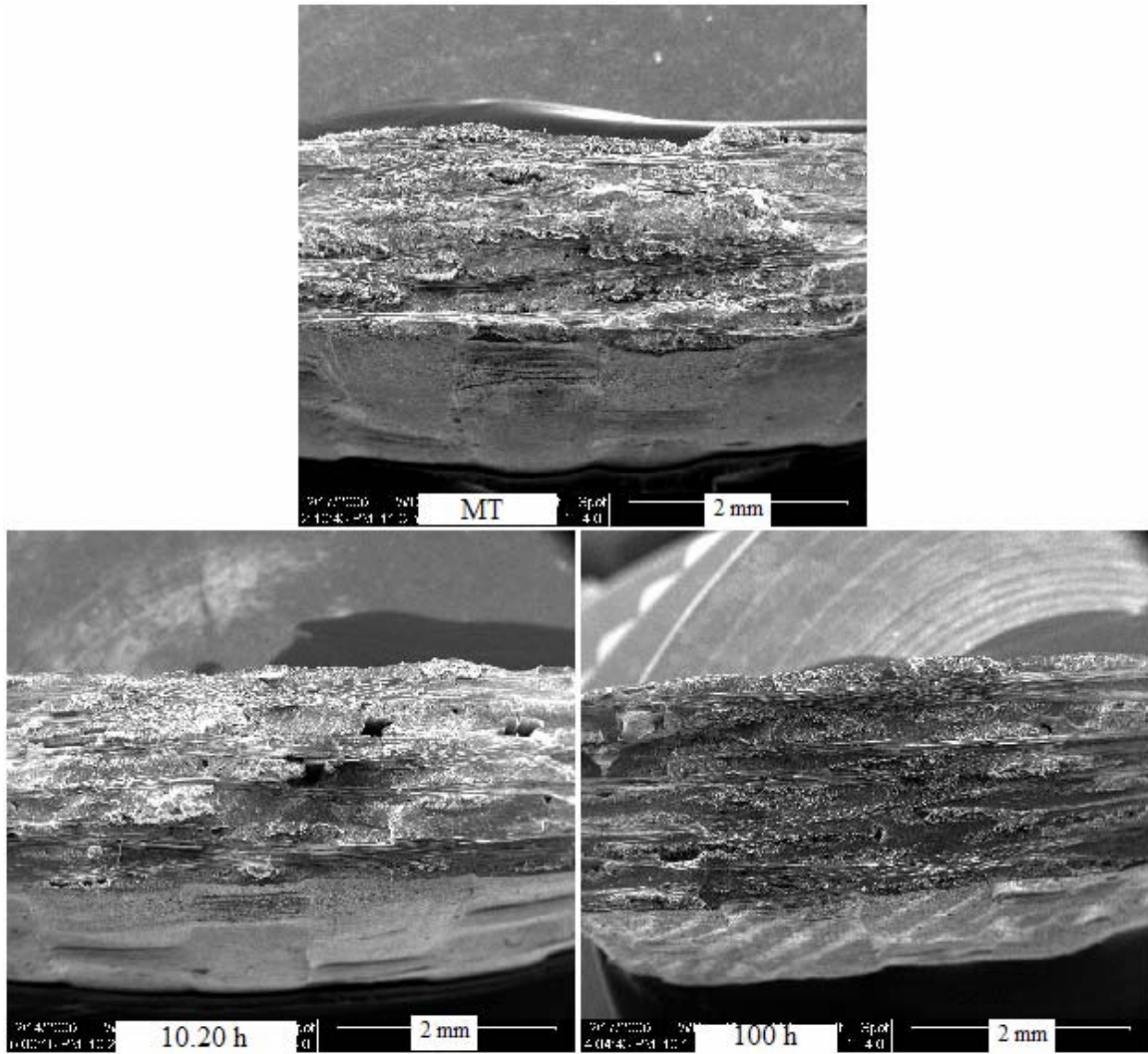
Figure 60: Stress Rupture Test - Ambient Air - 950°C - 50x
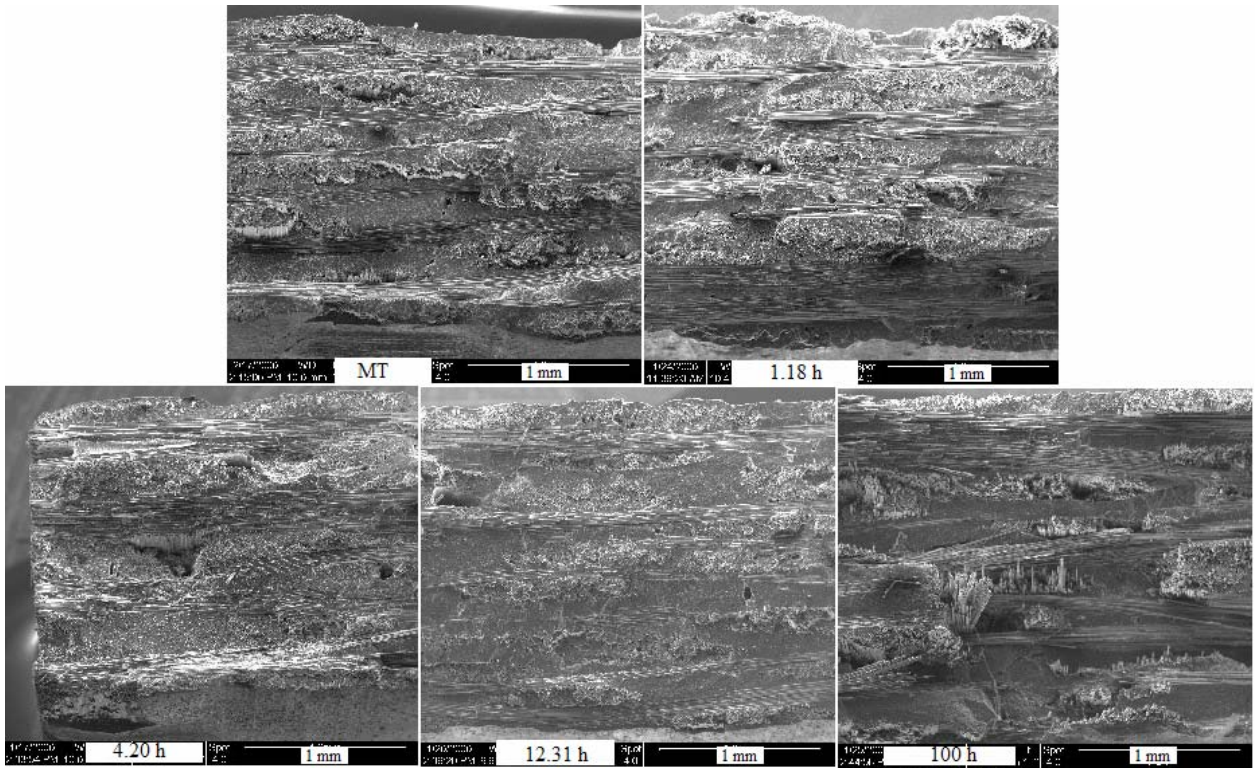
Figure 61: Stress Rupture Test - Humid Condition - 950°C - 100x

The images in Figure 61 and Figure 62 show again the fiber pullout in tows, with the exception of the 100h specimens, which had residual strength tests performed. These show some smaller groups of fiber pullout.

Figure 62: Stress Rupture Test - Ambient Air - 950°C - 100x
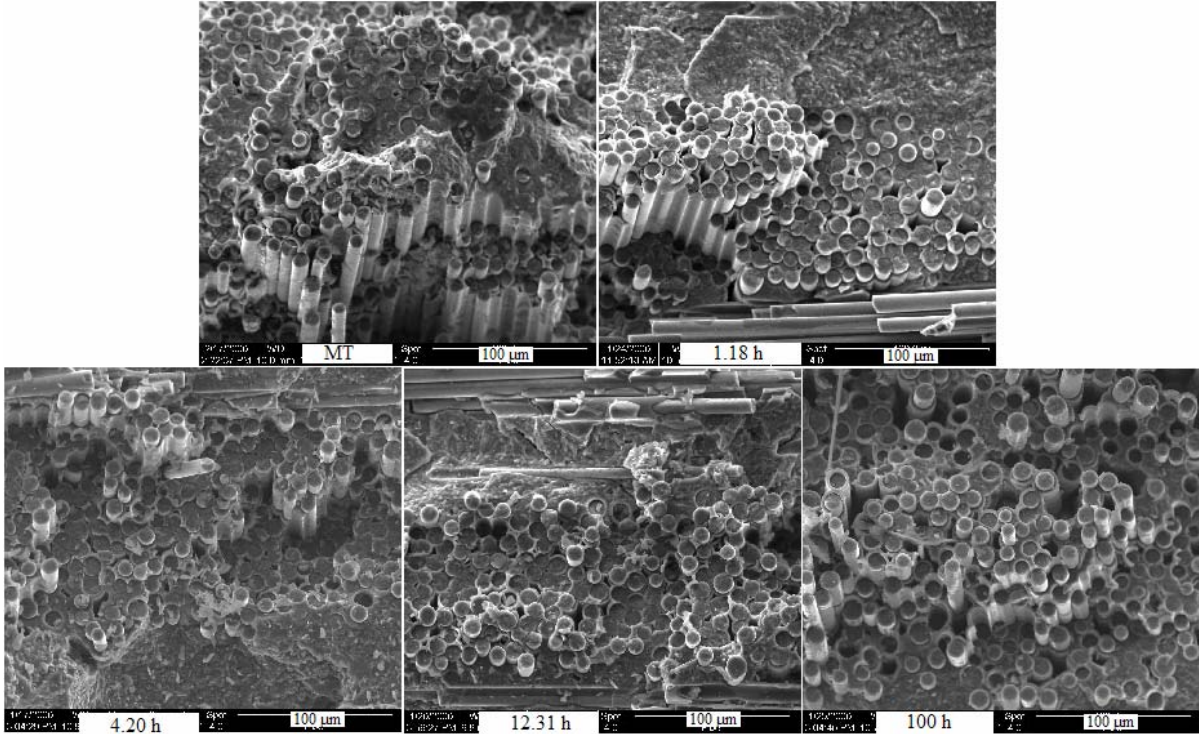
Figure 63: Stress Rupture Test - Humid Condition - 950°C - 1000x

The 1000x images show that the puddle formation has caused planar fracture in groups of fibers. However, there is still fiber pullout in tows. In both air and humid tests, little debonding of individual fibers is seen.
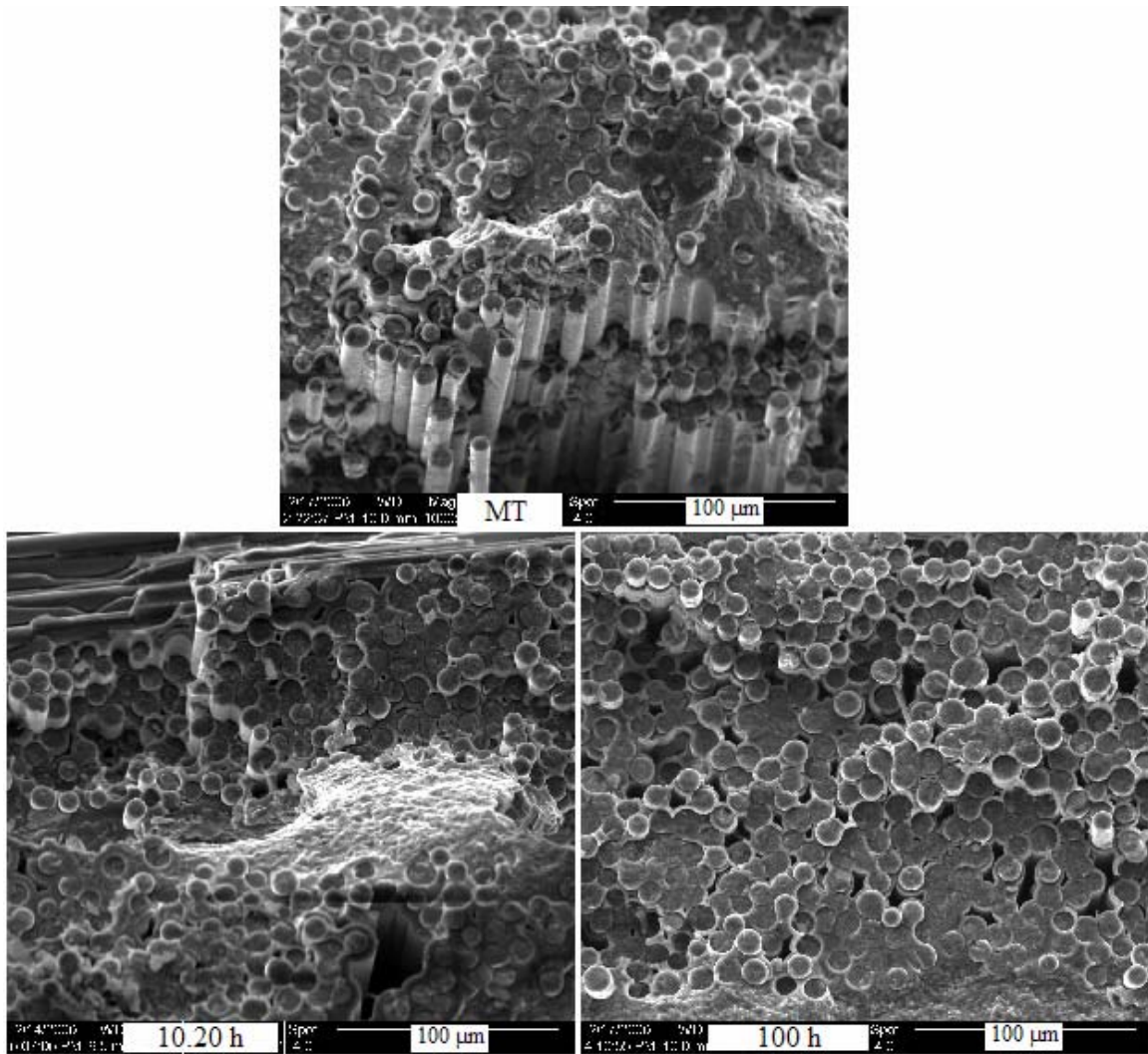
Figure 64: Stress Rupture Test - Ambient Air - 950°C - 1000x
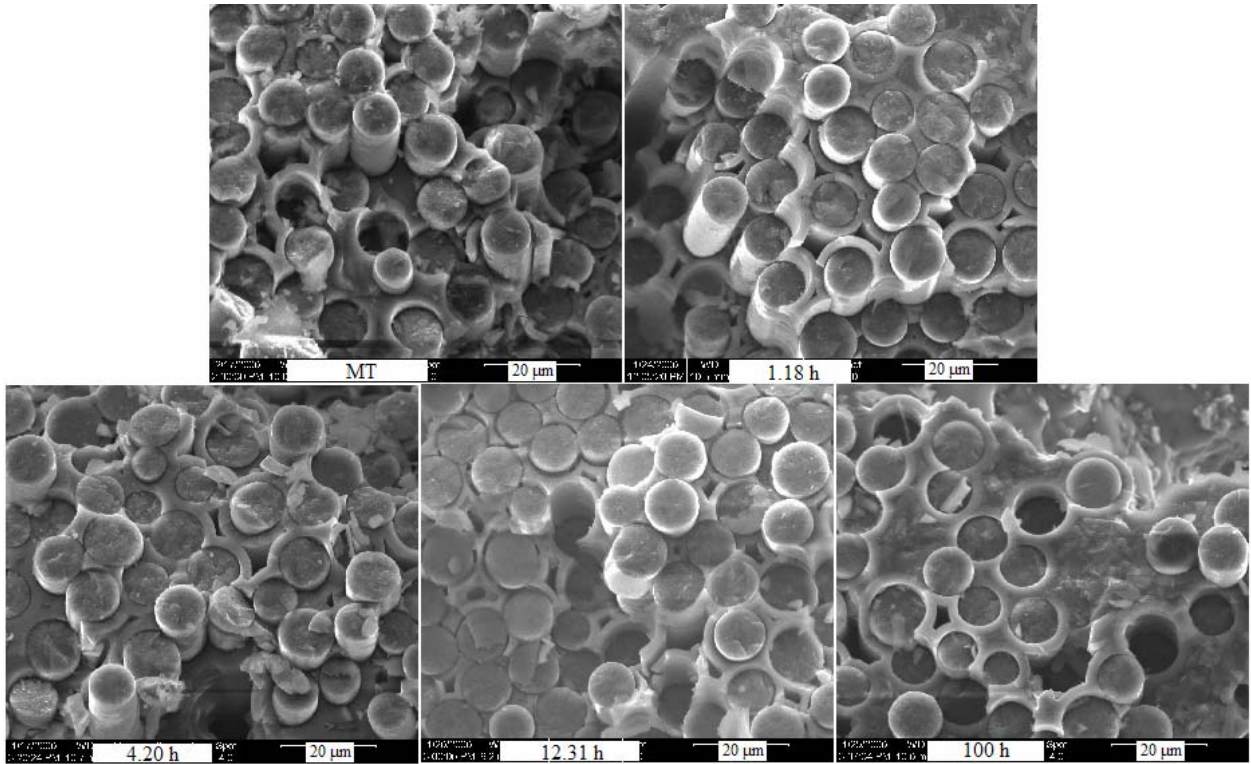
Figure 65: Stress Rupture Test - Humid Condition - 950°C - 3000x

The 3000x images show that pesting has occurred in many of the fibers. Neighboring fibers fail along the same fracture surfaces. The CVI SiC and MI SiC are distinguishable, and in tests with longer exposure times, one can see the featureless glass formation of the CVI SiC. In the 950°C fracture surfaces, there were sections with advanced embrittlement, and sections unaffected by moisture, unlike the 750°C tests, which experienced embrittlement across the fracture surface.

90

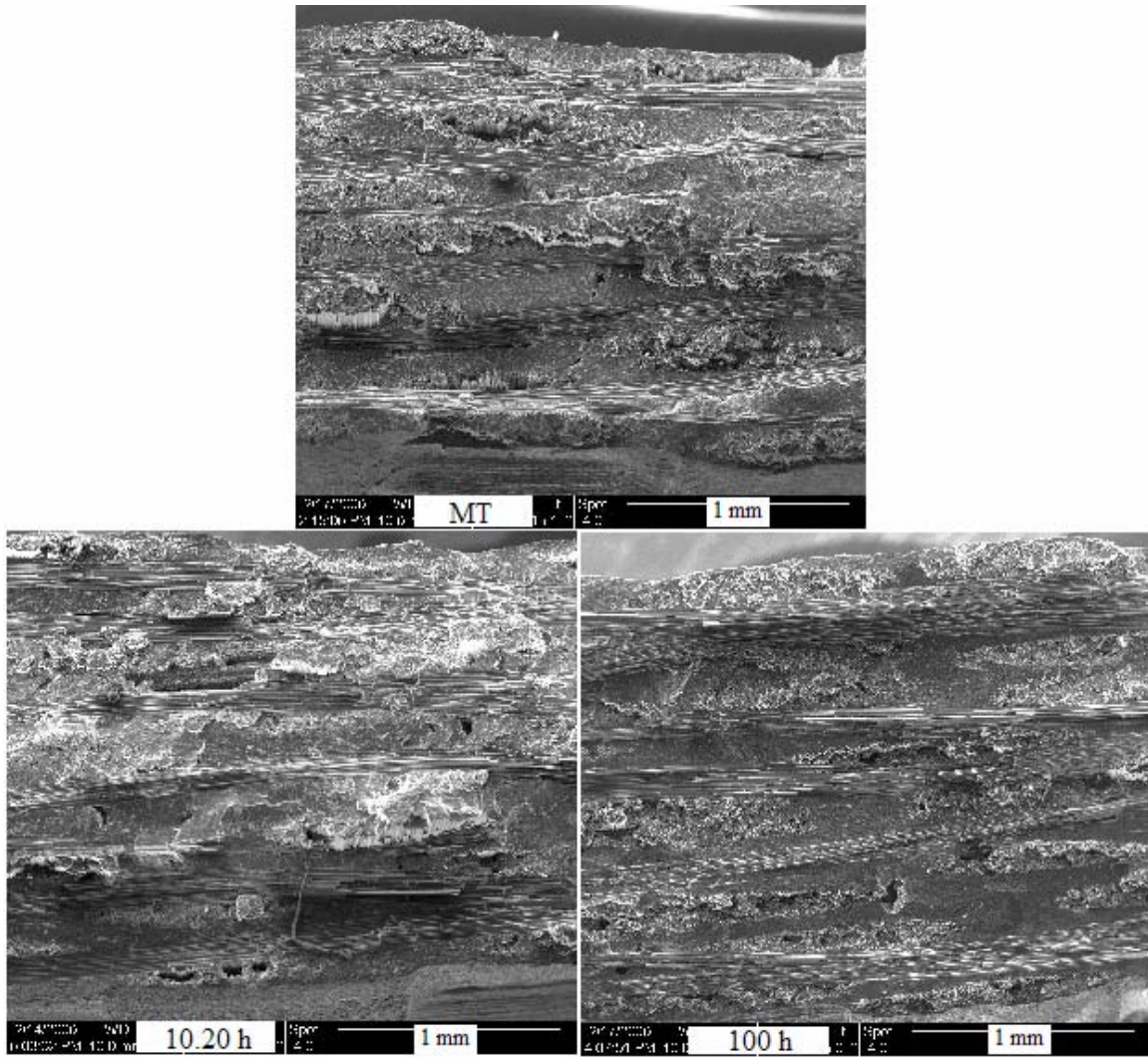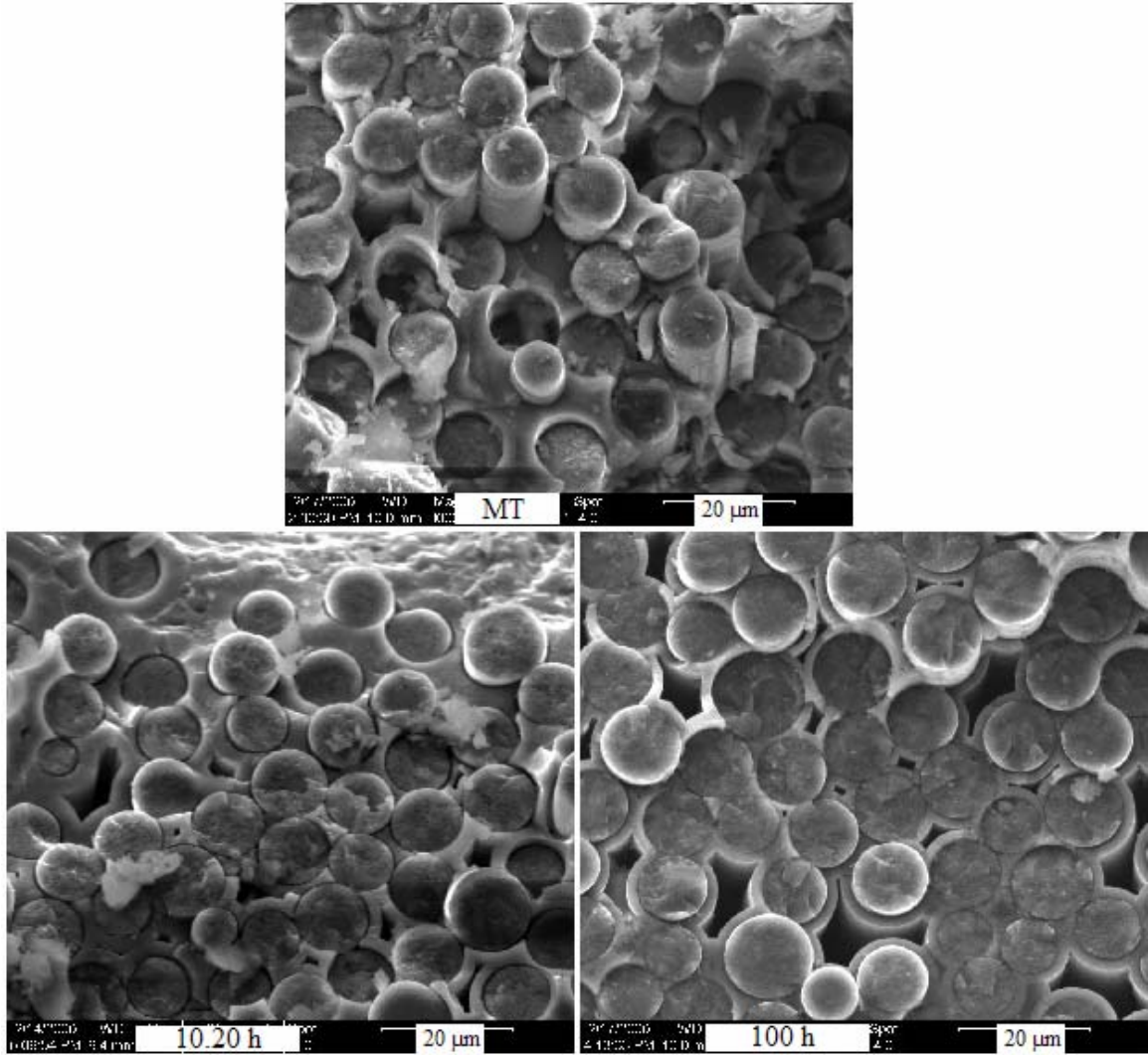**Figure 66: Stress Rupture Test - Ambient Air - 950°C - 3000x**
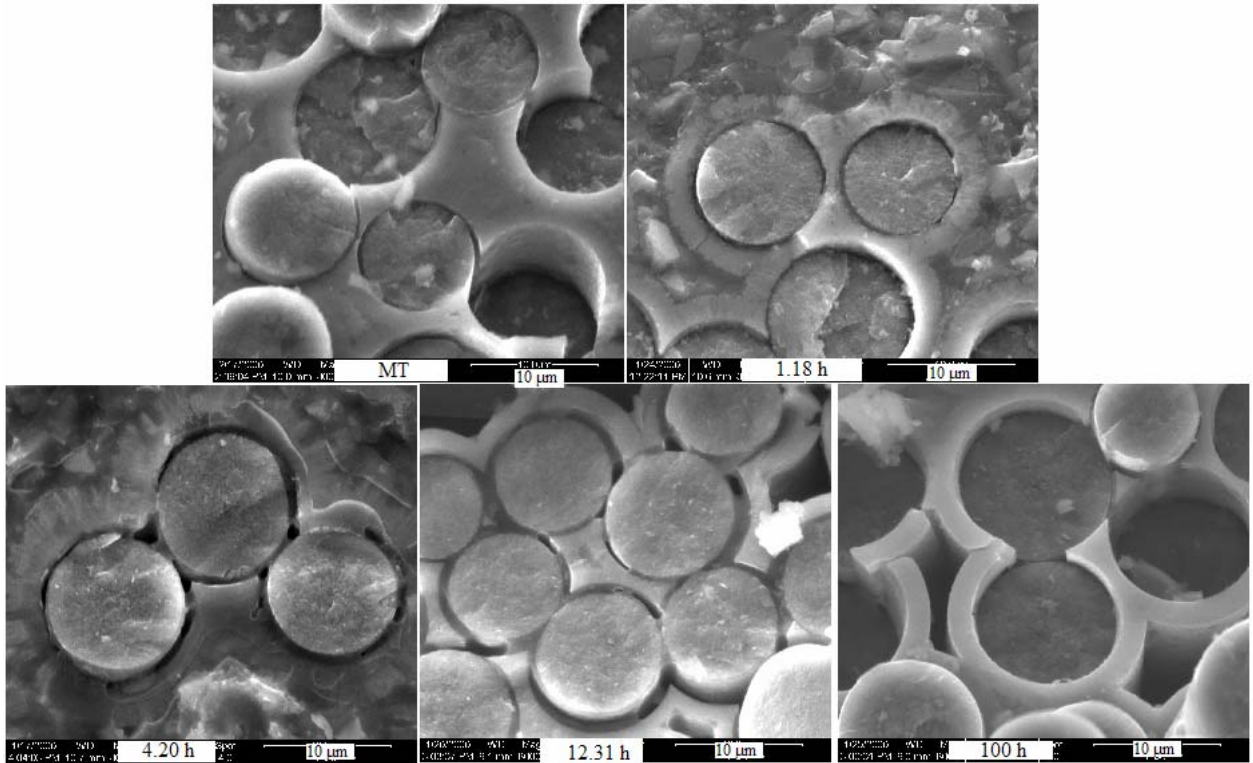
Figure 67: Stress Rupture Test - Humid Conditions - 950°C - 8000x

At this magnification, the damage done by moisture is apparent. The recession of the interphase and the pesting of the fibers is best displayed in the 4.20h and 12.31h tests in Figure 67. Under ambient air conditions, one can still observe the planar fracture, but the fibers and matrix are not bonded together as in the humid tests.
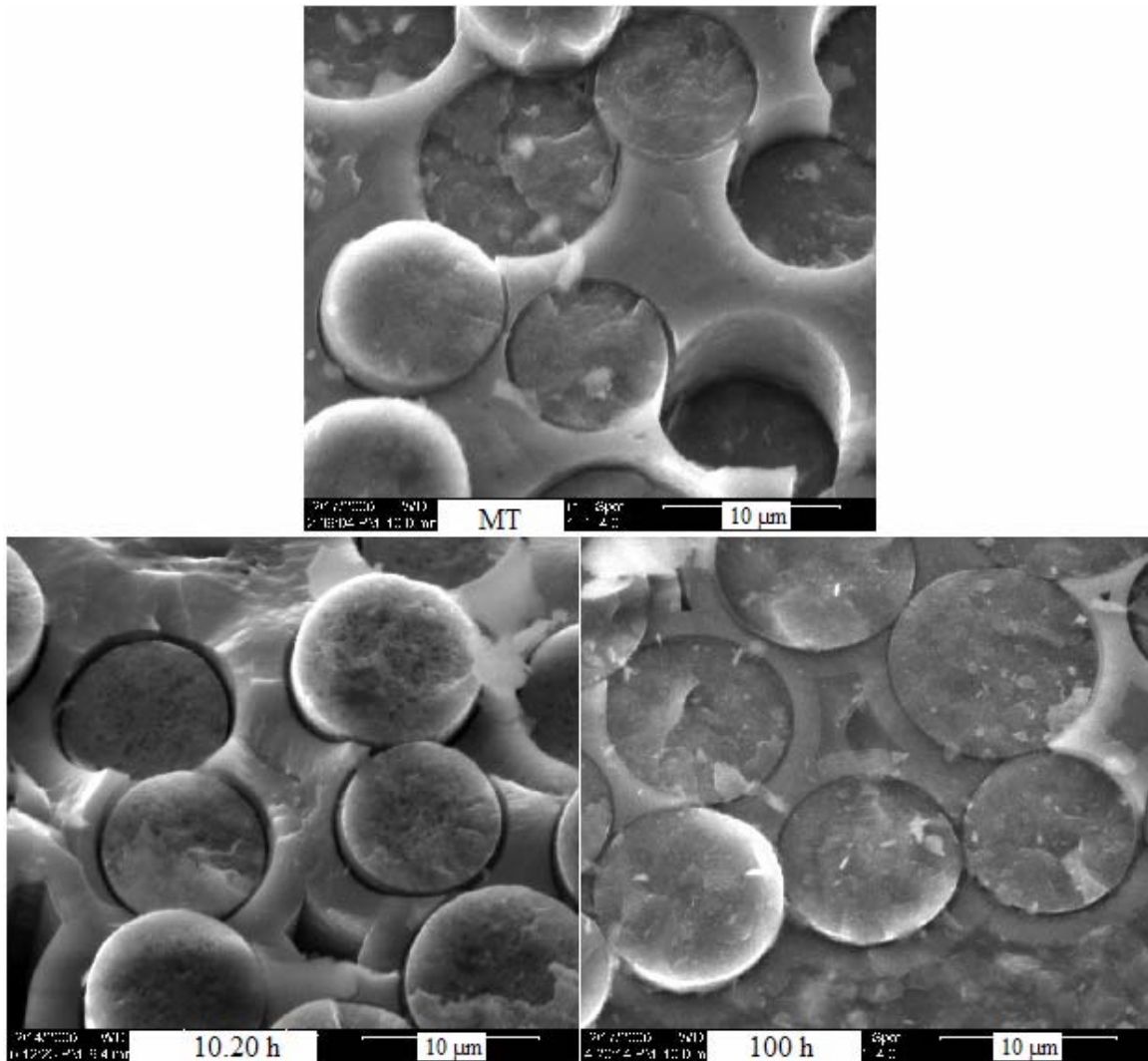
Figure 68: Stress Rupture Test - Ambient Air - 950°C - 8000x

Experiments were conducted to generate data to determine the effects of moisture and temperature on the stress rupture life of Syl-iBN/BN/SiC. It was found that moisture and temperature do not have a noticeable effect on the elastic modulus of the panels. In the monotonic tests, it was observed that moisture had no effect on the ultimate tensile strength of the specimens, only the temperature did. The higher the temperature, the more effect it had.

The SEM analysis showed the effect the exposure to high moisture, high temperature environment had on the constituents of a CMC. It was observed that the

93

moisture had no real effect below the intermediate range, at 400°C, but within the range, 750°C, and above the range, 950°C, moisture had a considerable effect on the life of the CMC. The higher the temperature, the more degradation in the strength of the material. High humidity led to more embrittlement and pesting in the material, and so premature failure.

5.2 Discussion

This research sought to answer two questions regarding the performance of a Syl-iBN/BN/SiC CMC in a humid environment at a temperature below the intermediate range, within the range, and above the intermediate range. The first question asked how the environment affects the constituents of the CMC. The second question concerned the response of the stress rupture life to the extreme environment. The method for answering these questions was to collect experimental data to understand the failure mechanisms of the CMC as the temperature was varied in ambient air and humid environments. This chapter discusses how the experimental results determined in this test provide more information on the effects of temperature and moisture on the Syl-iBN/BN/SiC CMC.

5.2.1 Environmental Effects on the Principal Constituents of the CMC

This research showed that the environment had the most effect on the interphase material of the Syl-iBN/BN/SIC CMC. The effect of the environment was expected, due to previous studies conclusions that the material properties of the fiber and matrix remained unchanged due to the environment. From literature previously reviewed in Chapter II, it was known that BN is susceptible to oxidation, which let to embrittlement and pesting. Heredia et al [12] believed that there was one temperature, called the pesting

94

temperature, for every loading condition, moisture level, and material where embrittlement would occur. His study concluded that the pesting temperatures for CMCs fell in the 600-900°C range. The study conducted by LaRochelle [4] found that for the Syl-iBN/BN/SiC, the pesting phenomenon occurred at a range of temperatures for a specific loading condition and environment. He concluded that the pesting phenomenon was dependent on the level of moisture in the environment. This research found that pesting does not only occur within the intermediate range, but that it can also occur at other temperatures, especially above the intermediate range. While the embrittlement in the 950°C tests was not as widespread as in the 750°C tests, where the 950°C samples were exposed to the environment, they experienced more advanced embrittlement. This is likely due to the sealing of cracks by silica formation.

5.2.2 Moisture Effects on the Life of the CMC

From previous research discussed in Chapter II, it is known that embrittlement is a primary mechanism of failure for the SiC/SiC composites, and in this case, the Syl-iBN/BN/SiC. The failure of the specimens was attributed to the decrease in strength resulting from the pesting of fibers. The pesting, or solidification, of fibers allowed cracks to propagate through the matrix and into the fibers, causing them to fail. With the fibers bonded together, as soon as the weakest fiber failed, the neighboring fibers would also fail. The failure of many fibers at once quickly increases the stress on other fibers, including those in other tows, causing premature failure throughout the specimen.

This research showed that an environment with a high moisture level is very detrimental to the lifetime of the CMC. The strength dependence on temperature is similar to results from previous tests [4], that higher temperatures lead to increased

strength degradation. It was also shown in Figure 27 and Figure 28 how the moisture level affected the residual strength of the specimens. Presence of high moisture levels in the environment caused the residual strength of the specimen to be much lower than that in the ambient air environment.

The areas of embrittlement were very similar in this research as in the research conducted by LaRochelle [4]. In regions untouched by the environment, the variations in fiber strength along the lengths of the fibers decided the length of the failed fiber, creating fiber pullout. In the embrittled regions, fibers failed in groups because of pested fibers failing when the first weak fiber failed, reducing the strength of the group of fibers to that of the weakest fiber. This effect is observed in the SEM images.

To summarize, the presence of moisture in a testing environment accelerates the embrittlement process, especially as the temperature is increased. This means the number of fibers pested together at a given moment is greater in a moisture environment than in the ambient air environment. The groups of pested fibers were incapable of handling increased loads, and when one fiber of a group would fail, the others would also fail, often along the same plane. This reduced the strength of the group of fibers to that of the weakest fiber.

VI. Conclusions and Recommendations

The focus of this study was to determine the effect of stress rupture loading, temperature, and moisture on the components of the Syl-iBN/BN/SiC CMC. The Syl-iBN/BN/SiC consisted of a Sylramic™ (Syl) fiber with an in-situ boron nitride (iBN) layer, boron nitride interphase, and silicon carbide (SiC) matrix. This study sought to investigate the stress rupture behavior of the material, or how it weakened over time, and how the environment affected this degradation.

During the study, tests were run in two separate environments – 100% humidity, and in air. A relationship was sought between the ceramic matrix composite degradation and the temperature, and/or the moisture content of the environment. Analysis of the failed specimens using a Scanning Electron Microscope showed how the introduction of high amounts of moisture into the testing environment affected the matrix, interphase, and fibers of the sample. Monotonic tensile tests at room temperature were conducted to show normal CMC failure mechanisms and, using the SEM, provided baseline images for comparison with tests run under the environmental conditions. Stress rupture tests were conducted in he various environments to collect data on strength reduction, and to provide fracture surfaces to show how time, temperature, and moisture content affect the embrittlement of the specimen. The research presented here is an insight into the effect of the intermediate temperature range on the embrittlement of a specimen compared with specimens tested outside the intermediate range.

6.1 Embrittlement of CMCs

Previous studies have investigated the stress rupture behavior of the NiC/SiC and HN/SiC CMCs at intermediate and high temperatures. LaRochelle [4] tested the Syl-iBN/BN/SiC CMC in the intermediate temperature range at various moisture levels. These studies found dramatic decreases in the strength of these systems due to embrittlement, especially in the intermediate temperature range. Embrittlement occurred in this range due to pesting of the fibers when the BN interphase was oxidized from exposure to the testing environment. Embrittlement changed the failure mechanism of the fibers from failing fiber by fiber to failing in groups when the weakest fiber failed.

This research focused on an area of interest that has not previously been studied: the effects of a high-moisture environment on the Syl-iBN/BN/SiC at a temperature below the intermediate range, within the range, and above the intermediate range. It tested the material at laboratory air and 100% humidity conditions at 400°C, 750°C, and 950°C. The tests run at 750°C were not only compared against the tests at 400°C and 950°C, they were compared with fracture surfaces from LaRochelle [4] so that the data could be assumed to be continued from his tests to this research.

The use of the SEM showed that both the presence of moisture and the temperature of the environment had negative effects of the strength of the Syl-iBN/BN/SiC CMC at all ranges by pesting the load bearing fibers in a through-the-thickness crack. It showed that as the temperature increased, the performance of the Syl-iBN/BN/SiC CMC worsened. Comparatively, the CMC strength degraded more in the intermediate range than outside the range, but quantitatively, it lasted longer than the tests run at 950°C.

When comparing the SEM pictures for the 400°C, 750°C, and the 950°C results with similar moisture content, the amount of embrittlement observed under ambient air conditions was similar for each temperature. However, under humid conditions, the amount of embrittlement increased as the temperature increased. In the 400°C tests, whatever embrittlement there was, it increased with the increased duration of the tests. For the 750°C and 950°C tests, the embrittlement advanced much earlier in a test.

6.2 Stress Rupture Life of CMCs

When compared to tests conducted in this research, the controlled humidity environment used in LaRochelle's tests [4] had a noticeable effect on the embrittlement of the CMC, but it did not cause a change in the mechanical characteristics. As seen in Figure 23, the test conducted under humid conditions in these tests matched extremely well with the curve set by the results obtained by LaRochelle [4]. As seen from these tests, the strength of the specimens decreased as the temperature was increased. The addition of moisture to the test environment accelerates the failure of the specimen, resulting in an earlier failure time.

6.3 Recommendations for Future Work

The work presented here has established that moisture has a discernable effect on the performance of Syl-iBN/BN/SiC within and above the intermediate temperature range. At these temperatures, pesting occurred more rapidly in the material, leading to premature failure. It would be of interest if Electron Dispersion Spectroscopy (EDS) were performed on the fracture surfaces to confirm the chemical reactions stated in Chapter II.

Another type of test that could be run on this material would be to test fatigue loading under humid and high temperature conditions. This would provide more data for the lifetime of the material, and perhaps expand its range of usefulness. Also, variable loading could be used, to achieve more complete stress strain curves.

Bibliography

1.   Hillig, W.B. *Tailoring Multiphase Composite Ceramics*. New York: Plenum Press, 1985.

2.   Prewo, K.M. and J.J. Brennan. "High Strength Silicon Carbide Fiber Reinforced Glass Matrix Composites," *Journal of Materials Science*, 15 [2]: 463-68 (1980)

3.   Brewer, D. "HSR/EPA combustor materials development program," *Materials Science Engineering*, A261: 284-291 (1999)

4.   LaRochelle, K. J. *Tensile Stress Rupture Behavior of a Woven Ceramic Matrix Composite in Humid Environments at Intermediate Temperature*. Ph. D. Dissertation, AFIT/DS/ENY/05-01. Air Force Institute of Technology (AU), Wright-Patterson AFB OH, March 2005.

5.   Chawla, K.K. *Ceramic Matrix Composites*, London: Chapman and Hall, 1993.

6.   Brennan, J.J. "Interfacial Characterization of Glass and Glass-Ceramic Matrix/Nicalon SiC Fiber Composites," *Materials Science and Research*, 20: 546-60 (1986).

7.   Cooper, R.F. and K. Chyung. "Structure and Chemistry of Fiber-Reinforced Ceramics," *Journal of Materials Science*, 22: 3148-60 (1987).

8.   Cao, H., E. Bischoff, O. Sbaizero, M. Ruhle, A.G. Evans, D.B. Marshall, and J.J. Brennan. "Effect of Interfaces on the properties of Fiber-Reinforced Ceramics," *Journal of the American Ceramic Society*, 73 [6]: 1691-99 (1990).

9.   Morscher, G.N. *Intermediate Temperature Stress Rupture of Woven SiC Fiber, BN Interphase, SiC Matrix Composites in Air*. Ph.D. Dissertation. Case Western Reserve University, Cleveland OH, (January 2000).

10.   Jacobson, N.S., S. Farmer, A. Moore, and H. Sayir. "High Temperature Oxidation Behavior of Boron Nitride Part I: Monolithic BN," *Journal of the. American Ceramic Society*, 82 [2]: 93-8 (1999).

11.   Jacobson, N.S., G.N. Morscher, D.R. Bryant, and R.E. Tressler. "High Temperature Oxidation of Boron Nitride Part II: BN Layers in Composites," *Journal of the American Ceramic Society,* 82 [6]: 1473-82 (1999).

12. Heredia, F.E., J.C. McNulty, F.W. Zok, and A.G. Evans. "Oxidation Embrittlement Probe for Ceramic Matrix Composites," *Journal of the. American Ceramic. Society*, 78 [8]: 2097-100 (1995).

13. Musil, S.S. *Characterization of Creep Behavior of Oxide/Oxide Composite with Monazite Coating at Elevated Temperature*. MS thesis, AFIT/GAE/ENY/05-M14. Air Force Institute of Technology (AU), Wright-Patterson AFB OH, March 2005.

14. More, K.L., E. Lara-Curzio, P. Tortorelli, A. Szweda, D. Carruthers, and M. Steware. "Evaluating the High-Temperature Stability of an Oxide/Oxide Composite Material at High Water Vapor Pressure," *Ceramic Engineering and Science Proceedings* (2004).

15. Committee on Advanced Fibers for High-Temperature Ceramic Composites, National Materials Advisory Board, Commission on Engineering and Technical Systems, National Research Council, Ceramic Fibers and Coatings: Advanced Materials for the Twenty-First Century, National Academy Press, Washington D.C., 1998 and 2000.

16. Evans, A.G. and D.B. Marshall. "Overview No. 85: The Mechanical Behavior of Ceramic Matrix Composites," *Acta Matall*, 37 [10]: 2567-2583 (1989).

17. Filipuzzi, L., G. Camus, R. Naslain, and J. Thebault. " Oxidation Mechanisms and Kinetics of 1D-SiC/C/SiC Composite Materials: I, An Experimental Approach," *Journal of the American Ceramics Society*, 77 [2]: 459-66 (1994).

18. Sheldon, B.W., E.Y. Sun, S.R. Nutt, and J.J. Brennan. "Oxidation of BN-Coated SiC Fibers in Ceramic Matrix Composites," *Journal of the American Ceramics Society*, 79 [2]: 539-43 (1996).

19. Ogbuji, Linus U.J.T. "A Pervasive Mode of Oxidation Degradation in a SiC-SiC Composite," *Journal of the American Ceramics Society*, 81 [11]:2777-84 (1998).

20. Lin, H.T. and P.F. Becher. "Stress-Temperature-Lifetime Response of Nicalon Fiber-Reinforced SiC Composites in Air," *ASTM Symposium of Thermal and Mechanical Test Methods and Behavior of Continuous-Fiber Ceramic Composites*. 128-41. ASTM STP 1309 (1997).

21. Lin, H.T., P.F. Becher, and P.F. Tortorelli. "Elevated Temperature Static Fatigue of a Nicalon Fiber-Reinforced SiC Composite," *MRS Symposium Proceedings, Vol. 365, Ceramic Matrix Composites/Advanced High Temperature Structural Materials*, 435-440. Materials Research Society, Pittsburg PA (1995).

22.   Lara-Curzio, E., M.K. Ferber, and P.F. Tortorelli. "Interface Oxidation and Stress-Rupture of Nicalon™/SiC CVCCs at Intermediate Temperatures," *Key Engineering Materials Vols. 127-131*. 1069-1082. Trans Tech Publications, Switzerland (1997).

23.   Lara-Curzio, E. "Stress-Rupture of Nicalon/SiC Continuous Fiber Ceramic Matrix Composites in Air at 950°C," *Journal of the American Ceramics Society*, 80 [12]: 3268-72 (1997).

24.   Lipetzky, P., N.S. Stoloff, and G.J. Dvorak. "Atmospheric Effects on High-Temperature Lifetime of Ceramic Composites," *Ceramic Engineering and Science Proceedings*, 18 [4]: 355-62 (1997).

25.   Martínez-Fernández, J. and G.N. Morscher. "Room and Elevated Temperature Tensile Properties of Single Tow Hi-Nicalon, Carbon Interphase, CVI SiC Matrix Minicomposites," *Journal of the European Ceramics Society*, 20: 2627-36 (2000).

26.   Morscher, G.N. " The Effect of Static and Cyclic Tensile Stress and Temperature of Failure for Precracked Hi-Nicalon/BN/CVD SiC Minicomposites in Air," *Ceramic Engineering and Science Proceedings*, (1997).

27.   Morscher, G.N. and J.D. Cawley. "Intermediate Temperature Strength Degradation in SiC/SiC Composites," *Journal of the European Ceramic Society*, 22[14]: 2777-88 (2002).

28.   Morscher, G.N., J. Hurst, and D. Brewer. "Intermediate-Temperature Stress Rupture of a Woven Hi-Nicalon, BN-Interphase, SiC-Matrix Composite in Air," *Journal of the American Ceramic Society*, 83 [6]: 1441-49 (2000).

29.   Budiansky, B., J.W. Hutchinson, and A.G. Evans. "Matrix Fracture in Fiber-Reinforced Ceramics," *Journal of the Mechanics and Physics of Solids*, 34 [2]: 167-89 (1986).

30.   Danchaivijit, S. and D.K. Shetty. "Matrix Cracking in Ceramic-Matrix Composites," *Journal of the American Ceramics Society*, 76 [10]: 2497-504 (1993).

31.   Yun, H.M. and J.A. DiCarlo. "Time/Temperature Dependent Tensile Strength of SiC and Al_2O_3-Based Fibers," *Ceramic Transactions Vol. 74, Advances in Ceramic Matrix Composites III*. 17-26, American Ceramic Society, Westerville OH (1996).

32.   Curtin, W.A., B.K. Ahn, and N. Tekeda. "Modeling Brittle and Tough Stress-Strain Behavior in Unidirectional Ceramic Matrix Composites," *Acta Material*, 46: 3409 (1998).

33.   Cofer, C.G. and J. Economy. "Oxidative and Hydrolytic Stability of Boron Nitride – A New Approach to Improving the Oxidation Resistance of Carbonaceous Structures," *Carbon*, 33 [4]: 389-95 (1995).

34.   Rockett, T.J. and W.R. Foster. "Phase Relations in the System Boron Nitride – Silica," *Journal of the American Ceramics Society*, 48 [2]: 75-80 (1965).

REPORT DOCUMENTATION PAGE

1. REPORT DATE (DD-MM-YYYY) 23-03-2006	2. REPORT TYPE **Master's Thesis**	3. DATES COVERED (From – To) Aug 2004 – Mar 2006

4. TITLE AND SUBTITLE

Creep Rupture Behavior of a Woven Ceramic Matrix Composite at Elevated Temperatures in a Humid Environment

5a. CONTRACT NUMBER

5b. GRANT NUMBER

5c. PROGRAM ELEMENT NUMBER

6. AUTHOR(S)

Ryba, Jennifer L., 2nd Lieutenant, USAF

5d. PROJECT NUMBER

5e. TASK NUMBER

5f. WORK UNIT NUMBER

7. PERFORMING ORGANIZATION NAMES(S) AND ADDRESS(S)

Air Force Institute of Technology
Graduate School of Engineering and Management (AFIT/EN)
2950 Hobson Way, Building 641
WPAFB OH 45433-7765

8. PERFORMING ORGANIZATION REPORT NUMBER

AFIT/GMS/ENY/06-M02

9. SPONSORING/MONITORING AGENCY NAME(S) AND ADDRESS(ES)

Mr. Larry Zawada
AFRL/MLLN
2230 Tenth St. Bldg. 655   DSN: 785-1352
WPAFB OH 45433-7817

10. SPONSOR/MONITOR'S ACRONYM(S)

11. SPONSOR/MONITOR'S REPORT NUMBER(S)

12. DISTRIBUTION/AVAILABILITY STATEMENT

APPROVED FOR PUBLIC RELEASE; DISTRIBUTION UNLIMITED.

13. SUPPLEMENTARY NOTES

14. ABSTRACT

This study focused on moisture and temperature effects on the embrittlement and stress-rupture life of the SiC/SiC CMC Syl-iBN/BN/SiC. The Syl-iBN/BN/SiC is composed of Sylramic™ fibers with an in-situ layer of boron nitride (Syl-iBN), boron nitride interphase (BN), and SiC matrix.
Stress rupture tests and monotonic tests were performed on the specimens. Tests were conducted under 100% humidity and laboratory air environments at three temperatures, 450°C, 750°C, and 950°C. These temperatures were chosen because they fall below the intermediate range, within the range, and above the range, respectively. This study found that while this CMC does experience embrittlement at intermediate temperatures, it also occurs at temperatures above the intermediate range. Scanning Electron Microscopy (SEM) analysis showed the embrittlement and pesting in the specimens increased with time, temperature, and moisture exposure, leading to premature failure. An analysis of the data confirmed that with increase in temperature and exposure to moisture, the stress-rupture life of the Syl-iBN/BN/SiC was considerably shortened.

15. SUBJECT TERMS

Creep, Silicon Carbides, Ceramic Matrix Composites, Embrittlement, Boron Nitrides

16. SECURITY CLASSIFICATION OF:			17. LIMITATION OF ABSTRACT	18. NUMBER OF PAGES	19a. NAME OF RESPONSIBLE PERSON Dr. S. Mall (ENY)
REPORT	ABSTRACT	c. THIS PAGE	UU	118	19b. TELEPHONE NUMBER (Include area code)
U	U	U			(937) 255-3636, e-mail: Shankar.Mall@afit.edu